All-Conjugated Diblock Copolyelectrolytes

Dissertation

Zur Erlangung des akademischen Grades

Doktor der Naturwissenschaften

(Dr. rer. nat.)

Bergische Universität Wuppertal

Fachbereich C – Mathematik und Naturwissenschaften

von

Andrea Gutacker

aus Wuppertal

Wuppertal, 2011

Die Dissertation kann wie folgt zitiert werden:

urn:nbn:de:hbz:468-20120403-101217-5
[http://nbn-resolving.de/urn/resolver.pl?urn=urn%3Anbn%3Ade%3Ahbz%3A468-20120403-101217-5]

Die vorliegende Arbeit wurde in der Zeit von Oktober 2007 bis Mai 2011 am Lehrstuhl für Makromolekulare Chemie des Fachbereichs C – Mathematik und Naturwissenschaften der Bergischen Universität Wuppertal unter Anleitung von Prof. Dr. Ullrich Scherf, sowie an der University of California, Santa Barbara, USA, unter Anleitung von Prof. Dr. Guillermo C. Bazan angefertigt.

Mein besonderer Dank gilt Herrn Prof. Dr. Ullrich Scherf für die interessante Themenstellung und zahlreiche Fragestellungen sowie seine vielfältige, persönliche Unterstützung und die angenehme Atmosphäre im Arbeitskreis.

Ebenso gilt mein Dank Herrn Prof. Dr. Guillermo C. Bazan für die freundliche Aufnahme in seinen Arbeitskreis an der University of California, Santa Barbara, USA.

1. Gutachter: Prof. Dr. Ullrich Scherf (Bergischen Universität Wuppertal, Deutschland)

2. Gutachter: Prof. Dr. Guillermo C. Bazan (University of California, Santa Barbara, USA)

3. Gutachter: Prof. Dr. Rachel C. Evans (Trinity College, University of Dublin, Ireland)

Eingereicht im Oktober 2011

Verteidigt im Dezember 2011

Meinen Eltern in Dankbarkeit

Life is what happens to you while you are busy making other plans.

John Lennon (1940-80)

Table of Contents

Table of Contents……..……IX

1. Introduction and Background 1

1.1. All-Conjugated Polyelectrolytes (CPE) 2

1.1.1. CPEs for Biomolecule Detection 3

1.1.2. CPEs for Optoelectronic Devices 7

1.2. All-Conjugated Block Copolyelectrolytes 10

1.3. Aim and Scope 12

1.4. References 13

2. All-Conjugated, Cationic Polyfluorene-*b*-Polythiophene Polyelectrolyte Block Copolymers 19

2.1. Introduction 19

2.2. Results and Discussion 21

2.2.1. Synthesis 21

2.2.2. Optical Properties 24

2.2.3. Aggregation Behavior in Methanol 27

2.2.3.1. Atomic Force Microscopy of Thin Films 27

2.2.3.2. Confocal Microscopy 31

2.2.4. Complexation with Anionic Surfactants 32

2.2.5. Incorporation into Organic Electronic Devices 33

2.3. Conclusion and Outlook 36

2.4. Experimental Section 38

2.5. References 47

3. All-Conjugated, "Rod-Rod" Diblock Copolyelectrolytes and their Complexes with Charged Molecules 51

3.1. Introduction 51

3.2. Results and Discussion 53
3.2.1. Synthesis and GPC Characterization 53
3.2.2. Complexation with DNA 54
3.2.3. Complexation with Anionic Surfactants 57
3.2.4. Interaction with Organic Acids 58
3.3. Conclusion and Outlook 59
3.4. Experimental Section 59
3.5. References 63
4. All-Conjugated, Cationic Polyfluorene-*b*-Polyfluorene "Rod-Rod" Diblock Copolymers 67
4.1. Introduction 67
4.2. Results and Discussion 69
4.2.1. Synthesis 69
4.2.2. Optical Properties 71
4.2.3. Atomic Force Microscopy of Thin Films 72
4.2.4. Confocal Microscopy 74
4.2.5. Incorporation into Organic Light-Emitting Diodes (OLEDs) 75
4.3. Conclusion and Outlook 77
4.4. Experimental Section 79
4.5. References 85
5. Summary 87
A Acknowledgement 89
B List of Publications 90
C Curriculum Vitae 92

Chapter 1

1. Introduction and Background

Polyelectrolytes (PEs) are defined as "polymers composed of macromolecules in which a substantial portion of the constitutional units contains ionic or ionizable groups or both".[1] These materials can dissociate in aqueous solution while leaving ions of one kind bound to the polymer chain and their corresponding counter ions in solution. Depending on the positively or negatively charged backbone a distinction is made between anionic [e.g. poly(sodium styrene sulfonate)] and cationic PEs (e.g. quaternized polyvinylpiridine) as shown in Scheme 1.1. Thus, there are also neutral PEs, containing both positive and negative charges (e.g. as zwitterions), so-called ampholytes.[2,3]

In contrast to most neutral hydrocarbon polymers, which are only soluble in less polar organic solvents, PEs are often soluble in more polar solvents, as methanol or water. Regarding to their dissociation behavior PEs are classified into strong and weak types. Strong ones dissociate completely in water independent of the pH value. In contrast, weak PEs dissociate only partly with the pH value having a big influence on the dissociation equilibrium. This is based on intra- or intermolecular Coulomb repulsion, osmotic and conformational effects.

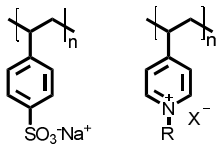

Scheme 1.1. Chemical structures of two PEs, anionic poly(sodium styrene sulfonate) [right] and a cationic, quaternized polyvinylpiridine [left].

The presence of ionic groups in PEs influences the polymer conformation drastically. Generally, also PEs, even with a high charge density, tend to form random coils like uncharged, linear polymers. But with decreased ion strength of the surrounding medium (e.g. by changing the solvent) intramolecular Coulomb interactions and osmotic effects come into play. Accordingly, intermolecular electrostatic repulsion and the Debye length increase. These effects result in a more extended chain conformation which is often called "ridgid-rod" conformation as illustrated in Figure 1.1.[3,4] Contrary, the addition of ions (salts) increases the

ion strength and supports a coiled conformation because of reduced electrostatic interactions within the PE chain. It is well known that these conformational changes also influence viscosity[5], turbidity[6] and conductivity[7] of the solutions.[4,8]

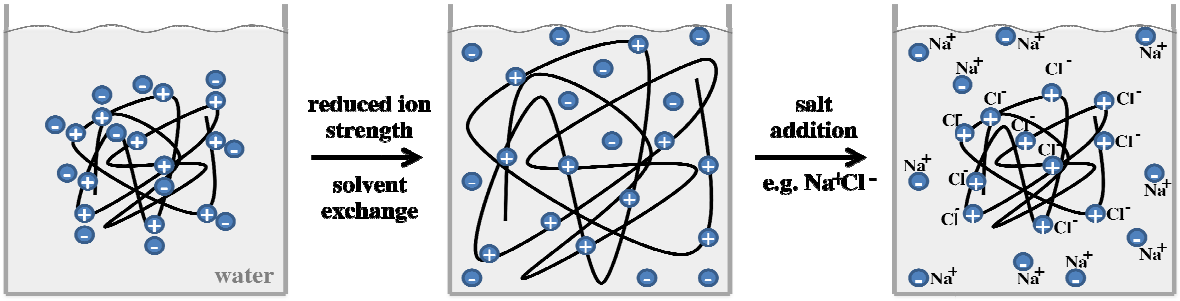

Figure 1.1. Conformational changes of a cationic PE dissolved in water when decreasing the ion strength from a coiled (left) to a "rigid rod" conformation (middle); and after salt addition (right).

With respect to the unique properties of PE they play an important role in biological systems as well as in industrial applications. For example, biological PEs as nucleic acids (DNA, RNA) act as carriers of the genetic information in organisms. Moreover, several PEs are of huge relevance for the metabolism of plants and animals. Water-soluble polyelectrolytes, natural as well as synthetic PEs, are widely used in many industrial applications. For instance, PEs are used in the textile industry as fixation agents, in cosmetics for a reduction of electrostatic effects and in the water treatment as a flocking agents.[4,9] Moreover, biocompatible PEs are added to many foods and drugs.[10,11]

1.1. All-Conjugated Polyelectrolytes (CPE)

This thesis focusses on a special class of PEs, PEs with π-delocalized backbones. So-called conjugated polyelectrolytes (CPEs) are polymer materials with electronically delocalized backbones and defined pendant groups with ionic functionalities.[11,12] Since the mid 1980s these materials have been available.[13,14] CPEs combine the characteristics of conjugated (or semiconducting) polymers[15] and the individual uniqueness of polyelectrolytes in which the properties are strongly determined by electrostatic forces.[10,16] Neutral conjugated polymers are nowadays important materials[17] for use in optoelectronic devices, such as organic solar cells (OSC)[18] and organic light emitting diodes (OLEDs)[19,20]. Primarily, the interest is based on the possibility of implementing solution-based deposition methods as part of the device fabrication process. With the addition of ionic side groups the solubility in polar and/or protic

solvents like methanol and water increases allowing for an orthogonal processing of multilayer stacks. In parallel, the manufacturing process may become environmentally friendlier.[10]

Much of the recent research into CPEs is focused towards applications in biological and chemical sensors. Design and synthetic schemes towards CPEs for biosensor applications have been developed by different scientists.[21,22] The integration of CPE layers into multilayer optoelectronic devices has resulted in improvements of organic field effect transistors (OFETs), photovoltaic devices[23], OLEDs[24] and organic light-emitting electrochemical cells[25]. Generally, there is a rising interest in novel CPEs for the optimization of device performance and processing. For instance, the strong interfacial dipole from the ionic groups can support charge injection and migration. The solubility of CPEs in polar solvents allows for their deposition atop of neutral organic semiconductors (principle of orthogonal solubility).[10,11,26]

1.1.1. CPEs for Biomolecule Detection

The majority of publications on the application of CPEs for biomolecule detection take advantage of absorbance changes or fluorescence quenching due to analyte-induced polymer aggregation[27] or electron/energy transfer processes.[11,28] This will be discussed exemplary for the following examples.

In the field of biosensing applications, a pioneer for CPE-based DNA detection was Leclerc and his team. In 2002, they first reported the synthesis of a cationic imidazolium-substituted poly(thiophene) (PImiT), which was made by oxidative coupling of the corresponding thiophene monomers by $FeCl_3$ (Scheme 1.2).

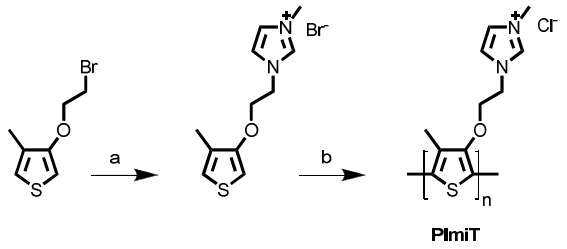

Scheme 1.2. Synthesis of PImiT, a) CH_3CN, 1,2-dimethylimidazole, b) $FeCl_3$, Bu_4NCl, ion exchange.

PImiT as water-soluble CPE is highly sensitive to the presence of oligonucleotides as depicted in Figure 1.2.[29] Upon addition of single-stranded DNA (ssDNA) to a solution of

PImiT in water the color changes from yellow (λ_{max} = 397 nm) to red (λ_{max} = 527 nm). This indicates complex ("duplex") formation between PImiT and ssDNA due to electrostatic interactions, as illustrated in Figure 1.3. Furthermore, the complementary ssDNA strand was added to the red mixture and the color of the solution turned again to yellow (λ_{max} = 421 nm). Leclerc *et al.* attributed this to a "triplex" formation, between PImiT and the hybridized double-stranded DNA (dsDNA). This color change from red to yellow is based on a conformational transition of the polythiophene backbone. Here, a highly conjugated and planar conformation of the polymer is present for the red colored "duplex", the yellow color of the "triplex" reflects a less conjugated, less planar (probably helical) PImiT conformation, respectively.[11,16,29]

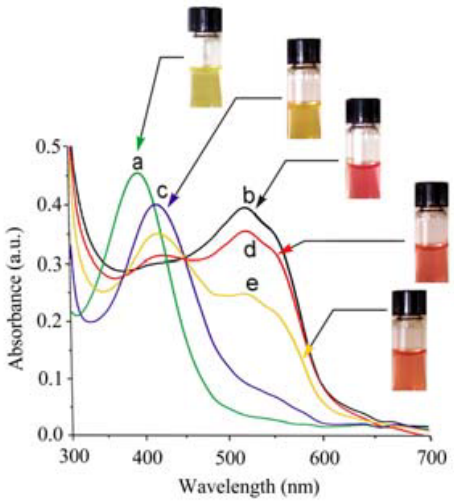

Figure 1.2. UV-Vis spectra of solutions of a) PImiT, b) PImiT/ssDNA complex ("duplex"), c) PImiT/dsDNA "triplex", d) PImiT/ssDNA "duplex" plus a complementary ssDNA strand with a two-base mismatch, and e) PImiT/ssDNA "duplex" plus a complementary ssDNA strand with a one-base mismatch after mixing the components, including images of the corresponding solutions.[29]

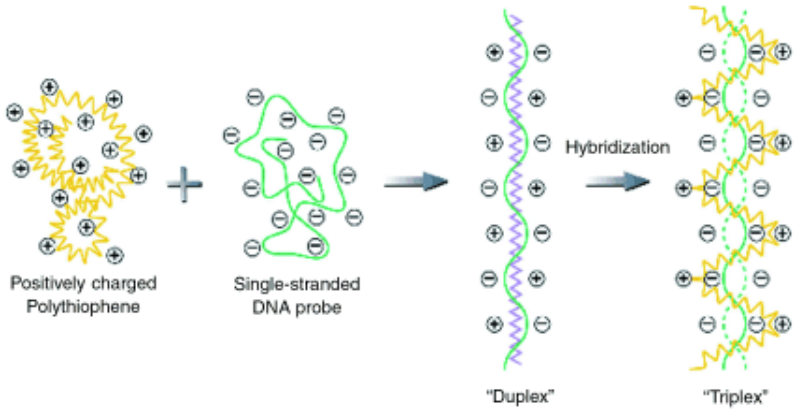

Figure 1.3. Schematic sketch of the formation of a planar PImiT/ssDNA "duplex"and a distorted, helical PImiT/dsDNA "triplex".[22,29]

One year later Nilsson *et al.* published a zwitterionic amino acid substituted poly(3-alkylthiophene) which confirmed the Leclerc observations for another system, that showed qualitatively similar changes of the optical spectra upon addition of oligonucleotides.[22,30]

Scheme 1.3 illustrates the straightforward synthesis of poly(3-[(*R*)-5-amino-5-carboxyl-3-oxapentyl]-2,5-thiophenylene hydrochloride) (POWT) after Nilsson *et al*., starting from N-*t*-BOC-L-serine (with BOC = *t*-butyloxycarbonyl) and thiophene-3-carboxylic acid. The amino acid-substituted monomer was polymerized as trifluoroacetate salt by chemical oxidation with $FeCl_3$ in toluene.[31]

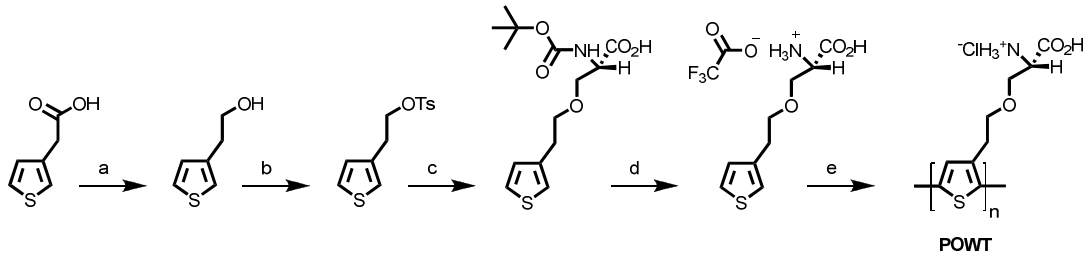

Scheme 1.3. Synthesis of POWT, a) $LiAlH_4$, ether, b) p-toluenesulfonyl chloride, pyridine, c) N-t-BOC-L-serine, K_2CO_3, DMF, d) trifluoroacetic acid, e) $FeCl_3$, tetrabutylammonium trifluoromethanesulfonate, $CHCl_3$.[31]

Further on, Nilsson *et al.* reported the interaction and the resulting conformational changes of this zwitterionic CPE in the presence of a synthetic oligopeptide. The negatively charged peptide (JR2E) was bounded to POWT via electrostatic attraction and hydrogen bonding. A red shift in the optical spectra indicates that the polymer backbone becomes more planar upon binding to the oligopeptide. Also, polymer aggregation was observed and attributed to interpeptide hydrogen bonding which brought several CPE and peptide chains into close neighborhood. By adding a positively charged peptide (JR2K), these polymer aggregates were broken as seen in a reverse blue shift of the emission maximum and an increased emission intensity. The authors attribute the deaggregation to interpeptide interactions thus leading to a disaggregation of the polyelectrolyte aggregates.[16,32]

In 2002, Gaylord, Bazan and Heeger reported an further example of CPE-based DNA detection based on a fluorescence resonance energy transfer (FRET) process[27c,33], also known as Förster energy transfer, including a cationic poly(fluorene-*co*-phenylene)s as CPE component.[34,35] The CPE was synthesized in two steps as shown in Scheme 1.4. First, 2,7-dibromo-9,9-*bis*(6-bromohexyl)fluorene and a 1,4-phenylenebisboronic ester were polymerized in a Suzuki coupling. The second step involved a polymer-analogous

quaternization reaction with trimethylamine thus generating poly[9,9-*bis*(6-(N,N,N-trimethylammonium)hexyl)-2,7-fluorene]-*co*-phenylene (PFP-Br). The sensing system consists of three parts: the quaternized CPE (PFP-Br), DNA of a specific sequence and a dye-labeled peptide nucleic acid (PNA).[36] Figure 1.4 depicts a schematic illustration of this sensing scheme using CPEs for direct visual DNA sensing based on FRET. The electrostatic attraction between the complementary ssDNA/PNA complex and the CPE chain brings energy donor (CPE) and acceptor (dye-labeled PNA) into close proximity thus enabling efficient FRET (A). The use of non-complementary ssDNA does not allow complex formation between donor (CPE) and acceptor (PNA) resulting in the absence of fluorescence energy transfer (B). They found that for this case that the electrostatic complexation only occurs between CPE and ssDNA while the CPE--- PNA distance remains too large for FRET. Therefore, the extent of hybridization between PNA and ssDNA can be directly estimated by the FRET efficiency or the intensity of dye emission.[34,37]

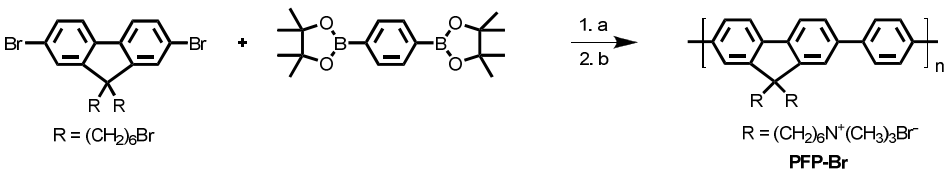

Scheme 1.4. Synthesis of PFP-Br, a) $Pd(PPh_3)_4$, 2 M Na_2CO_3, toluene, b) trimethylamine, THF/methanol.[34]

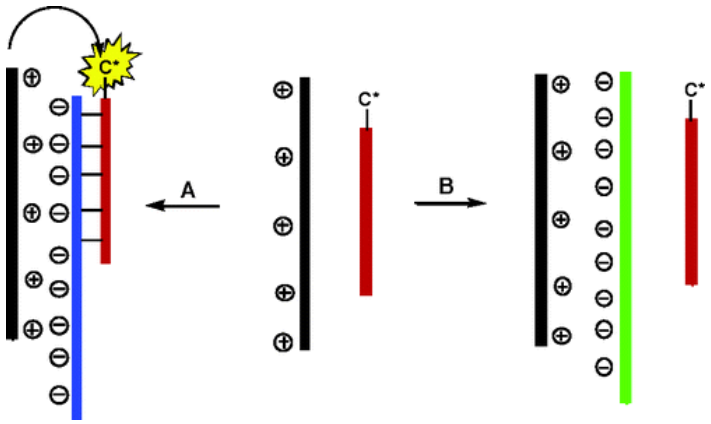

Figure 1.4. Schematic illustration of the dye-labeled PNA (red) / ssDNA-based sensing assay using a cationic CPE (black) and a specifically labeled PNA (red with C for fluorescein) as probe strand; the complementary ssDNA (blue) is shown in blue (A), the non-complementary ssDNA in green (B).[37]

Another class of CPE materials was introduced by Bazan *et al.* a few years later based on CPE backbones composed of donor-acceptor-type moieties. They represent a further advantage towards direct visual DNA detection. A cationic PFP derivative containing 5 mol%

2,1,3-benzothiadiazole (BT) on-chain units was generated by a Suzuki copolymerization of 1,4-phenylene bisboronic acid and a 95:5 mixture of 2,7-dibromo-9,9-*bis*(6-bromohexyl)fluorene and 4,7-dibromo-2,1,3-benzothiadiazole. The intermediate was quaternized with trimethylamine in THF/water (Scheme 1.5).[38] The resulting PFP-BT is soluble in polar and protic solvents as methanol or water and emits blue in solution. Complexation between the CPE and oppositely charged DNA molecules induces polymer aggregation, leading to enhanced interchain contacts and improved electronic coupling between the components. Under these condensed-state conditions, the energy transfer from the fluorene segments (donor) to the lower emission energy BT units (acceptor) is more efficient than in isolated chains. Thus, green emission from BT units dominates in the aggregated state. Such an aggregation-enhanced FRET allows for an efficient dsDNA detection in the concentration range from 0.6 nM to 0.15 μM.[11,39]

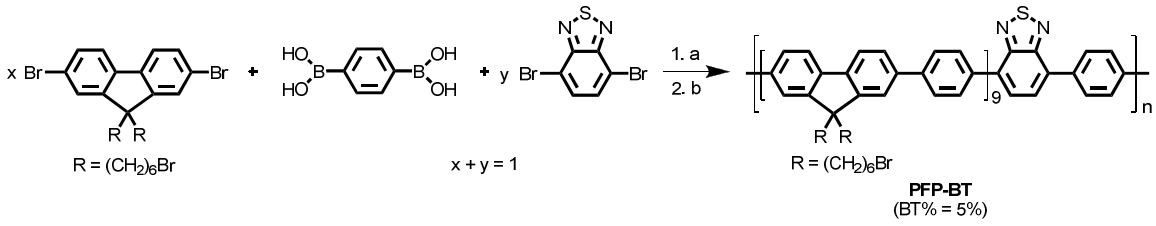

Scheme 1.5. Synthesis of PFP-BT, a) 2 M K_2CO_3, THF, $Pd(PPh_3)_4$, b) $N(CH_3)_3$, THF/H_2O.[38]

Variations of the chemical structure lead to an further extension of the dsDNA detection range. For this purpose, BT-containing CPEs with oligo(ethylene oxide) pendant groups on the fluorene or phenylene units were generated.[11,40] As a matter of fact, CPEs are very promising for future applications in biomolecule sensing devices.

1.1.2. CPEs for Optoelectronic Devices

There is an increasing number of publications on the incorporation of CPE interlayers as components of optoelectronic devices especially for an optimization of charge carrier injection/extraction. The use of CPE layers also offers new fabrication opportunities for multilayer stacks in organic light emitting diodes (OLEDs)[41,42], thin film transistors (OFETs)[43] as well as in organic solar cells (OSCs)[19,44,45]. The solubility of the CPEs in polar solvents allows, from a practical point of view, for the integration of CPE layers in multilayer devices using solution-casting methods (principle of orthogonal solubility).[41,46] Thin CPE

films with an optimized surface morphology and thickness can be precisely made using such solution processing techniques.[21c]

Exemplarily, two optoelectronic device applications (multilayer OLEDs and OSCs) including CPE layers are discussed in the following paragraph. Multilayer OLEDs including CPE-based electron injection/transport layers (EIL) for improving the device efficiency have been described by several groups. The improvements rely on a variety of mechanisms.[47] A study published by Hoven *et al.* revealed considerable details on how ion motion and energy level alignment of the OLED layers involved improve device performance. Their research work is based on poly[2-methoxy-5-(2-ethylhexyloxy)-1,4-phenylenevinylene] (MEH-PPV) as emissive layer and CPE layers of varying thickness as electron injection layers (EIL) of ITO/PEDOT:PSS/MEH-PPV/CPE/Au or Al devices [in which ITO stands for indium tin oxide and PEDOT:PSS for poly(3,4-ethylenedioxythiophene):poly(styrene-sulfonate)].[10,48] PFP-Br[34] with tetrakis(imidazolyl) borate as counter ion[41a] (PFP-BIm_4) was, hereby, used as the EIL (electron injection/hole blocking) layer (Figure 1.5). Because of the orthogonal solubility of MEH-PPV (soluble in non-polar solvents) and PFP-BIm_4 (soluble in polar solvents) multilayer fabrication can be easily realized. Gold or aluminum was used as cathode. The improved electron injection results from the combination of hole accumulation at the emissive layer/EIL interface and electric field screening within the EIL layers caused by the mobile counter ions. The device response time could be improved by reducing the thickness of the EIL layer and by using smaller, mobile counter ions, an important improvement when OLEDs are targeted for fast video applications.[48]

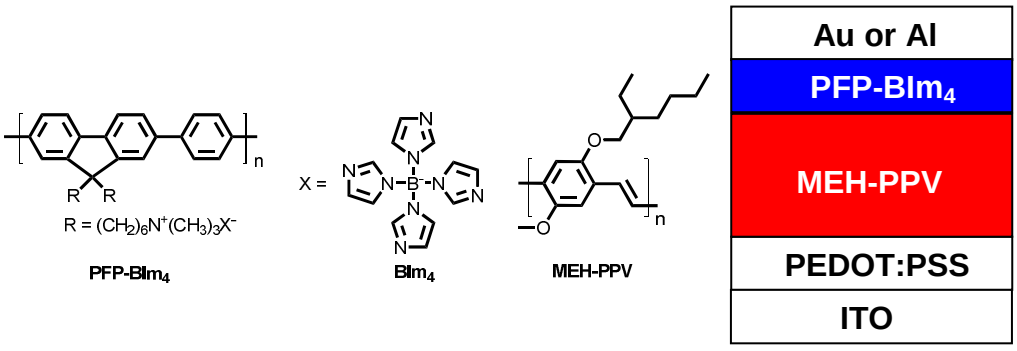

Figure 1.5. Schematic structures. of MEH-PPV and PFP-BIm_4. (left). OLED device structure (right).[48]

Bulk heterojunction (BHJ)-type organic solar cells are based on blends of electron-donating and electron-accepting materials as active layer. There are promising photovoltaic devices as they offer lightweight, shape-variable and low-cost solutions.[49,50] Main targets of this

technology are currently the optimization of the short circuit current density (J_{SC}), open circuit voltage (V_{OC}), and fill factor (FF), all influencing the resulting power conversion efficiency (PCE). These characteristic indicators are connected within the equilibration $PCE = \frac{V_{OC}J_{SC}FF}{P_{in}}$, where P_{in} is the incident light power.[51]

In 2009 Cao *et al.* showed that the V_{OC} can be increased by up to 0.3 V in BHJ-type organic solar cells by integrating a thin 5 nm CPE interlayer of a quaternized PFP derivate, relative to the situation in control devices.[52] FF and J_{SC} were also shown to increase slightly in comparison to the control device. The increased built-in potential across the device based on the interfacial dipole from the CPE interlayer is, herby, responsible for the enhanced device performance.[11,52]

One year later He *et al.* analyzed the dark currents of BHJ cells with different donor materials for a better understanding of the increase in V_{OC}.[53] The general assembly of their devices was ITO/PEDOT:PSS/active layer/CPE/Al, as illustrated in Figure 1.6. Quaternized poly(alkylfluorene) PF-Br with several counter ions (e.g. PF-BIm_4) was used as CPE, different conjugated polymers as poly(3-hexylthiophene) (P3HT), MEH-PPV, and poly[2,7-(9,9-dioctylfluorene)-*co*-(4,7-dithien-2-yl)-2,1,3-benzothiadiazole] (PFO-DBT35)[52] as donor and phenyl C_{61}-butyric acid methyl ester (PCBM) as acceptor materials. Regarding V_{OC}, the best results were achieved with PFO-DBT35 and PF-Br (V_{OC} = 1.07 V) or PF-BIm_4 (1.06 V). Relatively to the control device a V_{OC} rise of 140 to 150 mV occurred. These observations support the application potential of thin CPE interlayers. Similar results were obtained for P3HT and MEH-PPV as donor materials.

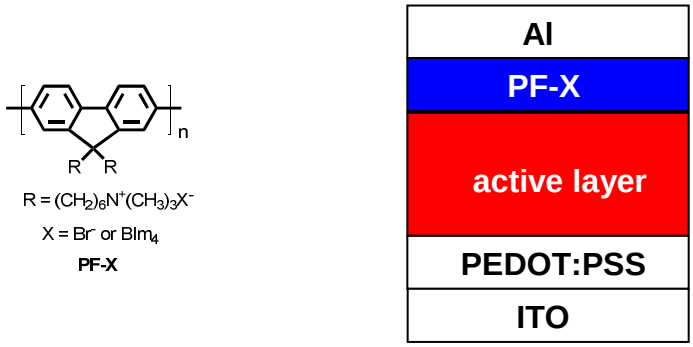

Figure 1.6. Molecular structures of PF-Br and PF-BIm_4. (left). OSC device structure (right).

Focussing on the dark current density-voltage (J-V) characteristics OSC devices with PFO-DBT35 as donor polymer display significantly suppressed dark current densities when applying thin CPE interlayers. Dark currents reduced by 1-2 orders of magnitude were observed for the OSC devices containing CPE interlayers, a reduction by ca. 1 order of

magnitude was observed for P3HT:PCBM- or MEH-PPV:PCBM-based devices. The authors propose that the decrease of dark currents is also responsible for the V_{OC} enhancement. Furthermore, Kim *et al.* published results on other polyfluorene-based polyelectrolyte derivatives used as interlayers of OSC devices showing a similar behavior.[11,54,55]

In summary, thin CPE interlayers can significantly improve the performance of optoelectronic devices. Multilayer devices can be easily obtained by orthogonal processing techniques.

1.2. All-Conjugated Block Copolyelectrolytes

All-conjugated block copolymers, comprising of two different blocks, are well known because of their spontaneous self organization in solution as well as in the solid state.[56,57] Emerging applications for conjugated (co)polymers in organic photovoltaics[58,59] and biotechnology often require the patterning of materials on the 10-100 nm length scale, and block copolymers may provide an elegant route to control the self-assembly into such nanostructured morphologies. However, the rod-like nature of most conjugated polymers complicates the self-assembly of corresponding block copolymers through a competition between crystalline and liquid crystalline interactions and the nanophase separation.[60,61] In comparison to coil-coil and rod-coil diblock copolymers, for all-conjugated rod-rod block copolymers a preferred assembly into low curvature vesicular and lamellar structures has been observed.[62] This tendency should be mainly independent of the chemical structure, size and composition of the block copolymer.

One nice example describing self-assembling in non-conjugated, rod-rod diblock copolymers was announced by Hayakawa and coworker in 2006, discussing the formation of a lamellar solid state morphology in oligo(ether sulphone)-*b*-oligo(ether ketone) diblock and triblock molecules.[63] Energy-filtering transmission electron microscopic (EFTEM) images of these diblock oligomers especially showed the formation of lamellar structures with a inter-lamellar spacing of 9.1 nm in full agreement with a molecular length of 9.2 nm for the fully elongated ("rigid rod") conformation of the aromatic oligomers.[64]

A second example was reported in 2011 by Wu *et al.*[65] They investigated synthesis and nanostructure formation of a polythiophene-*b*-poly(*γ*-benzyl L-glutamate) (P3HT-*b*-PBLG) diblock copolymer. The authors observed the formation of spherical particles with a diameter

of 200-300 nm as illustrated in transmission electron microscopy (TEM) images of Figure 1.7. Combined with the UV-Vis data, the researchers proposed that aggregates containing a P3HT core and a PBLG shell were formed.

Nowadays, conjugated polymers can be synthesized in high purity, with low amounts of structural defects, and high regioregularity by applying powerful transition metal-catalyzed or -mediated aryl-aryl coupling methods, e.g. after Suzuki, Stille or Yamamoto.[66]

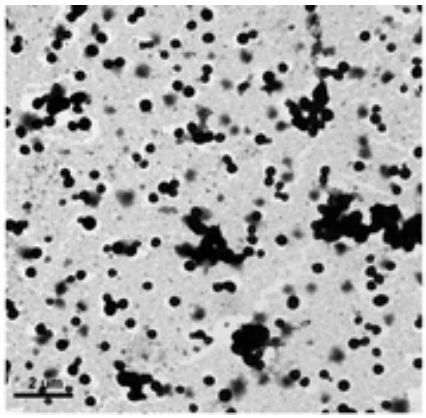

Figure 1.7. TEM image of nanoparticles formed from P3HT-b-PBLG (stained with 1 wt% aqueous solution of phosphotungstic acid).[65]

Novel protocols for an *in situ* generation of such conjugated polymers with defined, reactive end groups and a rather low polydispersity have also been developed. This kind of protocols is connected to the invention of chain-growth polycondensations.[67] Yokozawa *et al.* reported that the drastically reduced amount of chain termination events in such chain-growth polycondensations allows for a simple, step-by-step polycondensation of two (or more) different AB-type monomers in the aryl-aryl cross-coupling sequence thus leading to the formation of block copolymers. Since the chain-growth (or catalyst-transfer) polycondensation process allows for the generation of polyphenylenes, polyfluorenes, or N-substituted polypyrroles, Yokozawa *et al.* e.g. succeeded in the synthesis of a poly(2,5-dialkoxy-1,4-phenylene)-*b*-poly(N-hexyl-2,5-pyrrole) (PPy-*b*-PPP) diblock copolymer with a very narrow polydispersity of 1.16.[68] Based on the Yokozawa results also other research groups generated polythiophene-based diblock copolymers, for instance the rod-rod diblock copolymer poly(3-hexylthiophene)-*b*-poly[3-(2-ethylhexyl)thiophene] (P3HT-*b*-P3EHT) as shown in Scheme 1.6.[57,69]

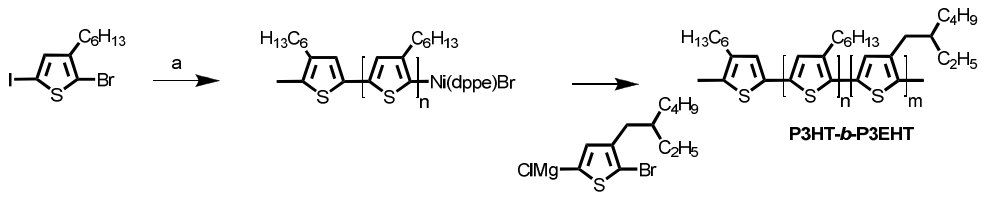

Scheme 1.6. Synthesis of a P3HT-b-P3EHT, a) i-C_3H_3MgCl, THF, Ni(dppe)Cl_2 with dppe = 1,2-bis(diphenylphosphino)ethane.[57]

Regarding to the self-assembly properties described above, P3HT-*b*-P3EHT shows the expected formation of a lamellar solid state morphology driven by the immiscibility of the two different poly(3-alkylthiophene) (P3AT) blocks mainly as a result of the different crystallization behavior of linear and branched octyl substituted P3ATs (Figure 1.8).[64,69]

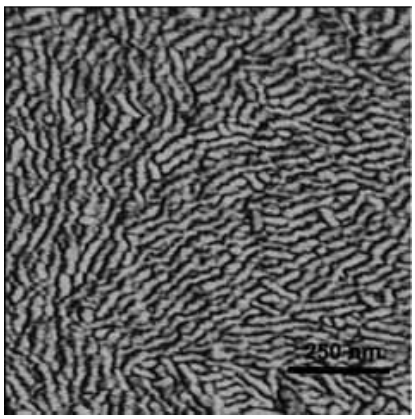

Figure 1.8. AFM images of lamellar nanostructure formed by P3HT-b-P3EHT; P3HT/P3EHT ratio: 83:17 (w/w, phase mode, image size: 1 × 1 µm², interlamellar distance: ca. 15 nm).[57]

In conclusion, conjugated rod-rod block copolymers are very promising candidates for future applications, especially based on their unique and tunable self-assembly behavior.

1.3. Aim and Scope

Inspired by the unique properties of CPEs and rod-rod block copolymers, a combination of both classes of materials seems very promising thus leading to all-conjugated block copolyelectrolytes composed of one ionic polyelectrolyte (CPE) block and one non-polar (CP) block. Such advanced materials based on electronically different conjugated polymer backbones and different pendant groups (including ionic side groups) have been synthesized within this project followed by studying their optical and self-assembly properties as well as

their complexation behavior with biomolecules and their incorporation into optoelectronic devices.

In the second chapter the synthesis of cationic polyfluorene-*b*-polythiophene diblock copolymers with varying ionic groups is described. The optical properties have been investigated dependent on the aggregation state and their application as electron extraction layer of organic solar cells. In chapter 3, the interaction of these all-conjugated block copolyelectrolytes with oppositely charged molecules (e.g. biomolecules, anionic surfactants, organic acids) is reported. Chapter 4 introduces novel diblock copolymers containing both a neutral and a charged (ionic) poly(alkylfluorene) block. UV-Vis absorption and photoluminescence (PL) of the diblock copolymer have been analyzed as well as their self-assembling behavior and an incorporation as thin EIL layer of OLEDs.

All three chapters are presented as independent chapters with separate experimental and references sections.

1.4. References

[1] M. Hess, R. G. Jones, J. Kahovec, T. Kitayama, P. Kratochvíl, P. Kubisa, W. Mormann, R. F. T. Stepto, D. Tabak, J. Vohlídal, E. S. Wilks, *Pure Appl. Chem.* **2006**, *78*, 2067.

[2] S. Traser: Gegenionenaktivität in neuartigen stäbchenförmigen und flexiblen, verzweigten Polyelektrolyten variabler Ladungsdichte, *Ph.D. Thesis*, Universität Potsdam, Germany **2005**.

[3] a) H. Dautzenberg, W. Jaeger, J. Kötz, B. Philipp, Ch. Seidel, D. Stscherbina, Polyelectrolytes: Formation, Characterization and Application **1994**, Carl Hanser Verlag, München. b) K. S. Schmitz: Macroions in solution and colloid suspension“ **1993**, VCH Publishers, New York. c) D.W. Heermann, Computer Simulation Methods of Theoretical Physics, Springer Verlag, Heidelberg, **1986**, 2te Auflage, Springer Verlag, Heidelberg, **1990**. d) F. Oosawa, „Polyelectrolytes“ **1971**, Marcel Dekker Verlag, New York.

[4] M. Mandel, *Encycl. Polym. Sci. Eng*. **1988**, *11*, 739.

[5] Y. Yamanaha, H. Matsuoka, M. Hasegawa, N. Ise, *J. Am. Chem. Soc*. **1990**, *112*, 587.

[6] a) S. Förster, M. Schmidt, *Adv. Polym. Sci*. **1995**, *120*, 51. b) G. Weill, *J. Phys. (France)* **1989**, *49*, 1049.

[7] a) L. Ghimici, S. Dragan, *Colloid Polym. Sci.* **2002**, *280*, 130. b) F. Bordi, R. H. Colby, C. Cametti, L. De Lorenzo, T. Gili, *J. Phys. Chem. B* **2002**, *106*, 6887.

[8] a) A. V. Dobrynin, M. Rubinstein, *Macromolecules* **1996**, *29*, 2974. b) J. Cohen, Z. Priel, Y. Rabin, *J. Chem. Phys.* **1988**, *88*, 7111. c) H. J. Limbach, C. Holm, *J. Phys. Chem. B* **2003**, *107*, 8041. d) U. Micka, C. Holm, K. Kremer, *Langmuir* **1999**, *15*, 4033. e) V. Lyulin, B. Dünweg, O. V. Borisov, A. A. Darinskii, *Macromolecules* **1999**, *32*, 3264. f) P. Chodanowski, S. Stoll, *J. Chem. Phys.* **1999**, *111*, 6069. g) F. J. Solis, M. O. de la Cruz, *Macromolecules* **1998**, *31*, 5502.

[9] a) D. A. Mortimer, *Polym. Int.* **1991**, *25*, 29. b) H. Spoor, *Angew. Makromol. Chem*. **1984**, *123*, 1.

[10] C. V. Hoven, A. Garcia, G. C. Bazan, T. Q. Nguyen, *Adv. Mater*. **2008**, *20*, 3793.

[11] A. Duarte, K.-Y. Pu, B. Liu, G. C. Bazan, *Chem. Mater*. **2011**, *23*, 501.

[12] M. R. Pinto, K. S. Schanze, *Synthesis* **2002**, *9*, 1293.

[13] a) A. O. Patil, Y. Ikenoue, F. Wudl, A. J. Heeger, *J. Am. Chem. Soc.* **1987**, *109*, 1858. b) S. Q. Shi, F. Wudl, *Macromolecules* **1990**, *23*, 2119.

[14] T. I. Wallow, B. M. Novak, *J. Am. Chem. Soc*. **1991**, *113*, 7411.

[15] a) U. Scherf, E. J. W. List, *Adv. Mater.* **2002**, *14*, 477. b) H. Shirakawa, E. J. Louis, A. G. MacDiarmid, C. K. Chiang, A. J. Heeger, *J. Chem. Soc., Chem. Commun.* **1977**, 578. c) C. K. Chiang, C. R. Fincher, Y. W. Park, A. J. Heeger, H. Shirakawa, E. J. Louis, S. C. Gau, A. G. MacDiarmid, *Phys. Rev. Lett.* **1977**, *39*, 1098. d) A. Heeger, *Rev. Mod. Phys.* **2001**, *73*, 681.

[16] W. Thomas III, G. D. Joly, T. M. Swager, *Chem. Rev*. **2007**, *107*, 1339.

[17] S. R. Forrest, *Nature* **2004**, *428*, 911.

[18] a) C. J. Brabec, N. S. Sariciftci, J. C. Hummelen, *Adv. Funct. Mater*. **2001**, *11*, 15. b) K. M. Coakley, M. D. McGehee, *Chem. Mater*. **2004**, *16*, 4533.

[19] R. H. Friend, R. W. Gymer, A. B. Holmes, J. H. Burroughes, R. N. Marks, C. Taliani, D. D. C. Bradley, D. A. Dos Santos, J. L. Bredas, M. Logdlund, W. R. Salaneck, *Nature* **1999**, *397*, 121.

[20] J. H. Burroughes, D. D. C. Bradley, A. R. Brown, R. N. Marks, K. Mackay, R. H. Friend, P. L. Burns, A. B. Holmes, *Nature* **1990**, *347*, 539.

[21] a) M. L. Davies, H. D. Burrows, S. Cheng, M. C. Morán, M. d. G. Miguel, P. Douglas, *Biomacromolecules* **2009**, *10*, 2987. b) F. Feng, F. He, L. An, S. Wang, Y. Li, D. Zhu, *Adv. Mater.* **2008**, *20*, 2959. c) H. Jiang, P. Taranekar, J. Reynolds, K. Schanze, *Angew. Chem. Int. Ed.* **2009**, *48*, 4300.

[22] M. Leclerc, A. Najari, S. Beaupré, *Can. J. Chem.* **2009**, *87*, 1201.

[23] T. Kawai, T. Yamaue, K. Tada, M. Onoda, S. H. Jin, S. K. Choi, K. Yoshino, *Jpn. J. Appl. Phys. Part* 2 **1996**, *35*, L741.

[24] a) J. Tian, C. C. Wu, M. E. Thompson, J. C. Sturm, R. A. Register, *Chem. Mater*. **1995**, *7*, 2190. b) A. F. Thunemann, *Adv. Mater*. **1999**, *11*, 127.

[25] V. Cimrova, W. Schmidt, R. Rulkens, M. Schulze, W. Meyer, D. Neher, *Adv. Mater*. **1996**, *8*, 585.

[26] W. L. Ma, P. K. Iyer, X. Gong, B. Liu, D. Moses, G. C. Bazan, A. J. Heeger, *Adv. Mater*. **2005**, *17*, 274.

[27] a) B. Liu, G. C. Bazan, *J. Am. Chem. Soc*. **2006**, *128*, 1188. b) Y. S. Wang, B. Liu, *Anal. Chem.* **2007**, *79*, 7214. c) B. Liu, S. Baudrey, L. Jaeger, G. C. Bazan, *J. Am. Chem. Soc.* **2004**, *126*, 4076.

[28] a) Q. Chen, Y. Cui, T. L. Zhang, L. Cao, B. H. Han, *Biomacromolecules* **2010**, *11*, 13. b) Y. Y. Wang, B. Liu, *Langmuir* **2009**, *25*, 12787. c) J. H. Liao, T. M. Swager, *Langmuir* **2007**, *23*, 112.

[29] H.-A. Ho, M. Boissinot, M. G. Bergeron, G. Corbeil, K. Doré, D. Boudreau, M. Leclerc, *Angew. Chem. Int. Ed.* **2002**, *41*, 1548.

[30] K. P. R. Nilsson, O. Inganäs, *Nat. Mater.* **2003**, *2*, 419.

[31] M. Andersson, P. O. Ekeblad, T. Hjertberg, O. Wennerström, O. Inganäs, *Polym. Commun*. **1991**, *32*, 546.

[32] K. P. R. Nilsson, J. Rydberg, L. Baltzer, O. Inganäs, *Proc. Natl. Acad. Sci. U.S.A.* **2003**, *100*, 10170.

[33] S. Wang, G. C. Bazan, *Adv. Mater.* **2003**, *15*, 1425.

[34] M. Kang, O. Kumar Nag, R. R. Nayak, S. Hwang, H. Suh H. Y. Woo, *Macromolecules* **2009**, *42*, 2708.

[35] B. S. Gaylord, A. J. Heeger, G. C. Bazan, *Proc. Natl. Acad. Sci. U.S.A.* **2002**, *99*, 10954.

[36] a) J. A. Wigenius, K. Magnusson, P. Björk, O. Andersson, O. Inganäs, *Langmuir* **2010**, *26*, 3753. b) F. Xia, X. Zuo, R. Yang, Y. Xiao, D. Kang, A. Valle-Blisle, X. Gong, A. J. Heeger, K. W. Plaxco, *J. Am. Chem. Soc*. **2010**, *132*, 1252.

[37] B. Liu, G. C. Bazan, *Chem. Mater*. **2004**, *16*, 4467.

[38] B. Liu, G. C. Bazan, *J. Am. Chem. Soc*. **2004**, *126*, 1942.

[39] J. W. Hong, W. L. Hemme, G. E. Keller, M. T. Rinke, G. C. Bazan, *Adv. Mater*. **2006**, *18*, 878.

[40] C. Y. Chi, A. Mikhailovsky, G. C. Bazan, *J. Am. Chem. Soc*. **2007**, *129*, 11134.

[41] a) R. Yang, H. Wu, Y. Cao, G. C. Bazan, *J. Am. Chem. Soc.* **2006**, *128*, 14422. b) A. Garcia, R. Yang, Y. Jin, B. Walker, T.-Q. Nguyen, *Appl. Phys. Lett*. **2007**, *91*, 153502.

[42] M. B. Ramey, J. Hiller, M. F. Rubner, C. Tan, K. S. Schanze, J. R. Reynolds, *Macromolecules* **2005**, *38*, 234.

[43] J. H. Seo, A. Gutacker, B. Walker, S. Cho, R. Yang, T.-Q. Nguyen, A. J. Heeger, and G. C. Bazan, *J. Am. Chem. Soc.* **2009**, *131*, 18220.

[44] a) J. Yang, A. Garcia, T.-Q. Nguyen, *Appl. Phys. Lett*. **2007**, *90*, 103514. b) L. Ding,M. Jonforsen, L. S. Roman, M. R. Andersson, O. Inganäs, *Synth. Met*. **2000**, *110*, 133. c) P. Taranekar, Q. Qiao, H. Jiang, I. Ghiviriga, K. S. Schanze, J. R. Reynolds, *J. Am. Chem. Soc*. **2007**, *129*, 8958.

[45] A. W. Grice, D. D. C. Bradley, M. T. Bernius, M. Inbasekaran, W. W. Wu, E. P. Woo, *Appl. Phys. Lett*. **1998**, *73*, 629.

[46] J. H. Seo, R. Yang, J. Z. Brzezinski, B. Walker, G. C. Bazan, T.-Q. Nguyen, *Adv. Mater*. **2009**, *21*, 1006.

[47] C. W. Tang, S. A. Vanslyke, *Appl. Phys. Lett.* **1987**, *51*, 913.

[48] C. V. Hoven, R. Q. Yang, A. Garcia, V. Crockett, A. J. Heeger, G. C. Bazan, T. Q. Nguyen, *Proc. Natl. Acad. Sci. U.S.A.* **2008**, *105*, 12730.

[49] J. C. Bravec, *Sol. Energy Mater. Sol. Cells* **2004**, *83*, 273.

[50] J. Peet, J. Y. Kim, N. E. Coates, W. L. Ma, D. Moses, A. J. Heeger, G. C. Bazan, *Nat. Mater*. **2007**, *6*, 497.

[51] B. Kippelen, J.-L. Brédas, *Energy Inviron. Sci*. **2009**, *2*, 251.

[52] J. Luo, H. B. Wu, C. He, A. Y. Li, W. Yang, Y. Cao, *Appl. Phys. Lett*. **2009**, *95*, 043301.

[53] C. He, C. Zhong, H. Wu, R. Yang, W. Yang, F. Huang, G. C. Bazan, Y. Cao, *J. Mater. Chem.* **2010**, *20*, 2617.

[54] S. H. Oh, S. I Na, J. Jo, B. Lim, D. Vak, D. Y. Kim, *Adv. Funct. Mater*. **2010**, *20*, 1977.

[55] S. I. Na, S. H. Oh, S. S. Kim, D. Y. Kim, *Org. Electron*. **2009**, *10*, 496.

[56] U. Scherf, A. Gutacker and N. Koenen, *Acc. Chem. Res.*, 2008, **41**, 1086.

[57] Y. Zhang, K. Tajima, K. Hirota and K. Hashimoto, *J. Am. Chem. Soc*., 2008, **130**, 7812.

[58] R. A. Segalman, B. McCulloch, S. Kirmayer, J. J. Urban, *Macromolecules* **2009**, *42*, 9205.

[59] a) M. Sommer, S. Huettner, M. Thelakkat, *J. Mater. Chem.* **2010**, *20*, 10788. b) S. B. Darling, *Energy Environ. Sci.* **2009**, *2*, 1266.

[60] Y. Liang, H. Wang, S. Yuan, Y. Lee, L. Gan, L. Yu, *J. Mater. Chem.* **2007**, *17*, 2183.

[61] H.-C. Kim, S.-M. Park, W. D. Hinsberg, *Chem. Rev*. **2010**, *110*, 146.

[62] U. Scherf, S. Adamczyk, A. Gutacker and N. Koenen, *Macromol. Rapid Commun.* **2009**, *30*, 1059.

[63] T. Hayakawa, R. Goseki, M. Kakimoto, M. Tokita, J. Watanabe, Y. Liao, S. Horiuchi, *Org. Lett. 2006, 8*, 5453.

[64] U. Scherf, A. Gutacker, N. Koenen, *Acc. Chem. Res*. **2008**, *30*, 1059.

[65] Z.-Q. Wu, R. J. Ono, Z. Chen, Z. Li, C. W. Bielawski, *Polym. Chem.* **2011**, *2*, 300.

[66] a) A. D. Schlüter, *J. Polym. Sci., A* **2001**, *39*, 1533. b) U. Scherf, *Topics Curr. Chem*. **1999**, *201*, 163. c) T. Yamamoto, *Macromol. Rapid Commun*. **2002**, *23*, 583.

[67] a) A. Yokoyama, H. Suzuki, J. Kubota, K. Ohuchi, H. Higashimura, T. Yokozawa, *J. Am. Chem. Soc*. **2007**, *129*, 7236. b) R. Miyakoshi, K. Shimono, A. Yokoyama, T. Yokozawa, *J. Am. Chem. Soc.* **2006**, *128*, 16012. c) R. Miyakoshi, A. Yokoyama, T. Yokozawa, *J. Am. Chem. Soc*. **2005**, *127*, 17542. d) E. E. Sheina, J. Liu, M. C. Iovu, D. W. Laird, R. D. McCullough, *Macromolecules* **2004**, *37*, 3526.

[68] A. Yokoyama, A. Kato, R. Miyakoshi, T. Yokozawa, *Macromolecules* **2008**, *41*, 7271.

[69] a) P.-T. Wu, G. Ren, C. Li, R. Mezzenga, S. A. Jenekhe, *Macromolecules* **2009**, *42*, 2317. b) Y. Zhang, K. Tajima, K. Hashimoto, *Macromolecules* **2009**, *42*, 7008. c) K. Ohshimizu, M. Ueda, *Macromolecules* **2008**, *41*, 5289. d) J. Ge, M. He, F. Qiu, Y. Yang, *Macromolecules* **2010**, *43*, 6422.

Chapter 2

2. All-Conjugated, Cationic Polyfluorene-*b*-Polythiophene Polyelectrolyte Block Copolymers

All-conjugated polyelectrolyte (CPE) diblock copolymers containing two "rigid rod" blocks, a non-ionic poly(alkylfluorene) block and a cationic, quaternary poly(ammoniumhexylthiophene) block can be generated in a "grafting from" scheme. They show a preferred tendency to self-assemble into low curvature, nano-scaled architectures in solution and the solid state. Their optical properties have been investigated by means of UV-Vis and photoluminescence (PL) spectroscopy in different solvents and solvent mixtures. By addition of oppositely charged molecules, e.g. surfactants, the aggregation leads to the formation of ordered polyelectrolyte/surfactant complexes. CPEs, especially also block copolymer-based CPEs, are promising candidates for an application in electronic devices or in functional membranes (e.g. for bio-/sensor applications). For bulk heterojunction (BHJ)-type organic solar cells (OSC) the power conversion efficiency (PCE) could be increased from 5% to 6.5% by incorporating a thin CPE interlayer between the active layer and the metal cathode.

2.1. Introduction

Block copolymers, which contain two chemically different chains that are covalently bound to each other, represent a fascinating field of synthetic macromolecular science.[1] Hereby, all-conjugated, rod-rod block copolymers are a novel, very recent development within this field.[2,3] They offer the opportunity to accomplish a defined microphase separation of the different conjugated segments in order to realize, materials with unique properties and to access new applications.[4,5]

These unique properties of all-conjugated block copolymers combine the electronic properties of conjugated polymers with the individual characteristics of block copolymers like solvent-dependent aggregation behavior.[6] The fact that both blocks of all-conjugated, rod-rod block copolymers are "rigid rods" mainly dictates their assembling behavior.[4] The structure of the conjugated blocks can be modified with different functional groups for tuning their electrical, physical (e.g. crystallization) and chemical properties leading to a variety of different nanostructures.[7,8,9] Polymer blends of the two components (blocks) of a diblock copolymer tend to demix. However, the covalent linkage between the blocks only allows for a nanoscale phase separation; macroscopic demixing cannot occur.[1]

Key to accessing the desired diblock copolymer structures is the development of suited reaction schemes for generating them. In 2007 Tu *et al.*[2] described a first all-conjugated, rod-rod diblock copolymer which contains one non-polar, hydrophobic poly[9,9-*bis*(2-ethylhexyl)fluorene] (PF2/6) and one polar, hydrophilic poly[3-(6-diethylphosphonatohexyl)thiophene] (P3PHT) block with different electronic properties of both blocks. The synthesis relies on a Suzuki-type step-growth polycondensation (cross-coupling)[10] as key step to yield a poly[9,9-*bis*(2-ethylhexyl)fluorene]-*b*-poly[3-(6-bromohexyl)thiophene] (PF2/6-*b*-P3BrHT) diblock copolymer intermediate. Phosphorylation of the bromohexyl side groups in a subsequent polymer-analogue step provides the target diblock copolymer poly[9,9-*bis*(2-ethylhexyl)fluorene]-*b*-poly[3-(6-diethylphosphonato-hexyl)thiophene] (PF2/6-*b*-P3PHT). A very similar synthetic approach towards PF-*b*-PT diblock copolymers was later on described by Darling *et al.*[11] Aggregated species of our "rigid rod"-type, amphiphilic PF-*b*-PT block copolymers show that different arrangements of the hydrophilic and hydrophobic blocks can be obtained by changing polarity and composition of solvent mixtures. Vesicle formation is, hereby, accompanied by distinct changes of the absorption and photoluminescence behavior.

The next, logical extension of our approach was the generation and characterization of the corresponding ionic analogues: amphiphilic, all-conjugated diblock copolymers incorporating ionic (polyelectrolyte) and non-polar blocks. Such systems with a positive charge of the conjugated polyelectrolyte block, i.e. cationic poly[9,9-dialkylfluorene]-*b*-poly[3-(6-trimethylammoniumhexyl)thiophene] (PF2/6-*b*-P3TMAHT or PFO-*b*-P3TMAHT, where PF2/6 or PFO denote branched 2-(ethyl)hexyl and linear octyl alkyl pendant groups), respectively, and poly(9,9-dialkylfluorene)-*b*-poly[3-(6-pyridylhexyl)thiophene] (PF2/6-*b*-

P3PyHT and PFO-*b*-P3PyHT) polyelectrolytes, all containing nitrogen-based cationic side groups, have been the target of this study.[12]

The synthesis of the ionic diblock copolyelectrolytes starts from the diblock copolymer PF2/6-*b*-P3BrHT and PFO-*b*-P3BrHT which was already uses for the generation of PF2/6-*b*-P3PHT and PFO-*b*-P3PHT.[13] Our approach in the generation of amphiphilic PF-*b*-PT systems is generally connected to three main advantages: I) the generation of the polyelectrolyte block copolymers follows a well-established synthetic approach; II) the well distinguishable optical properties of both blocks (absorption, emission) allow for an independent spectroscopic investigation of the self assembly process for the two blocks, and III) the amphiphilic character, i.e. the combination of hydrophobic and hydrophilic blocks additionally drives phase separation and self assembly.

2.2. Results and Discussion

2.2.1. Synthesis

Our synthetic approach uses two different monomer components, a bifunctional AB-type fluorene monomer (Scheme 2.1) and a polythiophene-based macromonomer Br-P3BrHT, prepared in a synthetic protocol previously described by McCullough *et al.*[14] (shown in Scheme 2.1).

In order to synthesize the AB-type fluorene monomer, 2,7-dibromofluorene was prepared from fluorene[15] and afterwards 9-alkylated with 2-ethylhexylbromide or 1-octylbromide into 2,7-dibromo-9,9-*bis*(2-ethylhexyl) or 2,7-dibromo-9,9-dioctylfluorene. In a next step, 2,7-dialkylfluorene is converted to the bifunctional AB-type monomers 2-bromo-9,9-*bis*(2-ethylhexyl)fluorene-7-boronic ester (F2/6) or 2-bromo-9,9-dioctylfluorene-7-boronic ester (FO).[16]

In order to synthesize the polythiophene-based macromonomer Br-P3BrHT 3-bromo-thiophene and 1,6-dibromohexane are first reacted to 3-(6-bromohexyl)thiophene (T6Br)[17]. After bromination of T6Br with NBS into 2-bromo-3-(6-bromohexyl)thiophene (BrT6Br) BrT6Br was coupled to monobromo-endcapped HT-poly[3-(6-bromohexyl)thiophene] (Br-P3BrHT) in a procedure after McCullough *et al.*[18]

The next synthetic step involves a Suzuki-type cross-coupling[10] of 2-bromo-9,9-dialkylfluorene-7-boronic ester using $Pd(PPh_3)_4$ as a catalyst and Br-P3BrHT as a macromolecular end-capper to synthesize the non-polar diblock copolymers PF2/6-*b*-P3BrHT and PFO-*b*-P3BrHT. The final polymer-analogous conversion involves the quaternization of the bromohexyl side groups with trimethylamine or pyridine to obtain the target polyelectrolyte diblock copolymers PF2/6-*b*-P3TMAHT / PFO-*b*-P3TMAHT or PF2/6-*b*-P3PyHT / PFO-*b*-P3PyHT.

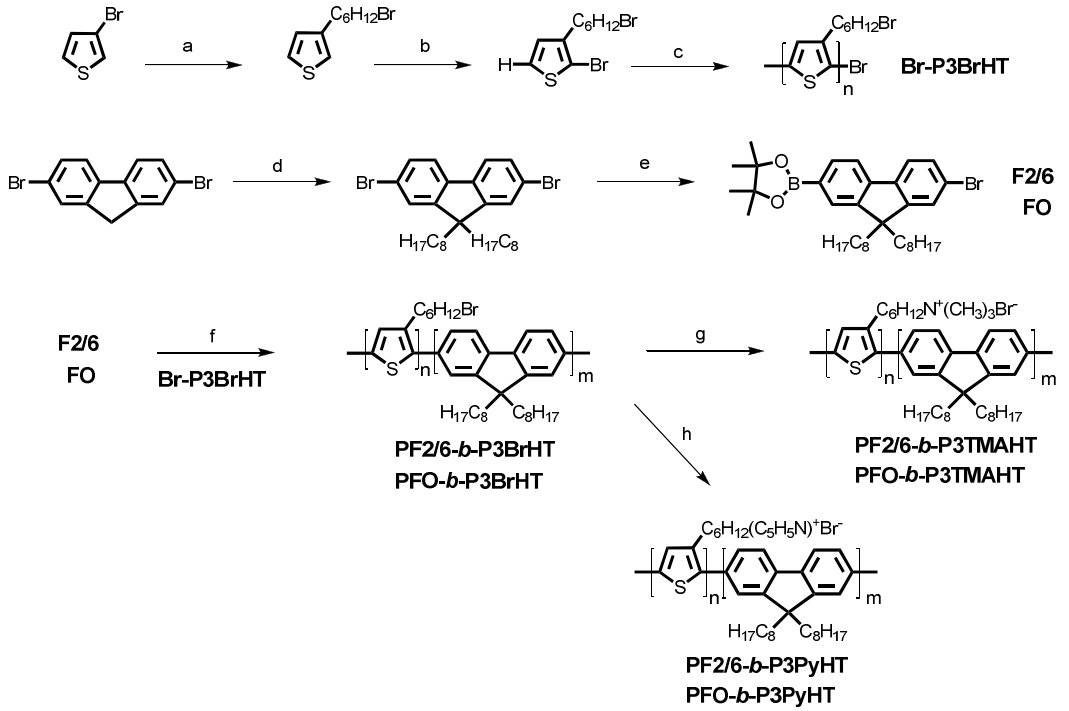

Scheme 2.1. Synthesis of the polyelectrolyte diblock copolymers PF2/6-b-P3TMAHT / PFO-b-P3TMAHT and PF2/6-b-P3PyHT / PFO-b-P3PyHT (C_8H_{17}: n-octyl for PFO, 2-ethylhexyl for PF2/6 series), a) n-BuLi, 1,6-dibromohexane, b) NBS, c) $ZnCl_2$, LDA, $Ni(dppp)Cl_2$, d) KOH, 2-ethylhexylbromide/1-octylbromide, e) n-BuLi, pinacolborane, f) $NaHCO_3$, $Pd(PPh_3)_4$, g) $N(CH_3)_3$, h) pyridine.

Standard characterization of the polymeric products was accomplished by gel permeation chromatography (GPC) analysis, nuclear magnetic resonance (NMR) spectroscopy and optical spectroscopy as well as atomic force microscopy (AFM) as imaging technique (see next chapter).

The results of the NMR analysis are in accordance with the proposed structure (see experimental section) and as confirmed by Darling *et al*. in 2011.[11]

The GPC analysis of the diblock copolymers uses multiple detection channels (RI, UV-Vis detection at the different absorption maxima of both blocks) to confirm the formation of block copolymers, preferably done at the stage of the non-polar diblock intermediates PF2/6-*b*-P3BrHT / PFO-*b*-P3BrHT.[2] The resulting average molecular weights M_n of the non-polar diblock copolymer precursors PF2/6-*b*-P3BrHT and PFO-*b*-P3BrHT were determined between 12,000 and 35,000 g/mol when starting from bromo-endcapped Br-P3BrHT macromonomers with a M_n between 6,000 and 17,500 g/mol (Table 2.1). We could not exactly measure the molecular weight of the cationic block copolymers by conventional GPC due to the strong interaction of the copolymer with the columns.

Table 2.1 lists the characterization data for four different batches. The polythiophene/polyfluorene mass ratio n of samples A-D remained relatively constant between 1.0 and 1.25 (as shown in Table 2.1). The polydispersity M_w/M_n of the diblock copolymers A-D varies between 1.38 and 2.0.

Table 2.1. Molecular weight data for four investigated diblock copolymers A-D.

sample	**structure**	**M_n**	**M_w**	**M_w/M_n**	**M_n (Br-P3BrHT)**	**M_w (Br-P3BrHT)**	**M_w/M_n (Br-P3BrHT)**	**M_n (PF) calc.**
A	PF2/6-*b*-P3BrHT	12,000	24,000	2.0	6,000	9,000	1.5	10,000
B	PF2/6-*b*-P3BrHT	13,000	18,000	1.38	6,500	9,100	1.4	6,500
C	PFO-*b*-P3BrHT	18,000	25,000	1.39	10,000	18,000	1.8	8,000
D	PF2/6-*b*-P3BrHT	35,000	65,000	1.86	17,500	24,500	1.41	17,500

The solubility of the diblock copolymers changes drastically after quaternization. PF2/6-*b*-P3BrHT and PFO-*b*-P3BrHT are soluble in typical organic solvents, such as chloroform, tetrachloroethane, or chlorobenzene. The cationic diblock copolymers are only soluble in polar solvents and solvent mixtures, including methanol, THF/water, or acetone/water. Dissolving PF2/6-*b*-P3TMAHT, PFO-*b*-P3TMAHT, PF2/6-*b*-P3PyHT or PFO-*b*-P3PyHT in pure water, turbid solutions are obtained that indicate formation of larger aggregates. The aggregation behavior is examined in the following paragraphs.

2.2.2. Optical Properties

Following, we studied the optical properties of the cationic, all-conjugated diblock copolymers PF2/6-*b*-P3TMAHT and PFO-*b*-P3TMAHT, as well as PF2/6-*b*-P3PyHT and PFO-*b*-P3PyHT in THF, methanol, water and THF/water 1:1 solution by UV-Vis absorption and photoluminescence (PL) spectroscopy. For simplicity, we will mainly concentrate on the trialkylammoniumhexyl-substituted derivative PF2/6-*b*-P3TMAHT. The resulting spectra are depicted in Figure 2.1 and summarized in Table 2.2.

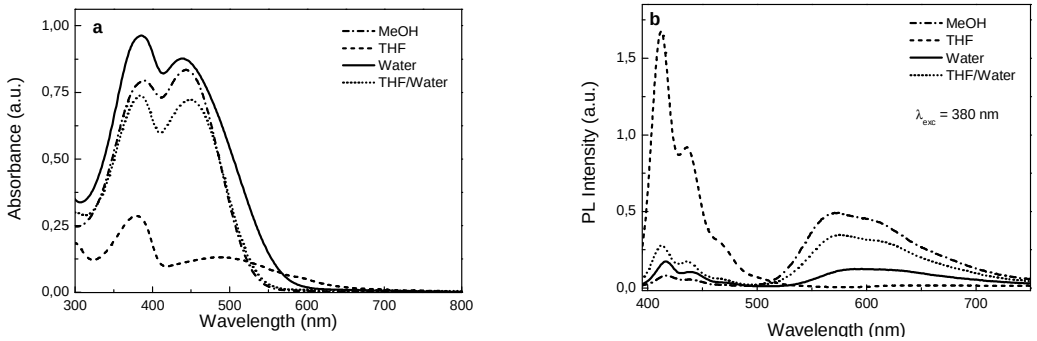

Figure 2.1. a) UV-Vis absorption and b) photoluminescence spectra of PF2/6-b-P3MAHT (made from precursor B) in methanol (dash-dotted line), THF (dashed line), water (solid line) and THF/water 1:1 (dotted line), at a polymer concentration of ~0.05 mg/mL (a) and ~0.002 mg/mL (b), λ_{exc} = 380 nm.

The absorption spectra show two characteristic bands peaking at 379-387 and 439-487 nm. Each of the two absorption bands is the spectral signature of one block. The higher energy maximum is attributed to the PF2/6 block.[19] The PF2/6 absorption band, is on contrast to the behavior of PFO, more or less insensitive to the aggregation state of the PF2/6 block.[19] The second band originates from the polar P3TMAHT blocks. The absorption band of the ionic P3TMAHT block in methanol, water and THF/water 1:1 appears at similar wavelengths as for the non-polar P3HT homopolymer.[20] Nevertheless, the absorption spectrum in water is slightly broadened with a red-shifted long-wavelength tail, most likely due to ongoing aggregation of the polar P3TMAHT blocks in pure water. Intensity changes in the ratio of the absorption maxima of the PF2/6 and P3TMAHT blocks between methanol (absorption PF2/6 < absorption P3TMAHT) and water (absorption PF2/6 > absorption P3TMAHT) are, at least in part, also a consequence of the band broadening in water. Contrary, the absorption spectrum in THF, as a less polar, non-protic solvent, shows a distinct red-shift of the P3TMAHT absorption feature to a λ_{max} at 487 nm, thus indicating aggregation of the ionic

P3TMAHT blocks in THF.[21] The solvatochromatic effect on the PT absorption band is visually detected as a color change from deep red in THF to pale orange in water.[22]

Figure 2.1 (and Table 2.2) also depicts the photoluminescence spectra (PL) of sample B obtained on selective excitation into the PF block at 380 nm. The occurrence of characteristic emissions of both blocks is observed, a blue PL feature at 400-500 nm for the PF2/6 block and a red PL feature at 500-700 nm for the P3TMAHT block. Here the P3TMAHT emission is (partially) sensitized by excitation energy transfer from the PF2/6 blocks. Further excitation experiments (not shown here) on detection at the P3TMAHT emission at 600 nm exhibit the characteristic PF absorption band thus further supporting the occurrence of PF→PT excitation energy transfer (FRET).[22] The emission features are again similar for methanol, water and THF/water 1:1. However, the PL of the P3TMAHT block shows an 18 nm red-shift when going from methanol to water while no corresponding shift in PL is observed for the PF2/6 block. The PL red-shift may indicate the formation of aggregates of the ionic P3TMAHT blocks in water. In THF we observed a dominant PF2/6 emission accompanied by a very weak and much red-shifted P3TMAHT PL component (λ_{max} = 630 nm). Higher intensity PL of the P3TMAHT blocks is observed with direct excitation into the P3TMAHT absorption band at 430 nm (not shown here), compare also to Figure 2.2). This finding indicates the formation of solid state-like P3TMAHT aggregates in THF with a distinct phase segregation thus strongly diminishing the excitation energy transfer. The overall photoluminescence quantum yields (PLQY) are 23% (THF), 16% (THF/water 1:1) and 3% (water).[21]

Table 2.2. Absorption and photoluminescence maxima of the PF2/6-b-P3TMAHT diblock copolymer (made from precursor B) in different solvents (PL: λ_{exc} = 380 nm).

solvent	**absorption $\lambda_{max\ abs}$ (nm)**	**photoluminescence $\lambda_{max\ PL}$ (nm)**
methanol	387 (PF2/6), 442 (P3TMAHT)	416/438 (PF2/6), 572 (P3TMAHT)
water	384, 439	416/438, 590
THF	379, 487	412/435, ca. 630 (very weak)
THF/water 1:1	383, 448	412/435, 576

Compared to the non-polar P3HT homopolymer the absorption and emission features of the P3TMAHT block display a somewhat larger Stokes loss, probably that resulting from a

distinctly more coiled, disordered confirmation of the individual, ionic P3TMAHT chains driven by electrostatic Coulombic repulsion between the charged, cationic side groups.

Very similar trends are seen for the pyridinium-derivative PF2/6-*b*-P3PyHT. In comparison with PF2/6-*b*-P3TMAHT, PF2/6-*b*-P3PyHT shows a slightly increased solubility of the polar P3PyHT block in non-polar and a decreased solubility in polar solvents thus indicating a somewhat reduced hydrophilic (or increased hydrophobic) character of the P3PyHT block, as expected. The analysis of the optical spectra of the corresponding diblock copolymers containing PFO blocks (with linear octyl side chains) instead of PF2/6 is complicated by β-phase formation leading to the occurrence of additional red-shifted absorption and emission features for the polyfluorene block. The details are not discussed here.[19,21,23]

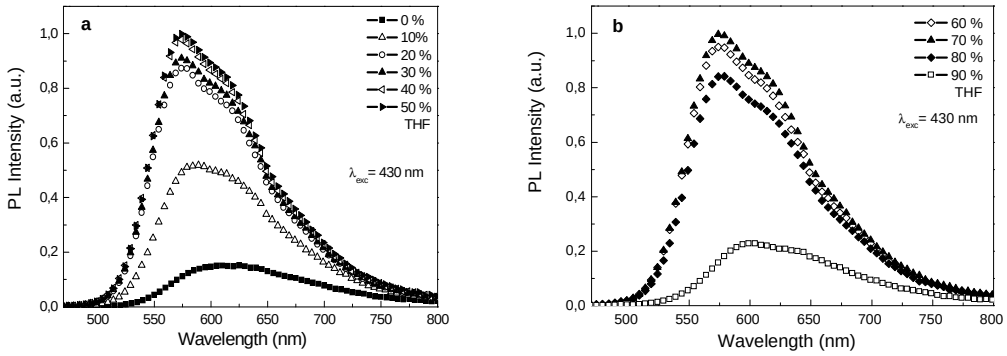

Figure 2.2 a/b). PL spectra of PF2/6-b-P3MAHT (made from precursor B; polymer concentration: 1.2×10^{-3} mg/mL) in THF/water mixtures (λ_{exc} = 430 nm).

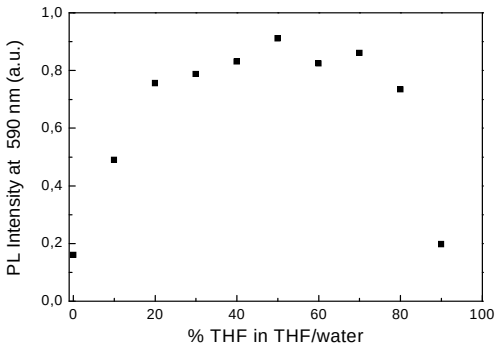

Figure 2.3. Photoluminescence intensity at 590 nm of PF2/6-b-P3TMAHT in THF/water mixtures (precursor B, polymer concentration: 1.2×10^{-3} mg/mL, λ_{exc} = 430 nm) as a function of composition (v/v).

PL spectra of PF2/6-*b*-P3TMAHT (excitation at 430 nm, thus leading to exclusive emission from the P3TMAHT block) in THF/water mixtures of varying composition are shown in

Figure 2.2. Starting from pure water to 10 and 20% THF, the PL band becomes more intense, and is accompanied by a blue shift of the emission maximum. This indicates an ongoing de-aggregation of the ionic polythiophene block. Further THF addition (to 30, 40, 50 and 60%) leads to a subsequent de-aggregation which is accompanied by a 50 nm blue shift of the P3TMAHT emission maximum. THF contents of 70, 80 and 90% again result in a decrease of the PL intensity and a red-shifted P3TMAHT PL band, thus reflecting the re-aggregation of the P3TMAHT blocks. For 50% THF the maximum PL intensity band is observed. The plot shown in Figure 2.3 visualizes this trend for the relative PL intensity at 590 nm of the P3TMAHT emission band after excitation of PF2/6-*b*-P3TMAHT at 430 nm as function of the composition indicating PL quenching by aggregation with increasing water contents. On excitation into the PF2/6 absorption band (at 380 nm) the intensity of the blue PF2/6 emission band is progressively reduced with decreasing THF content (not shown here).

A nearly identical trend in the PL spectra is observed for PF2/6-*b*-P3PyHT in THF/water mixtures, with the maximum PL intensity for the P3PyHT block observed for ca. 40% THF. The difference in the THF contents should reflect the slightly reduced hydrophilicity of the cationic P3PyHT block.

2.2.3. Aggregation Behavior in Methanol

Now we studied the aggregation of the diblock copolyelectrolytes PF2/6-*b*-P3TMAHT and PF2/6-*b*-P3PyHT by two different imaging techniques (AFM and confocal fluorescence microscopy). Here, we focus on the aggregation behavior in pure methanol.

2.2.3.1. Atomic Force Microscopy of Thin Films

AFM images of spin and drop cast layers of PF2/6-*b*-P3TMAHT or PF2/6-*b*-P3PyHT from dilute methanolic solution (0.03-0.08 mg/mL) onto mica substrates show the formation of spherical vesicles. The diameter of these vesicles (so-called polymersomes) ranges from several hundreds of nanometers up to several microns (ca. 0.2-4 μm). The results impressively demonstrate the tendency of rod-rod all-conjugated polyelectrolyte diblock copolymers towards formation of nanoaggregates with low curvature (vesicles or lamellae). This behavior

should be widely independent from the nature of the side chains at the polyfluorene block (PFO or PF2/6), the molecular weight of the diblock copolymer, the polydispersity, and the block length ratio.[12]

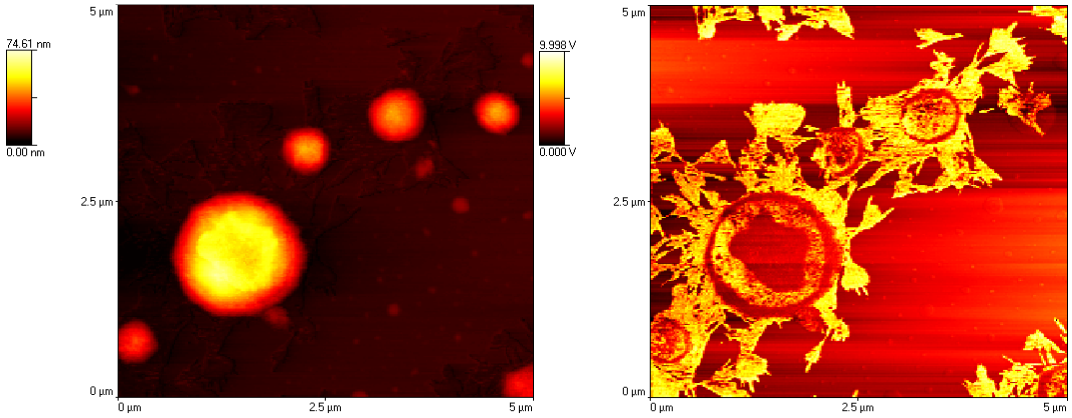

Figure 2.4. Tapping mode AFM images of PF2/6-b-P3PyHT (made from precursor B) deposited from methanolic solution onto a mica substrate (0.08 mg/mL, left: topography 5.0x5.0 µm², right: phase image 5.0x5.0 µm²).

Figure 2.4 illustrates the formation of vesicular PF2/6-*b*-P3PyHT (precursor B) aggregates from a methanolic solution of low diblock copolymer concentration. The layers were drop casted onto mica substrates and investigated by tapping mode AFM (left: topography; right: phase image). The occurrence of isolated, collapsed vesicles with a partially damaged vesicular shell, most likely a bilayer, is clearly visible in the AFM images (tapping mode). During collapse of the vesicles some diblock copolymer material was re-distributed on the surface as a very thin layer with a fractal shape.

Also contact mode AFM images show large vesicular structures from methanolic solution onto mica substrates (Figure 2.5). The polymersome formation seems similar if compared to the tapping mode AFM images from methanol. Comparable, but smaller vesicular structures have been observed for the uncharged amphiphilic poly[9,9-*bis*(2-ethylhexyl)fluorene]-*b*-poly[3-(6-diethylphosphonatohexyl)thiophene] by Tu *et al*. in 2007.[2]

Remarkably, drop casting of PF2/6-*b*-P3TMAHT from water (polymer concentration 0.1 mg/mL, Figure 2.6) followed by slow solvent evaporation leads to the formation of fractal-like, poorly structured aggregates as been also observed for triblock polyaniline-polyfluorene-polyaniline copolymers[24] and non-conjugated amphiphilic block copolymers (PS-*b*-PEO)[25].

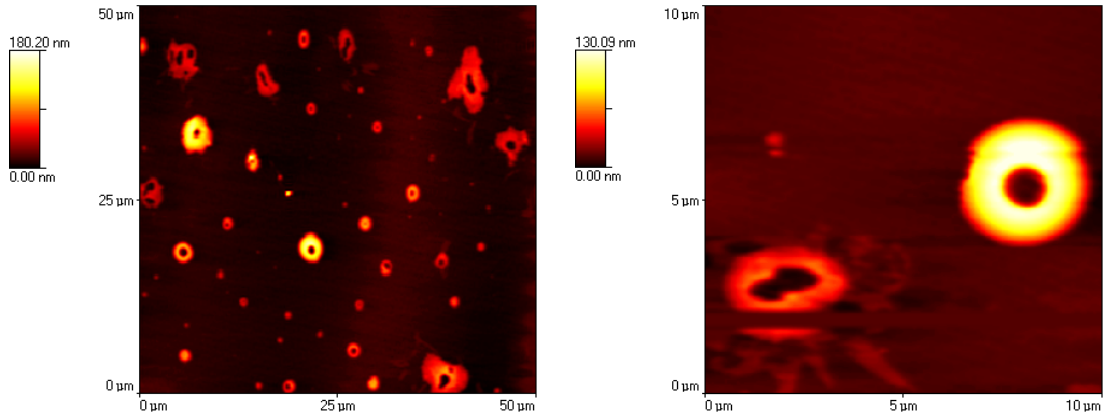

Figure 2.5. Contact mode AFM images of PF2/6-b-P3TMAHT (made from precursor B) deposited from methanolic solution onto a mica substrate (0.03 mg/mL; topography images, left: 50.0x50.0 μm^2, right: 10.0x10.0 μm^2).

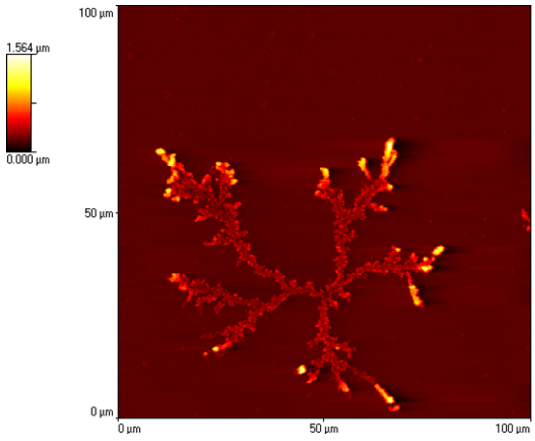

Figure 2.6. Contact mode AFM image of PF2/6-b-P3TMAHT (made from precursor C) deposited from aqueous solution onto a mica substrate (0.1 mg/mL; topography image, 100.0x100.0 μm^2).

Figure 2.7 depicts a structure model of the diblock copolymer vesicles (polymersomes) that are formed in methanol. The core region of the amphiphilic bilayers (vesicle walls) is generated in the aggregation of the non-ionic, hydrophobic PFO or PF2/6 segments (in red) while the outer shells of the vesicle walls are formed by the ionic, hydrophilic P3PyHT or P3TMAHT segments (in blue). Our structure model leads to the occurrence of an interfacial dipole within the vesicle walls.[26] The degree of interdigitation of the PF2/6 segments in the inner region of the vesicle walls cannot be derived from our data. However, the thickness of the collapsed vesicles (ca. 35-45 nm, see next paragraph) points to an interdigitation of the hydrophobic PF2/6 segments.

Further AFM experiments have been collected at higher concentrations of the polyelectrolyte diblock copolymer PF2/6-*b*-P3PyHT (precursor A, Figure 2.8) and PF2/6-*b*-P3TMAHT

(precursor D, Figure 2.9) in methanol. A denser coverage of the substrate accompanied by a transition to solid state-like films is obtained by drop-casting from methanol onto silica substrates.

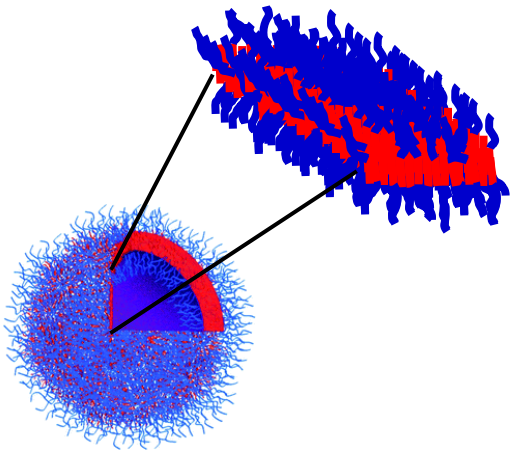

Figure 2.7. Graphical illustration of the vesicle structure formed by PF2/6-b-P3TMAHT and PF2/6-b-P3PyHT from methanolic solution (red: PF2/6 block, blue: P3TMAHT or P3PyHT block).

In Figure 2.8 vesicular and lamellar (fibrillar) aggregates with an inter-lamellar distance of ca. 20 nm coexist. The interlamellar distance well corresponds to the lateral dimension of extended copolymer chains (Figure 2.8).

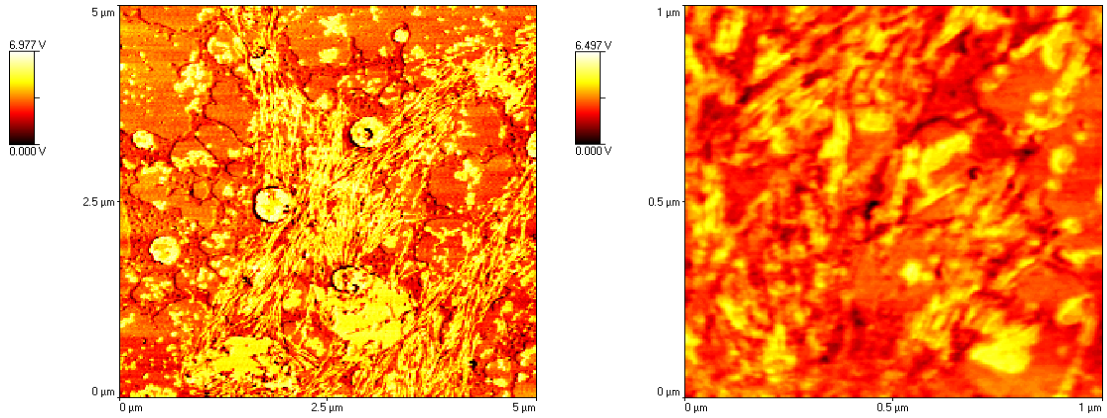

Figure 2.8. Tapping mode AFM images of PF2/6-b-P3PyHT (made from precursor A) drop-casted from methanolic solution onto a silica substrate (0.08 mg/mL, phase images, left: 5.0x5.0 μm^2, right: 1.0x1.0 μm^2).

Further experiments (Figure 2.9) at higher polymer concentration illustrate the transition from vesicular (region 1) to terrace-like morphologies (region 3) with a terrace height of ca. 35-45 nm. This step height should approximately correspond to the double lateral dimension of the copolymer bilayers which are formed in the collapse/fusion of the vesicles after

deposition. The layered assemblies should show a parallel orientation with respect to the silica surface.[21]

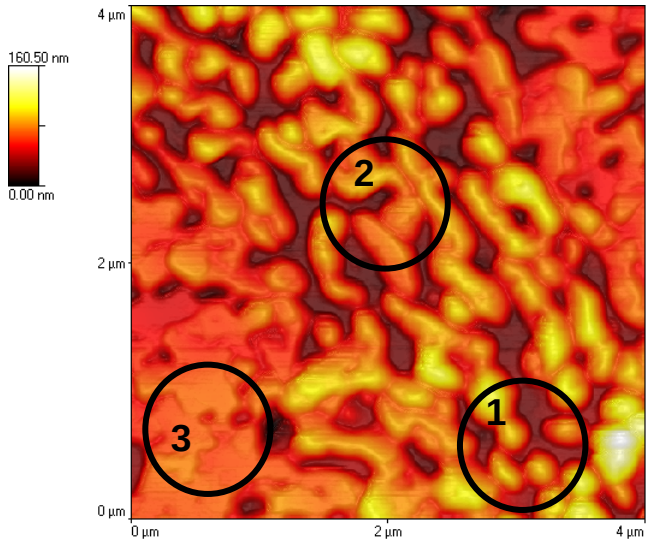

Figure 2.9. Tapping mode AFM images of PF2/6-b-P3MAHT (made from precursor D) deposited from methanolic solution onto a silica substrate (5 mg/mL, topography image, 4.0x4.0 µm^2). (1) vesicular, (2) mixed, and (3) terrace-like morphology.

2.2.3.2. Confocal Microscopy

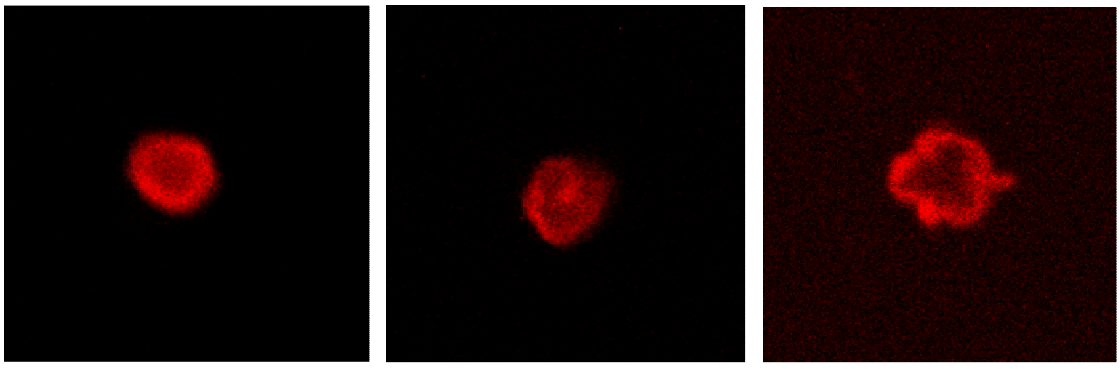

Figure 2.10. Confocal fluorescence microscopy images of three PF2/6-b-P3PyHT (made from precursor A*) vesicles in methanolic solution (10 mg/mL) on a glass substrate (vesicle size: 3-4 µm), left: single vesicle, middle and right: fused vesicles.*

Next, in addition to the AFM investigations, we have analyzed the vesicle (polymersome) formation of PF2/6-*b*-P3PyHT in solution directly by confocal fluorescence microscopy. Three confocal images of luminescent PF2/6-*b*-P3PyHT vesicles (precursor A) in methanol

with a diameter of 3-4 μm are depicted in Figure 2.10. The use of color filters showed that the photoluminescence of the vesicles is dominated by the red emission of the P3PyHT blocks that are located in the outer shell of the polymersomes. The left picture depicts a single vesicle, the middle and right images show fused vesicles that have been formed in the fusion of two or more initially formed single polymersomes.[21]

2.2.4. Complexation with Anionic Surfactants

In further experiments, the complexation of the block copolyelectrolyte PF2/6-*b*-P3TMAHT with the oppositely charged surfactant sodium dodecyl sulfate in water (SDS) has been studied. The PL spectra of PF2/6-*b*-P3TMAHT after addition of SDS to an aqueous solution of the diblock copolymer are depicted in Figure 2.11.

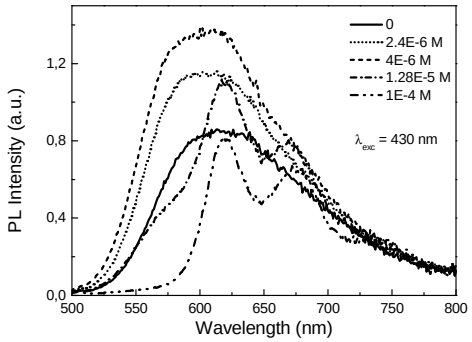

Figure 2.11. Photoluminescence spectra of PF2/6-b-P3TMAHT with the addition of sodium dodecyl sulfate (SDS) to an aqueous solution of the diblock copolymer (polymer concentration: 1.2×10^{-3} mg/mL ≈ 2.3×10^{-6} M charged repeat units; the SDS concentrations are given in the inset, at a SDS concentration of 2.4×10^{-6} M (dotted line) charge compensation should occur; λ_{exc} = 430 nm).

Excitation at 430 nm into the P3TMAHT absorption only causes emission of the polar P3TMAHT blocks. In contrast to the PF2/6 emission band, the P3TMAHT blocks show a distinct spectral response during surfactant addition. Incorporation of a charge equivalent of SDS leads to a significant PL enhancement without spectral changes after direct excitation at 430 nm. Starting at a 5-fold SDS excess a distinct red-shift of the PL spectral signature of the P3TMAHT blocks is observed that is accompanied by a spectral narrowing and the occurrence of well-resolved vibronic side bands. This spectral behavior is typical for an ongoing formation of highly ordered polyelectrolyte/surfactant (P3TMAHT/SDS) complexes of the diblock copolymer with SDS. At a 40-fold SDS excess, which still corresponds to an

SDS concentration considerably below its critical micelle concentration (cmc: 8.2 mM),[27] the re-organization process is mainly finished. This shows that not simply an incorporation of the diblock copolymer into micelles occurs. The finding that surfactant interactions with the diblock copolymers are observed at concentrations well below the surfactant cmc is in agreement with observations for other polyelectrolyte/surfactant systems as described by Jonsson *et al.*[28] The concept of ''critical association concentration'' (cac) describes the interaction of surfactants with oppositely charged polyelectrolytes at concentrations below their cmc, largely through electrostatic interactions and under formulation of polymer/surfactant aggregates.[28] A quite similar behavior, but at higher surfactant concentrations, is observed upon addition of sodium octyl sulfate (SOS). As has previously been seen with oppositely charged surfactants and alternating conjugated polyelectrolytes,[29,30] this strongly suggests that charge neutralization leads to self-assembly into ordered P3TMAHT/SDS complexes. In the case of our diblock copolymers this leads to a more rigid, planarized conformation of the ionic polythiophene chains. However, it should be pointed out, that the spectral changes only reflect the self-organization of the ionic P3TMAHT blocks upon formation of highly ordered P3TMAHT/SDS complexes. The consequences of SDS (or SOS) addition on the organization of the polyfluorene blocks cannot be derived from the PL spectra of Figure 2.11. Recently, similar observations were obtained by Yao *et al*. for the interaction of a cationic homopolythiophene poly{2-methyl-3-[3-(N,N,N-trimethylammonium)-1-propyloxy]-2,5-thiophene} with anionic surfactants.[31]

2.2.5. Incorporation into Organic Electronic Devices

The solubility of conjugated polyelectrolyte (CPE) block copolymers in highly polar solvents generally allows for a simple and reliable fabrication of multilayer-based organic devices, which may avoid one serious problem in the fabrication of multilayer devices by solution processing – the mixing of different components during the subsequent processing steps.[5,32] Recently, polyfluorene-based and related CPE's have been inserted between the active layer and the electron collecting electrode in bulk heterojunction (BHJ) devices for a more efficient charge carrier extraction.[33]

Consequently, we have used our novel CPE block copolymer PF2/6-*b*-P3TMAHT as well as the corresponding homopolymer P3TMAHT as charge extraction interlayer of BHJ-type

organic solar cells. Figure 2.12 shows the chemical structures of the used materials as well as the device structure with the CPE layer between active layer and metal electrode for charge extraction improvement.

BHJ-type organic solar cells were fabricated with an active PCDTBT/$PC_{71}BM$ blend onto a 40 nm thick poly(3,4-ethylenedioxythiophene):poly(styrenesulfonate) (PEDOT:PSS) layer on patterned ITO coated glass substrates. The blend films of poly[N-9"-heptadecanyl-2,7-carbazole-ail-5,5-(4',7'-di-2-thenyl-2',1',3'-benzothiadiazole)] (PCDTBT) and [6,6]-phenyl C70-butyric acid methyl ester ($PC_{71}BM$) were deposited by spin-coating (procedure described in the experimental section). The CPE layers were subsequently deposited by spin-coating 0.01% (w/v) P3TMAHT or 0.02% (w/v) PF2/6-*b*-P3TMAHT methanolic solutions. The low CPE concentrations were chosen to calibrate a thickness of only several nanometers thus minimizing possible complications due to ion motion.[34] We also fabricated a control device without CPE layer for comparison.

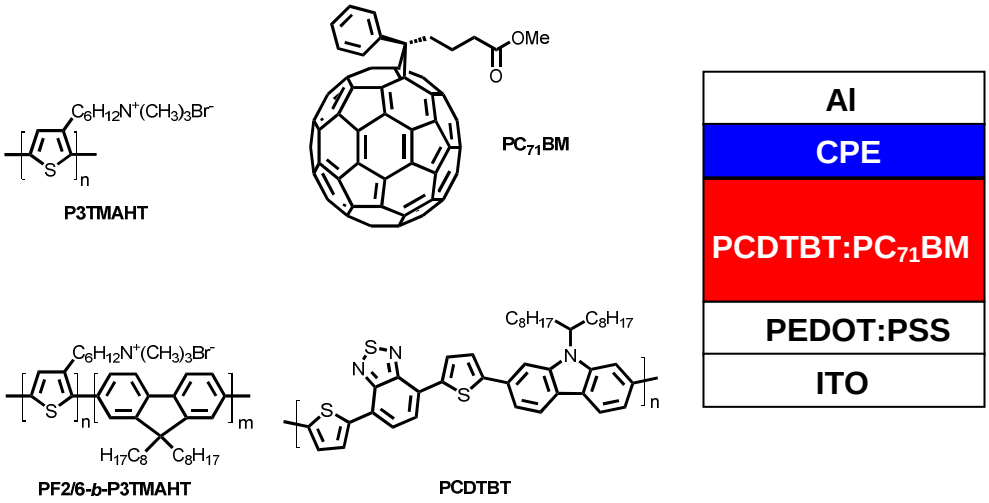

Figure 2.12. Chemical structure of the materials used for OSC device fabrication (left). Device configuration of an organic solar cell including a thin CPE layer (right).

Current density-voltage (J-V) characteristics of the devices measured under AM 1.5 illumination are shown in Figure 2.13. The obtained short circuit current (J_{SC}), open circuit voltage (V_{OC}), fill factor (FF) and power conversion efficiency (PCE), as determined from the J-V curves are summarized in Table 2.3. It is noteworthy that all devices with CPE layers show improved performances in comparison to control devices. The introduction of the CPE layer leads to increases of J_{SC} from 9.7 to 10.8 mA/cm² (P3TMAHT) and 10.6 mA/cm² (PF2/6-*b*-P3TMAHT). Similarly, an improvement in V_{OC} from 0.82 to 0.86 V (P3TMAHT) and 0.89 V (PF2/6-*b*-P3TMAHT) and FF from 63 to 66% (P3TMAHT) and 67% (PF2/6-*b*-

P3TMAHT) was observed. Therefore, the PCE increases from 5.3% for the control device to 6.3% (P3TMAHT) and 6.5% (PF2/6-*b*-P3TMAHT). [35]

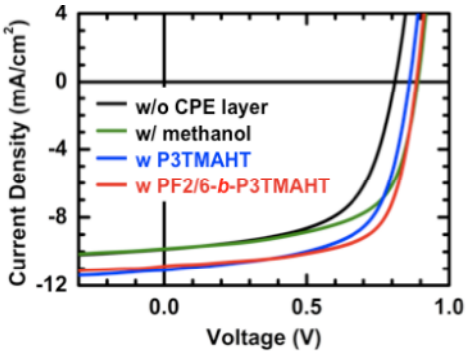

Figure 2.13. Current density-voltage (J-V) characteristics of PCDTBT:$PC_{71}BM$ devices without CPE layer (black), with a thin P3TMAHT (blue) or PF2/6-b-P3TMAHT interlayers (red) under illumination with an AM 1.5G solar simulator, 100 mW/cm^{-2}. Also pure methanol (green) was spin-cast on top of the active blend layer for comparison.

As a control experiment a possible influence of the solvent methanol used for CPE deposition was tested. These experiments involved spin-coating of pure methanol atop the active layer, followed by a sequence of steps similar to those for CPE layer deposition. Interestingly, the devices obtained after methanol treatment showed somewhat increased V_{OC} values and a somewhat higher PCE (Figure 2.13 and Table 2.3). However, the J_{SC} values are smaller in comparison to the devices containing CPE layers. We assume that the performance improvement for the devices with CPE layers may be due to a combination of several effects.[35]

In summary, we demonstrated the simple fabrication of high efficiency BHJ solar cells with a thin CPE interlayer between active layer and cathode. The introduction of P3TMAHT and PF2/6-*b*-P3TMAHT interlayers leads to a CPE increase from ca. 5.3 to 6.5%. Typically, the polythiophene backbones of the CPE are considered as hole transport/hole extraction materials. Cationic polythiophenes as well as block copolymers with cationic polythiophene-based CPE segments have been shown to be useful electron extracting interlayers. The reason for this effect may be due to the formation of interfacial dipoles and/or to the interfacial accumulation of ions. The main outcome is that a simple deposition of thin CPE layers simultaneously increases V_{OC}, J_{SC}, FF and PCE. However, further experiments are needed for a full understanding of the impact of CPEs interlayers on solar cell performance.[35] The available literature concerning this point is until now not consistent.

Table 2.3. Device performance of the PCDTBT:$PC_{71}BM$-based BHJ-type organic solar cells with and without CPE interlayers (J_{SC}: short circuit current density, V_{OC}: open circuit voltage, FF: fill factor, PCE: power conversion efficiency).

PCDTBT:$PC_{71}BM$	**J_{SC} (mA/cm²)**	**V_{OC} (V)**	**FF (%)**	**PCE (%) Average**	**PCE (%) Best**
w/o CPE layer	9.7 ± 0.3	0.82 ± 0.04	61 ± 1	5.0	5.3
w/methanol	9.7 ± 0.3	0.88 ± 0.01	62 ± 1	5.3	5.4
w/P3TMAHT	10.8 ± 0.3	0.86 ± 0.01	66 ± 1	6.1	6.3
w/PF2/6-*b*-P3TMAHT	10.6 ± 0.3	0.89 ± 0.01	67 ± 1	6.2	6.5

2.3. Conclusion and Outlook

In summary, we have developed a straightforward synthetic protocol towards novel all-conjugated, cationic diblock copolymers consisting of a non-ionic poly(dialkylfluorene) and a cationic poly(3-alkylthiophene) block. Pure PF2/6-*b*-P3TMAHT, PFO-*b*-P3TMAHT, PF2/6-*b*-P3PyHT and PFO-*b*-P3PyHT polyelectrolyte block copolymers were isolated by careful separation from homopolymeric products including repeated solvent extraction steps. Further on, we have studied the photophysical properties and aggregation behavior of them in solution and in the solid state.

Absorption and PL spectra of PF2/6-*b*-P3TMAHT, PFO-*b*-P3TMAHT, PF2/6-*b*-P3PyHT, and PFO-b-P3PyHT show spectral signatures of PF and PT blocks. Absorption and PL experiments in aqueous solution indicate the presence of strongly aggregated species. Addition of 30-70% THF leads to a subsequent de-aggregation which is accompanied by a blue shift of the emission maximum for the ionic polythiophene block. The all-conjugated, cationic block copolymers show the formation of micron-sized vesicular aggregates (polymersomes) mostly independent of the molecular weight of the ionic diblock copolymers. Vesicle formation was observed by imaging techniques such as contact/tapping mode atomic force microscopy (AFM) and confocal fluorescence microscopy.

Our CPEs have been tested as electron extraction interlayers of organic BHJ-type solar cells. The introduction of P3TMAHT or PF2/6-*b*-P3TMAHT as thin interlayers lead to an increase of the PCE from ca. 5.3 to ca. 6.5%.

Inspired by our preliminary results, future work will provide a more detailed studies of the self-organization properties. Concerning the poly(fluorene)-*b*-poly(thiophene) diblock copolyelectrolytes, a further improvement of the electronic properties seems possible by modification of the side groups (alkyl length, polar head groups). For this, ionic block copolymers with different quaternary ammonium groups, e.g. derived from quinoline or methylimidazole, as well as zwitterionic CPEs may be generated.

Hereby, the introduction of zwitterionic side groups seems especially interesting (exemplary shown for the PF-*b*-PT block copolymer in Scheme 2.2). An advantage of such zwitterionic CPE block copolymers is the absence of mobile counter ions due to the pinning of the sulfonate counter ions to the CPE side chain. This may also help to clarify the function of the thin CPE interlayers in OSCs. Such zwitterionic CPE interlayers may cause a further device improvement and are promising candidates for organic electronics devices.[36,37]

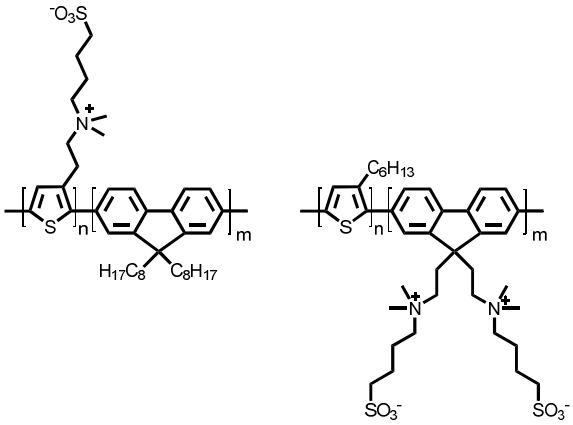

Scheme 2.2. Chemical structures of possible all-conjugated, zwitterionic diblock copolymers.

CPE-based sensors have already been developed for several kinds of analytes, as anions/cations, proteins or DNA.[38,39] In this context, block polyelectrolytes should be tested for an application in sensors/biosensors.

2.4. Experimental Section

Materials

Unless otherwise indicated, all reagents were obtained from commercial suppliers and were used without further purification. All reactions were carried out using standard and Schlenk techniques under an argon atmosphere. The solvents were used as commercial p.a. and HPLC quality.

3-(6-Bromohexyl)thiophene (T6Br)[17]

3-Bromothiophene (10.0 g, 61.3 mmol) was dissolved in dry *n*-hexane (85 mL) and cooled down to -50 °C. Then, 1.6 M *n*-butyllithium (38.3 mL, 61.3 mmol) was added drop-wise. After stirring for 10 min dry THF (8 mL) was introduced yielding a white precipitate. The mixture was stirred for 1 h and allowed to warm up to room temperature. Additional THF (3 mL) was added along with an excess of 1,6-dibromohexane (38 mL, 81.7 mmol). The yellow mixture was stirred for 2 h followed by extraction with diethyl ether for three times. The organic phase was isolated, washed with water, and dried over magnesium sulfate. After removing the organic solvents, the excess of alkylbromide was removed under reduced pressure. Further purification by vacuum distillation afforded 3-(6-bromohexyl)thiophene as a colorless oil (10.26 g, 68%).

^{1}H-NMR (400 MHz, CD_2Cl_2): δ (ppm): 7.17 (dd, *J = 5.1 Hz and 3.0 Hz*, 1H, Ar-H), 6.87 (dd, *J = 5.1 Hz and 1.2 Hz*, 1H, Ar-H), 6.86 (dd, *J = 3.0 Hz and 1.2 Hz*, 1H, Ar-H), 3.35 (t, *J = 6.6 Hz*, 2H, Br-CH_2), 2.56 (t, *J = 7.6 Hz*, 2H, Ar-CH_2), 1.78 (quint, *J = 7.1 Hz*, 2H, Br-CH_2-CH_2), 1.56 (quint, *J = 7.6 and 7.1 Hz*, 2H, Ar-CH_2-CH_2), 1.38 (quint, *J = 8.1 and 7.1 Hz*, 2H, Ar-$(CH_2)_2$-CH_2), 1.28 (quint, *J = 7.1 and 8.1 Hz*, 2H, Br-$(CH_2)_2$-CH_2). ^{13}C-NMR (100 MHz, CD_2Cl_2): δ (ppm): 143.3, 128.6, 125.5, 120.2, 34.7, 33.0, 30.6, 30.4, 28.7, 28.3. GC-MS: t_r = 7.5 min, 100% M^+: 246. Bp: 96 °C (± 1 °C) at 0.04 mbar.

2-Bromo-3-(6-bromohexyl)thiophene (BrT6Br)

3-(6-Bromohexyl)thiophene (4.95 g, 20.0 mmol) was dissolved in DMF (50 mL) in the dark at -20 °C. A solution of NBS (3.62 g, 20.5 mmol) in DMF (50 mL) was added drop-wise and

the resulting mixture stirred for 30 min at -20 °C and subsequently warmed up overnight to room temperature. Then, the reaction mixture was poured into ice (50 g). The resulting solution was extracted with dichloromethane for three times. The combined organic layers were dried over magnesium sulfate followed by the removal of volatile solvents at reduced pressure. The residue was purified by silica gel column chromatography (eluent: *n*-heptane) to afford 2-bromo-3-(6-bromohexyl)thiophene as a colorless oil (25.58 g, 73%).

DC: R_f = 0.50 (silica gel, *n*-heptane). ^{1}H-NMR (400 MHz, CD_2Cl_2): δ (ppm): 7.13 (d, *J = 5.6 Hz*, 1H, Ar-H), 6.73 (d, *J = 5.6 Hz*, 1H, Ar-H), 3.34 (t, *J = 7.1 Hz*, 2H, Br-CH_2), 2.45 (t, *J = 7.6 Hz*, 2H, Ar-CH_2), 1.78 (quint, *J = 7.1 Hz*, 2H, Br-CH_2-CH_2), 1.56 (quint, *J = 7.6 and 7.1 Hz*, 2H, Ar-CH_2-CH_2), 1.38 (quint, *J = 7.6 and 7.1 Hz*, 2H, Ar-$(CH_2)_2$-CH_2), 1.27 (quint, *J = 7.1 and 7.6 Hz*, 2H, Br-$(CH_2)_2$-CH_2). ^{13}C-NMR (100 MHz, CD_2Cl_2): δ (ppm): 142.0, 128.6, 125.7, 109.1, 34.7, 33.0, 29.7, 29.5, 28.6, 28.2. Elemental analysis: $C_{10}H_{14}Br_2S$, calculated (%): C 36.83, S 9.83, H 4.33, measured (%): C 36.95, S 9.72, H 4.59. GC-MS: t_r = 6.8 min, 100% M^+: 326.

General procedure for the synthesis of 2,7-dialkylfluorene

2,7-Dibromofluorene (15.8 g, 48.8 mmol), alkylbromide (488 mmol) and tetrabutylammonium bromide (1.57 g, 4.88 mmol) were added to an aqueous potassium hydroxide solution (300 mL, 45% w/w). The mixture was stirred for 1 h at 80 °C and then diluted with water (50 mL). The aqueous solution was extracted with dichloromethane for three times and the combined organic layers were washed with water, 1 M HCl, brine, and dried over magnesium sulfate. After removal of the organic solvent, the excess of alkylbromide was removed under reduced pressure. The crude product, a yellow oil, was purified by silica gel column chromatography to afford 2,7-dialkylfluorene as a colorless oil, which was recrystallized from ethanol yielding colorless crystals.

2,7-Dibromo-9,9-dioctylfluorene (BrFO)

According to the general procedure, 2,7-dibromofluorene (3.84 g, 14.76 mmol) was reacted with 1-bromooctane (28.50 g, 147.6 mmol) to yield, after purification by column chromatography (eluent: *n*-hexane), about 5.84 g (approx. 72%) of the target compound.

^{1}H-NMR (500 MHz, CD_2Cl_2): δ (ppm): 7.50 (d, *J = 8.0 Hz*, 2H, Ar-H), 7.49-7.46 (m, 4H, Ar-H), 1.95 (m, 4H, CH_2), 1.24-1.06 (m, 24H, CH_2), 0.59 (m, 6H, CH_3). ^{13}C-NMR (125 MHz, CD_2Cl_2): δ (ppm): 153.46, 139.9, 130.7, 126.9, 122.0, 121.8, 56.4, 40.7, 32.4, 30.5, 29.8, 24.3, 23.2, 22,5, 14.5. Elemental analysis: $C_{29}H_{40}Br_2$, calculated (%): C 63.51, H 9.79, measured (%): C 63.41, H 9.61. GC-MS: t_r = 8.5 min, 100% M^+: 548. Mp**:** 50 °C (± 1 °C).

2,7-Dibromo-9,9-bis(2-ethylhexyl)fluorene (BrF2/6)

According to the general procedure, 2,7-dibromofluorene (3.20 g, 12.30 mmol) was reacted with 3-(bromomethyl)heptane (23.60 g, 123 mmol) to yield, after purification by column chromatography (eluent: *n*-hexane), about 5.02 g (approx. 74%) of the target compound.

DC: R_f = 0.80 (silica gel, hexane). ^{1}H-NMR (400 MHz, $CDCl_3$): δ (ppm): 7.53 (d, *J = 7.6 Hz*, 2H, Ar-H), 7.46 (d, J = 1.5 Hz, 2H, Ar-H), 7.44 (d, *J = 1.5 Hz*, 2H, Ar-H), 1.98-1.89 (m, 4H, Ar-CH_2), 0.95-0.45 (m, 30H, alkyl-H). ^{13}C-NMR (100 MHz, $CDCl_3$): δ (ppm): 152.4, 139.2, 130.1, 127.1, 121.0, 120.8, 55.5, 44.4, 34.7, 33.7, 28.1, 27.1, 22.7, 14.0, 10.3. Elemental analysis: $C_{29}H_{40}Br_2$, calculated (%): C 63.51, H 9.79, measured (%): C 63.45, H 9.85. GC-MS: t_r = 8.5 min, 100% M^+: 548. Mp**:** 46 °C (± 1 °C).

General procedure for the synthesis of 2-(4',4',5',5'-tetramethyl-1',3',2'-dioxaborolane-2'-yl)-7-bromo-9,9-dialkylfluorene

2,7-Dibromo-9,9-dialkylfluorene (15.4 mmol) was dissolved in dry, degassed diethylether (300 mL) and placed in a 500 mL round bottle flask. The solution was cooled down to -78 °C and 0.98 equivalents of alkyl lithium (either *n*-butyllithium or *t*-butyllithium) were added drop-wise. The resulting solution was allowed to stir for one hour followed by addition of 2-isopropoxy-4,4,5,5-tetramethyl-1,3,2-dioxaborolane (12.6 mL, 61.5 mmol) in one shot. The reaction mixture was then stirred one more hour at -78 °C. The mixture was then allowed to warm up to room temperature overnight followed by quenching with water (50 mL). The two-phase solution was then extracted with dichloromethane for three times and the combined organic layers were washed with water and brine, and dried over magnesium sulfate. The solvent was removed under reduced pressure and the resulting yellow oil was purified by silica gel column chromatography to afford 2-(4',4',5',5'-tetramethyl-1',3',2'-dioxaborolane-2'-yl)-7-bromo-9,9-dioctylfluorene as a colorless oil.

2-(4',4',5',5'-Tetramethyl-1',3',2'-dioxaborolane-2'-yl)-7-bromo-9,9-dioctylfluorene (FO)

According to the general procedure, 2,7-dibromo-9,9-dioctylfluorene (6.0 g, 10.9 mmol) was reacted 1.6 M *n*-butyllithium (6.2 mL, 10.7 mmol) to yield, after purification by column chromatography (eluent: ethyl acetate/hexane = 5:95), about 3.20 g (approx. 49%) of the target compound.

^{1}H-NMR (500 MHz, $CDCl_3$): δ (ppm): 7.81 (d, 1H, Ar-H), 7.72 (s, 1H, Ar-H), 7.66 (d, 1H, Ar-H), 7.57 (d, 1H, Ar-H), 7.46 (s, 1H, Ar-H), 7.40 (m, 1H, Ar-H), 2.04-1.90 (m, 4H, Ar-CH_2), 1.39 (bs, 12H, $OC(CH_3)_2C(CH_3)_2O$), 1.29-1.00 (m, 20H, alkyl-H), 0.82 (t, 6H, CH_2-CH_3), 0.64-0.47 (m, 4H, alkyl-H). ^{13}C-NMR (125 MHz, $CDCl_3$): δ (ppm): 153.6, 149.5, 143.0, 140.0, 133.9, 129.9, 128.9, 126.2, 121.4, 119.0, 83.8, 55.5, 40.1, 31.8, 29.9, 29.1, 24.9, 23.6, 22.6, 14.0. Elemental analysis: $C_{35}H_{52}BBrO_2$, calculated (%): C 70.59, H 8.80, measured (%): C 70.42, H 8.39. GC-MS: t_r = 9.8 min, 100% M^+: 596.

2-(4',4',5',5'-Tetramethyl-1',3',2'-dioxaborolane-2'-yl)-7-bromo-9,9-bis(2-ethylhexyl)fluorene (F2/6)

According to the general procedure, 2,7-dibromo-9,9-*bis*(2-ethylhexyl)fluorene (4.94 g, 9.00 mmol) was reacted with 1.6 M *n*-butyllithium (6.2 mL, 10.7 mmol) to yield, after purification by column chromatography (eluent: ethyl acetate/hexane = 2:98), about 2.90 g (approx. 53%) of the target compound.

DC: R_f = 0.32 (silica gel, ethyl acetate/hexane = 2:98). ^{1}H-NMR (400 MHz, $CDCl_3$): δ (ppm): 7.82 (s, 1H, Ar-H), 7.78 (d, *J = 7.6 Hz*, 1H, Ar-H), 7.64 (d, *J = 7.6 Hz*, 1H, Ar-H), 7.56 (d, *J = 8.1 Hz*, 1H, Ar-H), 7.51 (s, 1H, Ar-H), 7.44 (d, *J = 8.1 Hz*, 1H, Ar-H), 2.05-2.00 (m, 2H, Ar-CH_2), 1.95-1.87 (m, 2H, Ar-CH_2), 1.36 (s, 12H, $OC(CH_3)_2C(CH_3)_2O$), 0.92-0.43 (m, 30H, alkyl-H). ^{13}C-NMR (100 MHz, $CDCl_3$): δ (ppm): 153.4, 149.2, 143.0, 140.1, 133.8, 130.4, 129.8, 127.5, 121.3, 118.9, 83.6, 55.2, 44.3, 33.7, 28.1, 27.3, 27.0, 24.8, 22.7, 14.0. Elemental analysis: $C_{35}H_{52}BBrO_2$, calculated (%): C 70.59, H 8.80, measured (%):71.24, H 8.89. GC-MS: t_r = 9.8 min, 100% M^+: 596.

Monobromo-endcapped poly[3-(6-bromohexyl)-2,5-thiophene] (Br-P3BrHT)

Fresh lithium diisopropylamide (LDA) was prepared from freshly distilled diisopropylamine (1.6 mL) and 1.6 M *n*-buthyllithium (6.25 mL in *n*-hexane). The product was added to dry

THF (50 mL) under Ar atmosphere at -78 °C via a syringe. The resulting solution was allowed to warm up to room temperature. The solution was stirred for 5 min at room temperature and again cooled down to -78 °C followed by addition of 2-bromo-3-(6-bromohexyl)thiophene (3.26 g, 10.0 mmol). After stirring for 2 h the reaction mixture was added to a cooled solution (-78 °C) of dry zinc(II) chloride (1.40 g, 10.3 mmol) in dry THF (3 mL) via a syringe followed by additional stirring for 1 h at -78 °C. After warming up the mixture to room temperature the catalyst Ni(dppp)Cl_2 (43 mg, 0.0065 mmol) was added in the dark and the resulting reaction solution stirred for 30 min. The reaction product was poured into cold methanol (500 mL) and the precipitate isolated by filtration. The crude polymer was re-dissolved in $CHCl_3$ and washed with water, brine, and saturated $NaHCO_3$. Then, the solution was concentrated and the polymer re-precipitated by pouring the viscous solution into cold methanol (500 mL). The polymer was purified by Soxhlet extraction with methanol, acetone, and *n*-hexane. The residue was re-dissolved in chloroform and the polymer isolated by removing the chloroform under reduced pressure. The resulting polymer was dried in vacuum to yield Br-P3BrHT as a dark red solid (1.82 g, 56%).

^{1}H-NMR (400 MHz, CD_2Cl_2): δ (ppm): 6.94 (s, 1H, Ar-H), 3.37 (t, 2H, *J = 6.6 Hz*, -CH_2), 2.87-2.74 (t, 2H, Ar-CH_2), 1.91-1.73 (m, 2H, alkyl-H), 1.72-1.55 (m, 2H, alkyl-H), 1.54-1.11 (m, 4H, alkyl-H). ^{13}C-NMR (100 MHz, CD_2Cl_2): δ (ppm): 140.0, 133.9, 130.8, 128.9, 34.7, 33.0, 30.5, 29.6, 28.9, 28.3. Elemental analysis: $(C_{10}H_{13}BrS)_n$, calculated (%): C 48.92, S 13.08, H 5.34, measured (%):C 48.68, S 12.97, H 5.38. UV-Vis ($CHCl_3$): $\lambda_{max,\ abs}$ = 435 nm. PL ($CHCl_3$, λ_{exc} = 380 nm): $\lambda_{max,\ em}$ = 570 nm.

General procedure for the synthesis of poly(9,9-dialkyl-2,7-fluorene)-b-poly[3-(6-bromohexyl)-2,5-thiophene]

2-(4',4',5',5'-Tetramethyl-1',3',2'-dioxaborolane-2'-yl)-7-bromo-9,9-dialkylfluorene (1.80 mmol), and tetrakis(triphenylphosphine)palladium(0) (34 mg, 0.030 mmol) were dissolved in toluene (5 mL) followed by addition of 2 M aqueous sodium carbonate solution (5 mL). The resulting mixture was allowed to react under inert atmosphere for 8 h at 80 °C. After that, Br-P3BrHT (200 mg) in toluene (5 mL) was added. The reaction mixture was further reacted for 40 h at 80 °C. Upon completion of the reaction the mixture was poured into methanol (500 mL) resulting in polymer precipitation. The solid was collected and washed/fractionated by Soxhlet extraction with methanol and hexane for 24 h each, followed by Soxhlet extraction with chloroform. The chloroform fraction was characterized and used.

Poly(9,9-dioctyl-*2,7-fluorene)-b-poly[3-(6-bromohexyl)-2,5-thiophene] (PFO-b-P3BrHT)*

According to the general procedure, 2-(4',4',5',5'-tetramethyl-1',3',2'-dioxaborolane-2'-yl)-7-bromo-9,9-dioctylfluorene (FO) (0.56 mg, 0.90 mmol) and poly[3-(6-bromohexyl)-2,5-thiophene] (Br-P3BrHT) (51 mg) as macromolecular endcapper were reacted to yield, after Soxhlet extraction, about 178 mg (approx. 31%, related to the amount of fluorene monomer) of the target compound as a dark red solid.

^{1}H-NMR (400 MHz, $CDCl_3$): δ (ppm): 7.88-7.56 (m, PF-block), 7.00-6.97 (m, PT-block), 3.43-3.37 (m, alkyl-H), 2.89-2.77 (m, alkyl-H), 2.20-0.63 (m, alkyl-H). UV-Vis ($CHCl_3$): $\lambda_{max, abs}$ = 385, 435 nm. PL ($CHCl_3$, λ_{exc} = 380 nm): $\lambda_{max, em}$ = 415, 572 nm.

Poly[9,9-bis(2-ethylhexyl)-2,7-fluorene]-b-poly[3-(6-bromohexyl)-2,5-thiophene] (PF2/6-b-P3BrHT)

According to the general procedure, 2-(4',4',5',5'-tetramethyl-1',3',2'-dioxaborolane-2'-yl)-7-bromo-9,9-*bis*(2-ethylhexyl)fluorene (F2/6) (3.096 mg, 5.20 mmol) and poly[3-(6-bromohexyl)-2,5-thiophene] (Br-P3BrHT) (716 mg) as macromolecular endcapper were reacted to yield, after Soxhlet extraction, about 805 mg (approx. 26%, related to the amount of fluorene monomer) of the target compound as a dark red solid.

^{1}H-NMR (400 MHz, $CDCl_3$): δ (ppm): 7.89-7.56 (m, PF-block), 7.00-6.96 (m, PT-block), 3.75-3.70 (m, alkyl-H), 2.89-2.78 (m, alkyl-H), 2.23-0.50 (m, alkyl-H). UV-Vis ($CHCl_3$): $\lambda_{max, abs}$ = 390, 439 nm. PL ($CHCl_3$, λ_{exc} = 380 nm): $\lambda_{max, em}$ = 424, 571 nm.

General procedure for the quaternization reaction

A large excess of the amine (10 mmol) was added to a solution of the neutral polymer (50 mg) in dry THF (5 mL). After stirring for 1 day at 80 °C the formation of a precipitate was observed, which was re-dissolved by addition of methanol (10 mL). After filtration to remove some insoluble material the solvents were removed under reduced pressure. The residue was purified by dialysis against water/methanol 1:1 using a dialysis membrane with a cut-off of 3,500 g/mol.

Poly(9,9-dioctyl-2,7-fluorene)-b-poly[3-(6-trimethylammoniumhexyl)-2,5-thiophene] (PFO-b-P3TMAHT)

According to the general procedure, PFO-*b*-P3BrHT (50 mg) was reacted with 45 wt% aqueous trimethylamine solution (2 mL) to yield, after purification by dialysis (water/methanol 1:1), about 41 mg (approx. 80%) of the target compound as a dark red solid.

^{1}H-NMR (400 MHz, MeOD): δ (ppm): 7.31-7.15 (m, PF-block), 7.14-7.01 (m, PT-block and pyridine), 3.14 (m, alkyl-H), 2.93-2.74 (m, alkyl-H), 1.91-0.73 (m, alkyl-H). UV-Vis (MeOH): $\lambda_{max,\ abs}$ = 388 (PF-block), 422 nm (PT-block). PL (MeOH, λ_{exc} = 380 nm): $\lambda_{max,\ em}$ = 417 (PF-block), 572 nm (PT-block).

Poly[9,9-bis(2-ethylhexyl)-2,7-fluorene]-b-poly[3-(6-trimethylammoniumhexyl)-2,5-thiophene] (PF2/6-b-P3TMAHT)

According to the general procedure, PF2/6-*b*-P3BrHT (43 mg) was reacted with 45 wt% aqueous trimethylamine solution (2 mL) to yield, after purification by dialysis (water/methanol 1:1), about 41 mg (approx. 85%) of the target compound as a dark red solid.

^{1}H-NMR (400 MHz, MeOD): δ (ppm): 7.30-7.17 (m, PF-block), 7.16-7.00 (m, PT-block), 3.52-3.26 (m, CH_3-N), 3.15 (m, alkyl-H), 2.96-2.77 (m, alkyl-H), 1.92-0.76 (m, alkyl-H). UV-Vis (MeOH): $\lambda_{max,\ abs}$ = 387 (PF-block), 422 nm (PT-block). PL (MeOH, λ_{exc} = 380 nm): $\lambda_{max,\ em}$ = 416, 438 (PF-block), 572 nm (PT-block).

Poly[9,9-bis(2-ethylhexyl)-2,7-fluorene]-b-poly{3-[6-pyridylhexyl]-2,5-thiophene} (PF2/6-b-P3PyHT)

According to the general procedure, PF2/6-*b*-P3BrHT (200 mg) was reacted with pyridine (5 mL) to yield, after purification by dialysis (water/methanol 1:1), about 120 mg (approx. 51%) of the target compound as a dark red solid.

^{1}H-NMR (400 MHz, D_2O): δ (ppm): 8.95-8.66 (m, pyridine-H), 8.57-8.40 (m, pyridine-H), 8.10-7.80 (m, pyridine-H), 7.30-6.66 (m, PF- and PT-block), 4.64-4.33 (m, alkyl-H), 2.79-2.26 (m, alkyl-H), 2.05-1.75 (m, alkyl-H), 1.64-0.97 (m, alkyl-H). DSC: T_g = 75.5 °C. UV-Vis (MeOH): $\lambda_{max,\ abs}$ = 389 (PF-block), 423 nm (PT-block). PL (MeOH, λ_{exc} = 380 nm): $\lambda_{max,\ em}$ = 419 (PF-block), 570 nm (PT-block).

Poly{3-[6-(N,N,N-trimethylammonium)hexyl]-2,5-thiophene} (P3TMAHT)

According to the general procedure, Br-P3BrHT (151 mg) was reacted with aqueous 45 wt% trimethylamine solution (2 mL) to yield, after purification by dialysis (water), about 142 mg (approx. 76%) of the target compound as a dark red solid.

^{1}H-NMR (400 MHz, D_2O). δ (ppm): 7.56-6.57 (m, 1H, Ar-H), 3.64-2.33 (m, 11H, N-CH_3 and alkyl-H), 2.04-0.57 (m, 10H, alkyl-H). Elemental analysis: $(C_{13}H_{22}BrNS)_n$, calculated (%): C 51.31, S 10.54, H 7.29, measured (%): C 51.42, S 10.05, H 7.00. UV-Vis (MeOH): $\lambda_{max,\ abs}$ = 429 nm. PL (MeOH, λ_{exc} = 390 nm) $\lambda_{max,\ em}$= 562 nm.

Device Part

Organic bulk heterojunction-type solar cells were fabricated by spin-coating the active PCDTBT/PC_{71}BM blends onto a 40 nm layer of PEDOT:PSS on patterned ITO glass substrates. The PCDTBT:PC_{71}BM (1:4 ratio) blends were, hereby, spin casted at 5000 rpm for 40 sec from solution in a chlorobenzene/1,2- dichlorobenzene (1:3) mixture onto the PEDOT:PSS layer. The films were annealed on a hot plate at 70°C for 10 min in a glove box. The CPE layers were subsequently deposited by spin-coating a 0.01% (w/v) P3TMAHT or 0.02% (w/v) PF2/6-*b*-P3TMAHT methanolic CPE solution. Finally, 100 nm thick Al electrodes were deposited by thermal evaporation in vacuum. The *J-V* characteristics of all devices were measured using a Keithley 236 Source Measure Unit.The solar cell performance was determined with an Air Mass 1.5 Global (AM 1.5 G) solar simulator with an irradiation intensity of 100 mW/cm^2. An aperture (9.84 mm^2) was used on top of the cell to eliminate extrinsic effects such as crosstalk, wave guiding and shadow effects. The spectral mismatch factor was calculated by comparison of the spectrum of the solar simulator and the AM 1.5 spectrum at RT.

Instrumentation

NMR

The ^{1}H and ^{13}C NMR spectra were recorded on Bruker ARX 400 and Avance III 600 spectrometers with use of solvent proton or carbon signals as internal standards.

Elemental analyses

Elemental analyses were performed on a Vario EL II (CHNS) instrument.

GC-MS

GC-MS measurements were obtained on a Shimadzu GC-17a with a Shimadzu GCMS-QP 5050 mass spectrometer (column: FS-OV1-CB-0.25) under helium. Injection temperature: 280 °C, starting temperature: 250 °C, heating rate: 6 °C, end temperature: 280 °C, end time: 30 min.

DSC

Differential Scanning Calorimetry (DSC) measurements were collected with a Perkin Elmer DSC 7 (heating/cooling rate 10 K/,min).

GPC

Gel permeation chromatography (GPC) measurements were carried out using Jasco PU 1580 equipped with Column “MZ plus linear 5 μ and 300 mm” columns, RI (Jasco RI-2031) and UV (Jasco UV-2031) detectors, toluene or THF as a solvent using polystyrene (PSS) calibration. The measurements were obtained at 30 °C.

UV-Vis absorption spectroscopy

UV-Vis absorption spectra were recorded on a Jasco V 550 spectrophotometer at room temperature.

Photoluminescence spectroscopy

Fluorescence measurements were carried out on a Varian Cary Eclipse instrument at room temperature.

Confocal flourescence microscope

Confocal fluorescence images were collected using a Leica TCS SP high resolution spectral confocal microscope equipped with a Millennia® series argon laser S-10 excitation source. The polymer samples were prepared by depositing a polymer solution onto glas slide followed by placement of a cover slip. The slide was inverted and placed onto the microscope stage (cover slip down) and the sample imaged in the epi-fluorescence mode.

AFM

Atomic force microscopy measurements were recorded using two instruments. 1) A diInnova microscope from Bruker in the tapping mode at room temperature under ambient conditions. The silicon cantilevers used were between 215-235 μm in length and had a resonance frequency of approximate 84 kHz; the tip height was between 15-20 μm. The polymer films are prepared by drop-casting of polymer solutions onto mica and dried in the exsiccator at room temperature. The solutions were filtered through 0.25 μm PTFE-filters. 2) AFM measurements were recorded using a under nitrogen environment using a commercial scanning probe microscope (MultiMode and Nanoscope Controller IIIa, Veeco Inc.). Surface potential measurements were collected using a Veeco diDimension Icon atomic force microscope instrument.

2.5. References

[1] a) H.-C. Kim, S.-M. Park, W. D. Hinsberg, *Chem. Rev.* **2010**, *110*, 146. b) H. Wang, M. K. Ng, L. Wang, L. Yu, B. Lin, M. Meron, Y. Xiao, *Chem. Eur. J.* **2002**, *8*, 3246.

[2] G. Tu, H. Li, M. Forster, R. Heiderhoff, L. Balk, R. Sigel, U. Scherf, *Small* **2007**, *3*, 1001.

[3] T. Hayakawa, R. Goseki, M.-a. Kakimoto, M. Tokita, J. Watanabe, Y. Liao, S. Horiuchi, *Org. Lett.* **2006**, *8*, 5453.

[4] Y. Liang, H. Wang, S. Yuan, Y. Lee, L. Gan, L. Yu, *J. Mater. Chem.* **2007**, *17*, 2183.

[5] C. V. Hoven, A. Garcia, G. C. Bazan, T. Q. Nguyen, *Adv. Mater*. **2008**, *20*, 3793.

[6] H. Plank, R. Güntner, U. Scherf, E. List, *Adv. Funct. Mater.* **2007**, *17*, 1093.

[7] Y. Zhang, K. Tajima, K. Hirota, K. Hashimoto, *J. Am. Chem. Soc.* **2008**, *130*, 7812.

[8] D. M. Vriezema, M. C. Aragone`s, J. A. A. W. Elemans, J. J. L. M. Cornelissen, A. E. Rowan, R. J. M. Nolte, *Chem. Rev*. **2005**, *105*, 1445.

[9] A. Kros, W. Jesse, G. A. Metselaar, J. J. L. M. Cornelissen, *Angew. Chem., Int. Ed. Engl*. **2005**, *44*, 4349.

[10] A. D. Schlüter, *J. Polym. Sci. A Polym. Chem.* **2001**, *39*, 1533.

[11] R. Verduzco, I. Botiz, D. L. Pickel, S. M. Kilbey, K. Hong, E. Dimasis, S. B. Darling, *Macromolecules*, **2011**, *44*, 530.

[12] A. Gutacker, N. Koenen, S. Adamczyk, U. Scherf, J. Pina, S. M. Fonseca, J. Seixas de Melo, A. J. M. Valente, H.D. Burrows, *Macromol. Rapid Commun.* **2008,** *29*, F50.

[13] U. Scherf , S. Adamczyk, A. Gutacker, N. Koenen, *Macromol. Rapid Commun.* **2009**, *30*, 1059.

[14] L. Zhai, R. D. McCullough, *Adv. Mater.* **2002**, *14*, 901.

[15] H.-G. Nothofer, *Ph.D. Thesis*, Universität Potsdam, Germany 2001; Logos Verlag, Berlin, **2001**, ISBN 3-89722-6685.

[16] a) A. Sandee, C. Williams, N. Evans, J. Davies, C. Boothby, A. Kohler, R. Friend, A. Holmes, *J. Am. Chem. Soc.* **2004**, *126*, 7041. b) F. Schindler, J. Jacob, A. Grimsdale, U. Scherf, K. Müllen, J. Lupton, J. Feldmann, *Angew. Chem., Int. Ed. Engl.* **2005**, *44*, 1520. c) Y. Wu, J. Li, Y. Fu, Z. Bo, *Org. Lett.* **2004**, *6*, 3485. d) M. Ranger, D. Rondeau, M. Leclerc, *Macromolecules* **1997**, *30*, 7686. e) X. Zhang, H. Tian, Q. Liu, L. Wang, Y. Geng, F. Wang, *J. Org. Chem.* **2006**, *71*, 4332.

[17] K. K. Stokes, K. Heuzé, R. D. McCullough, *Macromolecules* **2003**, *36*, 7114.

[18] M. Jeffries-EL, G. Sauve and R. D. McCullough, *Adv. Mater.* **2004**, *16*, 1017.

[19] U. Scherf, E. J. W. List, *Adv. Mater.* **2002**, *14*, 477.

[20] R. D. McCullough, *Adv. Mater.* **1998**, *10*, 93.

[21] A. Gutacker, S. Adamczyk, A. Helfer, L. E. Garner, R. C. Evans, S. M. Fonseca, M. Knaapila, G. C. Bazan, H. D. Burrows, U. Scherf, *J. Mater. Chem.* **2010**, *20*, 1423.

[22] M. Knaapila, R. C. Evans, A. Gutacker, V. M. Garamus, M. Torkkeli, S. Adamczyk, M. Forster, U. Scherf, and H. D. Burrows, *Langmuir* **2010**, *26*, 5056.

[23] L. L. G. Justino, M. L. Ramos, M. Knaapila, A. T. Marques, C. J. Kudla, U. Scherf, L. Almásy, R. Schweins, H. D. Burrows, A. P. Monkman, *Macromolecules*, **2011**, *44*, 334

[24] M. Knaapila, V. M. Garamus, L. Almásy, J. S. Pang, M. Forster, A. Gutacker, U. Scherf, and A. P. Monkman, *J. Phys. Chem. B* **2008**, *112*, 16415.

[25] J. Peng, Y. Han, W. Knoll, H. D. Kim, *Macromol. Rapid Commun.* **2007**, *28*, 1422.

[26] J. L. Casson, D. W. McBranch, J. M. Robinson, H.-L. Wang, J. B. Roberts, P. A. Chiarelli, M. S. Johal, *J. Phys. Chem. B* **2000**, *104*, 11996.

[27] P. Mukerjee, K. J. Mysels, *Critical Micelle Concentration of Aqueous Surfactant Systems*, National Bureau of Standards, Washington, DC, **1970**.

[28] B. Jonsson, B. Lindman, K. Holmberg, B. Kronberg, *Surfactants and Polymers in Aqueous Solution*, Wiley, Chichester, **1998**, 219.

[29] M. J. Tapia, H. D. Burrows, A. J. M. Valente, S. Pradhan, U. Scherf, V. M. M. Lobo, J. Pina and J. Seixas de Melo, *J. Phys. Chem. B* **2005**, *109*, 19108.

[30] M. Monteserin, H. D. Burrows, A. J. M. Valente, V. M. M. Lobo, R. Mallavia, M. J. Tapia, I. X. Garcia Zubiri, R. E. Di Paolo and A. L. Macanita, *J. Phys. Chem. B* **2007**, *111*, 13560.

[31] Z. Yao, Y. Li, C. Li, G. Shi, *Chem. Commun.* **2010**, *46*, 8639.

[32] a) F. Hung, B. Wu, Y Cao, *Chem. Soc. Rev*. **2010**, *39*, 2500. b) C. Wang, A. Garcia, H. Yan, K. E. Sohn, A. Hexemer, T.-Q. Nguyen, G. C. Bazan, E. J. Kramer, H. Ade, *J. Am. Chem. Soc*. **2009**, *131*, 12538.

[33] a) J. Luo, H. Wu, C. He, A. Li, W. Yang, Y. Cao, *Appl. Phys. Lett.* **2009**, *95*, 043301. b) C. He, C. Zhong, H. Wu, R. Yang, W. Yang, F. Huang, G. C. Bazan, Y. Cao, *J. Mater. Chem.* **2010**, *20*, 2617. (c) L. Ding, M. Jonforsen, L. S. Roman, M. R. Andersson, O. Inganäs, *Synthetic Metals* **2000**, *110*, 133. d) S.-H. Oh, S.-I. Na, J. Jo, B. Lim, D. Vak, D.-Y. Kim, *Adv. Func. Mater.* **2010**, *20*, 1997.

[34] a) J. H. Seo, A. Gutacker, B. Walker, S. Cho, R. Yang, T.-Q. Nguyen, A. J. Heeger, and G. C. Bazan, *J. Am. Chem. Soc.* **2009**, *131*, 18220. b) J. H Seo, E. B. Namdas, A. Gutacker, A. J. Heeger, G. C. Bazan, *Appl. Phys. Lett*. **2010**, *97*, 043303.

[35] J. H. Seo, A. Gutacker, Y. Sun, H. Wu, F. Huang, Y. Cao, U. Scherf, A. J. Heeger, G. C. Bazan, *J. Am. Chem. Soc.* **2011**, *133*, 8416.

[36] a) J. Fang, B. H. Wallikewitz, F. Gao, G. Tu, C. Müller, G. Pace, R. H. Friend, W. T. S. Huck, *J. Am. Chem. Soc.* **2011**, *133*, 683. b) Q. B. Pei, Y. Yang, G. Yu, C. Zhang, A. J. Heeger, *J. Am. Chem. Soc.* **1996**, *118*, 3922. c) Q. B. Pei, G. Yu, C. Zhang, Y. Yang, A. J. Heeger, *Science* **1995**, *269*, 1068. d) J. Fang, P. Matyba, N. D. Robinson, L. Edman, *J. Am. Chem. Soc*. **2008**, *130*, 4562. e) U. Scherf, *Angew. Chem. Int. Ed*. **2011**, *50*, 5016.

[37] G. Pace, G. Tu, E. Fratini, S. Massip, W. T. S. Huck, P. Baglioni, R. H. Friend, *Adv. Mater*. **2010**, *22*, 2073.

[38] S. W. Thomas III, G. D. Joly, T. M. Swager, *Chem. Rev*. **2007**, *107*, 1339.

[39] a) B. Liu, G. C. Bazan, *Proc. Natl. Acad. Sci*. **2005**, *102*, 589. b) K. Ding, F. E. Alemdaroglu, M. Börsch, R. Berger, A. Herrmann, *Angew. Chem. Int. Ed*. **2007**, *119*, 1191.

Chapter 3

3. All-Conjugated, “Rod-Rod” Diblock Copolyelectrolytes and their Complexes with Charged Molecules

All-conjugated block copolymers of the “rod-rod”-type have gained an enormous interest because of their unique and attractive combination of nanostructure formation and electronic activity. Potential applications for this class of block copolymer materials for (bio)sensors or photovoltaic devices have been demonstrated. Combining the active optical and electronic function of conjugated polymers with (cat)ionic polyelectrolytes in all-conjugated block copolyelectrolytes is, therefore, a very challenging goal of synthetic polymer chemistry. First examples of such all-conjugated block copolymers from a couple of research groups demonstrate possible synthetic approaches and the rich application potential in biosensors and electronic devices.

3.1. Introduction

The majority of research on block copolymers has focused on coil-coil[1] and rod-coil[2,3] block copolymers. Much less studied are rod-rod block copolymers, which can be attributed to the challenges in synthesizing these types of materials. Driven by the increasing interest in all-conjugated, rod-type block copolymers as components of target structures with biological [copolymers with polypeptide or deoxyribonucleic acid (DNA) blocks] or electronic (conjugated polymer blocks) function[3], investigations into rod-rod block copolymers have strongly intensified during the last five years. Two, or more, different “rigid rod” blocks covalently bound to each other, will allow for a controlled spatial arrangement of these blocks. As a result, functional nanostructures arising from aggregation and phase separation of the different blocks have much application potential.[4]

Conjugated polyelectrolytes (CPEs) are often synthesized by polycondensation reactions of dihalides and a second, correspondingly substituted, difunctional monomer (e.g. with $B(OR)_3$[5], SnR_3[6], ZnX[7], and phosphonates[8] as functional groups). Within the class of metal-catalyzed or -mediated aryl-aryl coupling methods, novel synthetic routes for a preparation of conjugated polymers with defined and appropriately reactive end groups have been developed by McCullough *et al.*[9] They synthesized several end-functionalized regioregular poly(3-alkylthiophene) via a so-called Grignard metathesis polymerization reaction in one step. Furthermore, the method of chain-growth polycondensation, which lead to conjugated polyarylenes with rather low polydispersity[10-12], allows for novel synthetic schemes towards all-conjugated block copolymers. Yokozawa *et al.* are one of the pioneering groups in the development of such catalyst transfer (or chain-growth) polycondensations, and applied this method for polyphenylene and polyfluorene synthesis, respectively.[11] They recently adapted their procedure for the step-wise generation of all-conjugated diblock copolymers.[12] The drastically reduced amount of chain termination events in such catalyst-transfer polycondensations allows for a simple, step-by-step polycondensation of two, or more, AB-type monomers in the step-wise aryl-aryl cross-coupling sequence. Utilizing this, the authors successfully synthesized a poly(2,5-dialkoxy-1,4-phenylene)-*b*-poly(N-hexyl-2,5-pyrrole) diblock copolymer (PPy-*b*-PPP) with a rather narrow molecular weight distribution of 1.16.[12]

We have now studied synthesis and nanostructure formation of ionic, all-conjugated, rod-rod diblock copolymers containing two conjugated blocks of different polarity. Thereby, one rational was to introduce an additional driving force for self-organization by using conjugated, amphiphilic block copolymers. So, we have synthesized and characterized a cationic, all-conjugated, rod-rod diblock copolymer PF2/6-*b*-P3TMAHT which is composed of a non-polar poly[9,9-*bis*(2-ethylhexyl)fluorene] (PF2/6) and a polar, cationic poly[3-(6-trimethylammoniumhexyl)-2,5-thiophene] (P3TMAHT) block. The resulting PF2/6-*b*-P3TMAHT block copolyelectrolyte is expected to exhibit solubility in polar protic solvents including methanol and water. Solubility in water is a crucial prerequisite for potential application in biosensors.

One advantage of conjugated polyelectrolytes as component of biosensors over small molecule-based systems stems from the amplification of both fluorescence quenching[13,14] and Förster resonance energy transfer to appropriate dyes.[15] This can lead to extremely high sensitivity. For example, genetic material (DNA) can be detected up to the zeptomole level.[16] So, cationic, conjugated polyelectrolytes are of particular importance for a use as DNA

sensors.[17] However, although CPE-based fluorescent probes with more than one emission feature have been developed,[18] it would appear desirable to develop a CPE-based ratiometric fluorescence sensor which output signal can be related to an internal standard (and follows changes of the nucleic acid concentration).

All-conjugated, diblock copolymers consisting of polyfluorene (PF) and polythiophene (PT) are valuable advanced materials.[19,20] The chain conformation of both blocks, especially the polythiophene block can be modulated by its environment. The introduction of cationic side chains at the PT-segment introduces water solubility and the possibility of tuning the electronic and optical properties by changing solvent or by addition of appropriate additives such as anionic surfactants.[21] Following the well-established effects of nucleic acids on the spectral and photophysical properties of cationic polythiophenes,[22] we report the use of the cationic diblock copolyelectrolyte PF2/6-*b*-P3TMAHT in an assay for anionic surfactants like sodium dodecylsulfate (SDS), DNA as well as organic acids.

3.2. Results and Discussion

3.2.1. Synthesis and GPC Characterization

For synthesizing the cationic, all-conjugated diblock copolymer PF2/6-*b*-P3TMAHT we used a “grafting-from” approach starting from a monobromo-endcapped, regioregular poly[3-(6-bromohexyl)-2,5-thiophene] Br-P3BrHT precursor with a mean average molecular weight (M_n) of 10,000 (weight average molecular weight M_w = 18,000, polydispersity M_n/M_w = 1.8) that was generated in a coupling protocol by McCullough and coworkers.[23] In the next step, the non-polar diblock copolymer PF2/6-*b*-P3BrHT was synthesized under Suzuki cross-coupling conditions with 2-bromo-9,9-*bis*(2-ethylhexyl)fluorene-7-boronic ester (F2/6) as bifunctional AB-type monomer and the monobromo-terminated Br-P3BrHT macromonomer as end-capper (Scheme 3.1). After subsequent purification (removal of homopolymeric by-products which was accomplished by several solvent extraction steps based on the rather different solubility behavior of the components) the bromoalkyl side groups of the diblock copolymer intermediate were converted into the charged target copolymer with trimethylamine leading to the NR_4^+-type cationic side groups of PF2/6-*b*-P3TMAHT.[19,24] (See also chapter 2 for more synthetic details.)

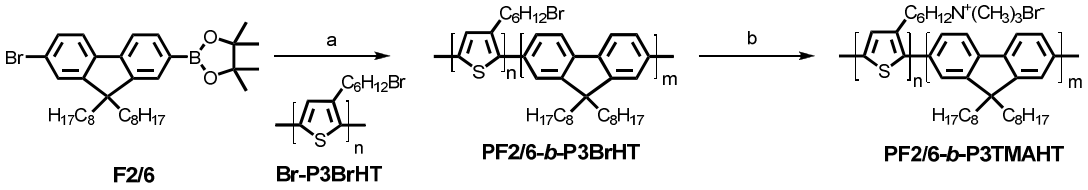

Scheme 3.1. Synthesis of the polyelectrolyte diblock copolymer PF2/6-b-P3TMAHT (C_8H_{17}: 2-ethylhexyl for PF2/6), a) $NaHCO_3$, $Pd(PPh_3)_4$, b) $N(CH_3)_3$.

The M_n of the non-polar diblock copolymer PF2/6-*b*-P3BrHT was determined to be 18,000 (M_w = 25,000, M_n/M_w = 1.4), corresponding to a M_n of the PF2/6 block of about 8,000. During GPC characterization of P3BrHT-*b*-PF2/6, the detection of the GPC elugrams was carried out both at 380 and 450 nm, respectively, corresponding to the long wavelength absorption maxima of the related homopolymers PF2/6 and P3BrHT in dilute solution. The GPC profiles of PF2/6-*b*-P3BrHT display a very similar shape and very similar M_n/M_w values at both detection wavelengths supporting that the resulting block copolymer is not a mixture/blend with one or both homopolymers.

3.2.2. Complexation with DNA

CPE-based biosensors are sensitive to variations in the environment and instrumental conditions, therefore, they need appropriate standards for quantitative applications. Fluorescence sensors can use ratiometric methods that compare the luminescence from more than one emitting species.[25] For example, CPE-based systems with two emission features have been developed for DNA quantification using ratiometric fluorescence methods.[15] Furthermore, selective fluorescence quenching is an attractive option. Here, we report the potential use of cationic diblock CPEs for ratiometric nucleic acid sensing.

The ionic nature of the copolymer PF2/6-*b*-P3TMAHT leads to an increased solubility in polar solvents as methanol and water compared to the neutral precursor PF2/6-*b*-P3BrHT. Although PF2/6-*b*-P3TMAHT aggregates in water, which may influence its interactions with other macromolecules/analytes, these aggregates can be broken up by addition of 20 - 80% of a cosolvent, such as THF (compare chapter 2.2.2).[26] We used PF2/6-*b*-P3TMAHT solutions of 20% THF / 80% water mixtures to study the interaction between the cationic diblock

copolymer and DNA. This solution mixture was found to provide a balance between photophysical properties and aggregation.

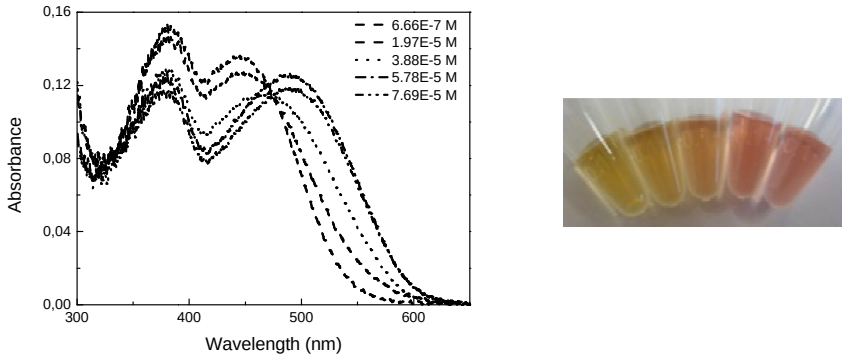

Figure 3.1. UV-Vis absorption spectra of PF2/6-b-P3TMAHT during addition of ssDNA to a polymer solution (9.86×10^{-6} M) in 20% / THF 80% water, the ssDNA concentrations are given in the inset, together with a photograph of the solutions before and during the addition of increasing ssDNA amounts.

Spectral signatures of both blocks were seen in the UV-Vis absorption spectrum of PF2/6-*b*-P3TMAHT solutions (Figure 3.1) and are attributed to PF (λ_{max} ~ 382 nm) and PT (λ_{max} ~ 445 nm) blocks. Upon addition of DNA, a slight decrease in absorption and an ongoing red shift of the polythiophene band is observed. This red shift is more pronounced with ssDNA (46 nm) than with double stranded dsDNA (27 nm, spectra not shown in here), possibly due to an increased conformational flexibility of ssDNA allowing a stronger interaction with the diblock copolymer. Similar effects have previously been reported for the interaction of DNA with the cationic poly{9,9-*bis*[6-*N*,*N*,*N*-trimethylammonium)hexyl]fluorene-*co*-1,4-phenylene} (PFP-Br) system.[27] The colorimetric effects may be attributing to conformational changes of the polythiophene blocks in the presence of DNA, thus increasing the conjugation length. In pure aqueous solutions of PF2/6-*b*-P3TMAHT the red shift of the polythiophene band upon addition of ssDNA is even larger (60 nm), which opens up more opportunities for imaging applications.

The photoluminescence spectra (PL) (Figure 3.2) following excitation of the polyfluorene absorption band at 385 nm show the occurrence of characteristic emission features of both blocks, a blue PL feature at 400-500 nm for the PF block and a red PL feature at 500-700 nm for the PT block. Under these conditions, the polythiophene emission is sensitized by excitation energy transfer from the polyfluorene block.[21b] Strong and selective quenching of the polythiophene block PL is observed upon addition of DNA, while the polyfluorene PL is

almost not influenced. In addition, the quenching of the polythiophene PL is accompanied by a red shift of the emission maximum. As observed with the absorption spectra, the red shift of fluorescence with ssDNA (36 nm) is larger than with double stranded dsDNA (18 nm).

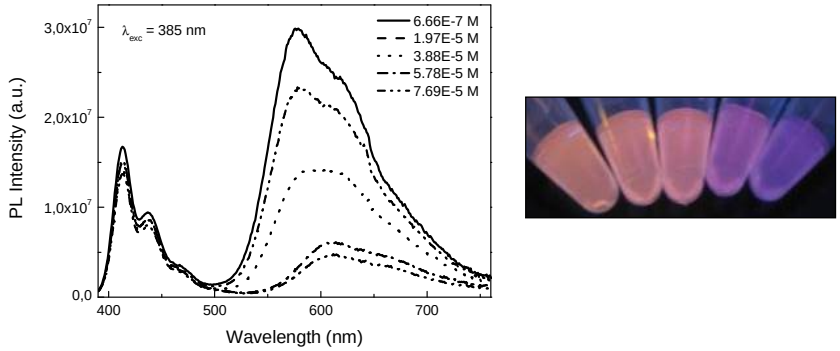

Figure 3.2. Photoluminescence spectra of PF2/6-b-P3TMAHT during addition of ssDNA to a polymer solution (9.86×10^{-6} M) in 20% / THF 80% water, the ssDNA concentrations are given in the inset, together with a photograph of the solutions before and during the addition of increasing ssDNA amounts. (λ_{exc}=385 nm).

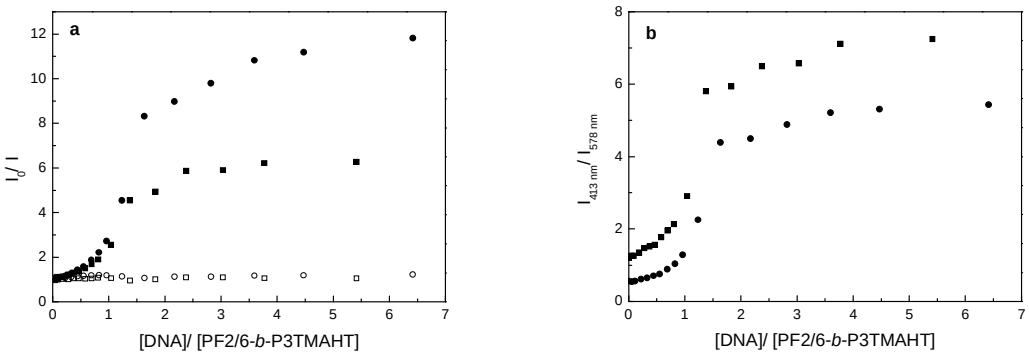

Figure 3.3. a) Stern-Volmer plots for the photoluminescence quenching of the polyfluorene (λ_{em} = 413 nm, open symbols) and polythiophene (λ_{em} = 578 nm, solid symbols) related PL with ssDNA (circles) and dsDNA (squares) and b) PL intensity ratio of PF/PT block as a function of the [DNA]/[PF2/6-b-P3TMAHT] ratio for ssDNA (circles) and dsDNA (squares).

The quenching behavior was analyzed by using Stern-Volmer plots[28,29]of the emission intensity at the PL maxima of the PT and PF block in the presence (I) and absence (I_0) of the analyte as a function of the [DNA]/[PF2/6-*b*-P3TMAHT] ratio for ssDNA and dsDNA (Figure 3.3). The corresponding Stern-Volmer plots for the PL quenching of the polythiophene blocks show a sigmoidal behavior, reminiscent of a titration curve, where the steep slope occurs for a [DNA]/[PF2/6-*b*-P3TMAHT] ratio corresponding to charge

neutralization (molar concentrations in terms of the respective monomeric repeat units). In contrast, no significant quenching is seen for the PL of the polyfluorene block. Fluorescence titrations using this system permit DNA quantification at the submicromolar level. From Figure 3.3, it can also be seen that the polythiophene PL quenching upon addition of ssDNA is twice that with the double-stranded one thus providing a potential ratiometric fluorescence detection route for distinguishing between single and double stranded DNA.

3.2.3. Complexation with Anionic Surfactants

The addition of an oppositely charged anionic surfactant like sodium dodecyl sulfate (SDS) to an aqueous solution of PF2/6-*b*-P3TMAHT leads to an ongoing compensation of the charges and the formation of highly ordered polyelectrolyte/surfactant complexes as shown by a distinct red shift of the PL maximum (polythiophene component) with the occurrence of a well-resolved vibronic structure in the PL band as known from aggregated PT (Figure 3.4).[20] Almost the same results were observed with the addition of sodium octyl sulfate, but significant changes in the spectrum were only seen at higher surfactant concentrations (for more details compare chapter 2.2.4.

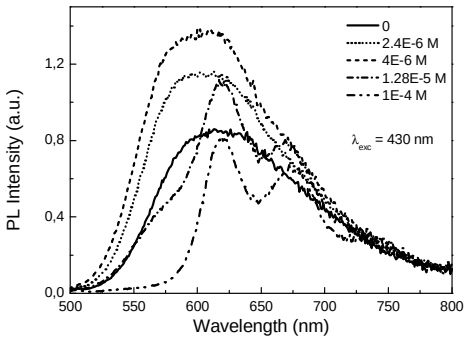

Figure 3.4. Photoluminescence spectra of PF2/6-b-P3TMAHT with the addition of sodium dodecyl sulfate (SDS) to an aqueous solution of the diblock copolymer (polymer concentration: 1.2×10^{-3} mg/mL ≈ 2.3×10^{-6} M charged repeat units; the SDS concentrations are given in the inset, at a SDS concentration of 2.4×10^{-6} M (dotted line) charge compensation should occur; λ_{exc} = 430 nm).

Recently, similar observations were obtained by Yao *et al*. for a cationic homopolythiophene poly{2-methyl-3-[3-(N,N,N-trimethylammonium)-1-propyloxy]-2,5-thiophene} and anionic surfactants and supported the validity of our results.[30]

3.2.4. Interaction with Organic Acids

To study the interaction of the cationic diblock copolymer PF2/6-*b*-P3TMAHT with organic acids (like p-toluenesulfonic acid and acetic acid) absorption spectra were recorded in the presence of different amounts of the organic acids (Figure 3.5). Increasing the amounts of p-toluenesulfonic acid caused a red-shift of the PT band in the absorption spectra from 440 nm to 510 nm. These spectral changes are due to the transition from random-coil PT chains (without acid) to well-ordered aggregates i.e. π-stacked complexes (addition of acid).[31,32] In contrast, the effect of acetic acid on the polyelectrolyte absorption maxima is very small. This leads us to the consideration that p-toluenesulfonic acid as a "soft" base has a stronger aggregation-tendency with the "soft" acid of the quaternary ammonium head group in the side chains of the PT block than acetic acid as a "hard" base. The so-called hard-soft acid-base (HSAB) principle by Pearson[33] predicts that hard-hard or soft-soft combinations are better stabilized and helps us to understand why the electrostatic interaction between a quaternary ammonium group and a sulfonate group is stronger than a carboxylate group with a quaternary ammonium group.[34] Furthermore, the type of electrostatic interaction influences the formation of π-stacked PT complexes. For comparison, similar interactions of a cationic homopolymer with organic acids have been observed by a Chinese group in 2010.[35]

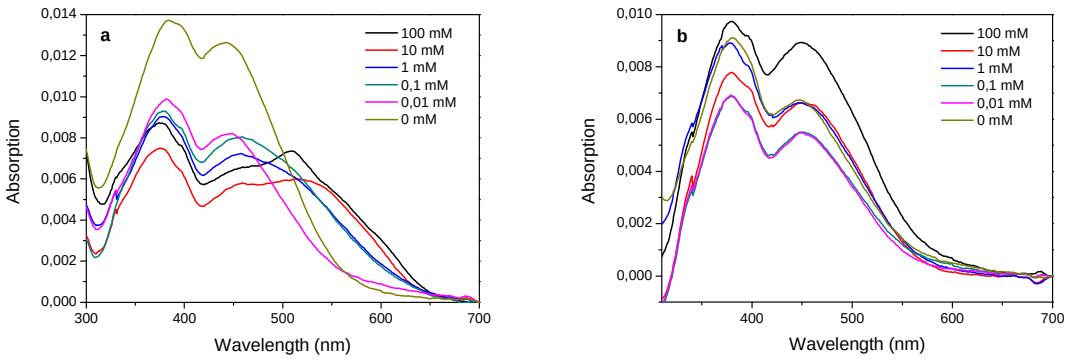

Figure 3.5. UV-Vis absorption spectra of PF2/6-b-P3TMAHT with the addition of p-toluenesulfonic acid (a) and acetic acid (b), (polymer concentration: 0.1 mg/mL; the acid concentrations are given in the inset).

3.3. Conclusion and Outlook

In conclusion, the all-conjugated, rod-rod diblock copolyelectrolyte PF2/6-*b*-P3TMAHT has been successfully synthesized. Selective quenching and/or a red shift of the PT-related photoluminescence band of the cationic polythiophene block is seen upon addition of either surfactants or DNA. Binding of nucleic acids to PF2/6-*b*-P3TMAHT leads to red shifts in the absorption and emission maxima due to conformational changes. Fluorescence titration of the diblock conjugated polyelectrolyte with DNA can be used for nucleic acid quantification at the submicromolar level. In addition, differences in the fluorescence quenching response can be used to distinguish between single and double strand DNA. As for DNA interactions with other cationic conjugated polyelectrolytes[36] at high nucleic acid concentrations the complexation is accompanied by the formation of nanostructured networks.

Additionally, we have shown the interaction of the block copolyelectrolyte with organic acids. The interaction can be realized with the HSAB principle. “Soft-soft” combinations with sulfonic acids favor the electrostatic interaction between PF2/6-*b*-P3TMAHT and p-toluenesulfonic acid under formation of π-stacked PT complexes.

However, a lot of further research is necessary to optimize all-conjugated block copolymers for a use in biosensors e.g. for DNA. Future work will be directed towards characterization of the solid state structures of conjugated block polyelectrolytes at high nucleic acid concentrations. Moreover, the complexation behavior of PF2/6-*b*-P3TMAHT with anionic polyelectrolytes as polystyrene sulfonic acid (PSSA) seems interesting and will be investigated in further studies.

3.4. Experimental Section

Materials

Unless otherwise indicated, all reagents were obtained from commercial suppliers and were used without further purification. All reactions were carried out using standard and Schlenk techniques under an argon atmosphere. The solvents were used as commercial p.a. and HPLC quality.

2-(4',4',5',5'-Tetramethyl-1',3',2'-dioxaborolane-2'-yl)-7-bromo-9,9-bis(2-ethylhexyl)fluorene (F2/6)

2,7-Dibromo-9,9-*bis*(2-ethylhexyl)fluorene (4.94 g, 9.00 mmol) was dissolved in dry, degassed diethylether (250 mL) and placed in a 500 mL round bottle flask. The solution was cooled down to -78 °C and 0.98 equivalents of 1.6 M *n*-butyllithium (6.2 mL, 10.7 mmol) were added drop-wise via a syringe. The resulting solution was stirred for one hour followed by addition of 2-isopropoxy-4,4,5,5-tetramethyl-1,3,2-dioxaborolane (12.6 mL, 61.5 mmol) in one shot. The reaction mixture was stirred for one more hour at -78 °C. The mixture was allowed to warm up to room temperature overnight followed by quenching with water (50 mL). The two-phase solution was then extracted with dichloromethane for three times and the combined organic layers were washed with water and brine, and dried over magnesium sulfate. The solvent was removed under reduced pressure and the resulting yellow oil was purified by silica gel column chromatography (eluent: ethyl acetate/hexane = 98:2), to afford 2.90 g (approx. 53%) of 2-(4',4',5',5'-tetramethyl-1',3',2'-dioxaborolane-2'-yl)-7-bromo-9,9-dioctylfluorene as a colorless oil.

DC: R_f = 0.32 (silica gel, ethyl acetate/hexane = 98:2). ^{1}H-NMR (400 MHz, $CDCl_3$): δ (ppm): 7.82 (s, 1H, Ar-H), 7.78 (d, *J = 7.6 Hz*, 1H, Ar-H), 7.64 (d, *J = 7.6 Hz*, 1H, Ar-H), 7.56 (d, *J = 8.1 Hz*, 1H, Ar-H), 7.51 (s, 1H, Ar-H), 7.44 (d, *J = 8.1 Hz*, 1H, Ar-H), 2.05-2.00 (m, 2H, Ar-CH_2), 1.95-1.87 (m, 2H, Ar-CH_2), 1.36 (s, 12H, $OC(CH_3)_2C(CH_3)_2O$), 0.92-0.43 (m, 30H, alkyl-H). ^{13}C-NMR (100 MHz, $CDCl_3$): δ (ppm): 153.4, 149.2, 143.0, 140.1, 133.8, 130.4, 129.8, 127.5, 121.3, 118.9, 83.6, 55.2, 44.3, 33.7, 28.1, 27.3, 27.0, 24.8, 22.7, 14.0. Elemental analysis: $C_{35}H_{52}BBrO_2$, calculated (%): C 70.59, H 8.80, measured (%): C 71.24, H 8.89. GC-MS: t_r = 9.8 min, 100% M^+: 596.

Poly[3-(6-bromohexyl)-2,5-thiophene] (Br-P3BrHT)[23]

Fresh lithium diisopropylamide (LDA) was prepared from freshly distilled diisopropylamine (1.6 mL) and 1.6 M *n*-buthyllithium (6.25 mL in *n*-hexane). The product was added to dry THF (50 mL) under Ar atmosphere at -78 °C via a syringe. The resulting solution was allowed to warm up to room temperature. The solution was stirred for 5 min at room temperature and again cooled down to -78 °C followed by addition of 2-bromo-3-(6-bromohexyl)thiophene (3.26 g, 10.0 mmol). After stirring for 2 h the reaction mixture was added to a cooled solution (-78 °C) of dry zinc(II) chloride (1.40 g, 10.3 mmol) in dry THF

(3 mL) via a syringe followed by additional stirring for 1 h at -78 °C. After warming up the mixture to room temperature the Ni(dppp)Cl_2 catalyst (43 mg, 0.0065 mmol) was added in the dark and the resulting reaction solution stirred for 30 min. The reaction product was poured into cold methanol (500 mL) and the precipitate isolated by filtration. The crude polymer was re-dissolved in $CHCl_3$ and washed with water, brine, and saturated $NaHCO_3$. Then, the solution was concentrated and the polymer re-precipitated by pouring the viscous solution into cold methanol (500 mL). The polymer was purified by Soxhlet extraction with methanol, acetone, and *n*-hexane. The residue was re-dissolved in chloroform and the polymer isolated by removing the chloroform under reduced pressure. The resulting polymer was dried in vacuum to yield Br-P3BrHT as a dark red solid (1.82 g, 56%).

^{1}H-NMR (400 MHz, CD_2Cl_2): δ (ppm): 6.94 (s, 1H, Ar-H), 3.37 (t, 2H, -CH_2), 2.87-2.74 (t, 2H, Ar-CH_2), 1.91-1.73 (m, 2H, alkyl-H), 1.72-1.55 (m, 2H, alkyl-H), 1.54-1.11 (m, 4H, alkyl-H). ^{13}C-NMR (100 MHz, CD_2Cl_2): δ (ppm): 140.0, 133.9, 130.8, 128.9, 34.7, 33.0, 30.5, 29.6, 28.9, 28.3. Elemental analysis: $(C_{10}H_{13}BrS)_n$, calculated (%): C 48.92, S 13.08, H 5.34, measured (%):C 48.68, S 12.97, H 5.38. GPC Anal. (THF, 254 nm): M_n = 10 000 g/mol, M_w = 18 000 g/mol, M_n/M_n = 1.8. UV-Vis ($CHCl_3$): $\lambda_{max,\ abs}$ = 435 nm. PL ($CHCl_3$, λ_{exc} = 385 nm): $\lambda_{max,\ em}$ = 570 nm.

Poly[9,9-bis(2-ethylhexyl)-2,7-fluorene]-b-poly[3-(6-bromohexyl)-2,5-thiophene] (PF2/6-b-P3BrHT)

2-(4’,4’,5’,5’-Tetramethyl-1’,3’,2’-dioxaborolane-2’-yl)-7-bromo-9,9-*bis*(2-ethylhexyl)-fluorene (F2/6) (3.096 mg, 5.20 mmol), and tetrakis(triphenylphosphino)-palladium(0) (95 mg, 0.084 mmol) were dissolved in toluene (15 mL) followed by addition of 2 M aqueous sodium carbonate solution (15 mL). The resulting mixture was allowed to react under inert atmosphere for 8 h at 80 °C. After that Br-P3BrHT (716 mg) in toluene (15 mL) was added. The reaction mixture was allowed to react for 40 h at 80 °C. Upon completion of the reaction the mixture was poured into methanol (1000 mL) resulting in polymer precipitation. The solid was collected and washed/fractionated by Soxhlet extraction with methanol and hexane for 24 h each, followed by Soxhlet extraction with chloroform to yield about 805 mg (approx. 26%, related to the fluorene monomer) of the target compound as a dark red solid. The chloroform fraction was characterized and further used.

^{1}H-NMR (400 MHz, $CDCl_3$): δ (ppm): 7.89-7.56 (m, PF-block), 7.00-6.96 (m, PT-block), 3.75-3.70 (m, alkyl-H), 2.89-2.78 (m, alkyl-H), 2.23-0.50 (m, alkyl-H).GPC Anal. (THF, 254, 380 and 450 nm): M_n = 18,000 g/mol, M_w = 25,000 g/mol, M_w/M_n = 1.4. UV-Vis ($CHCl_3$): $\lambda_{max, abs}$ = 390, 439 nm. PL ($CHCl_3$, λ_{exc} = 254, 385 and 430 nm): $\lambda_{max, em}$ = 424, 571nm.

Poly[9,9-bis(2-ethylhexyl)-2,7-fluorene]-b-poly[3-(6-trimethylammoniumhexyl)-2,5-thiophene] (PF2/6-b-P3TMAHT)

A large excess of aqueous 45 wt% trimethylamine (2 mL) was added to a solution of the neutral polymer PF2/6-*b*-P3BrHT [43 mg, M_n = 18,000 g/mol, M_n (Br-P3BrHT) = 10,000 g/mol] in dry THF (5 mL). After stirring for 1 day at 80 °C the formation of a precipitate was observed, which was re-dissolved by addition of methanol (10 mL). After filtration to remove some insoluble material, the solvent was removed under reduced pressure. The residue was purified by dialysis against water/methanol 1:1 using a dialysis membrane with a cut-off of 3,500 g/mol to yield, after evaporating the solvent, about 41 mg (approx. 85%) of the target compound as a dark red solid.

^{1}H-NMR (400 MHz, MeOD): δ (ppm): 7.30-7.17 (m, PF-block), 7.16-7.00 (m, PT-block), 3.52-3.26 (m, CH_3-N), 3.15 (m, alkyl-H), 2.96-2.77 (m, alkyl-H), 1.92-0.76 (m, alkyl-H). UV-Vis (20% THF/80% H_2O): $\lambda_{max, abs}$ = 382 (PF-block), 445 nm (PT-block). PL (20% THF/80% H_2O, λ_{exc} = 385 nm): $\lambda_{max, em}$ = 412, 437 (PF-block), 576 nm (PT-block).

Instrumentation

NMR

The ^{1}H and ^{13}C NMR spectra were recorded on a Bruker ARX 400 spectrometer with use of the solvent proton or carbon signals as internal standard.

Elemental analyses

Elemental analyses were performed on a Vario EL II (CHNS) instrument.

GC-MS

GC-MS measurements were obtained on a Shimadzu GC-17a coupled with a Shimadzu GCMS-QP 5050 mass spectrometer (column: FS-OV1-CB-0.25) under helium gas, injection temperature: 280 °C, starting temperature: 250 °C, heating rate: 6 °C, end temperature: 280 °C, end time: 30 min.

GPC

Gel permeation chromatography (GPC) measurements were carried out using Jasco PU 1580, Column “MZ plus linear 5 µ and 300 mm”, RI (Jasco RI-2031) and UV (Jasco UV-2031) detectors, toluene or THF as solvents using polystyrene (PSS) calibration. The measurements were obtained at 30 °C.

UV-Vis absorption spectroscopy

UV-Vis absorption spectra were recorded on a Jasco V 550 and on a Shimadzu UV-2401 PC spectrophotometer at room temperature.

Photoluminescence spectroscopy

Fluorescence measurements were carried out on a Varian Cary Eclipse and on a Shimadzu UV-2401 instrument room temperature.

3.5. References

[1] a) F. S. Bates, G. H. Frederickson, *Phys. Today* **1999**, *52*, 32. b) P. Bahadur, *Curr. Sci*. **2001**, *80*, 1002.

[2] H.-A. Klok, S. Lecommandoux, *Adv. Mater*. **2001**, *13*, 1217.

[3] Y. Liang, H. Wang, S. Yuan, Y. Lee, L. Gan, L. Yu, *J. Mater. Chem.* **2007**, *17*, 2183.

[4] T. Hayakawa, R. Goseki, M.-a. Kakimoto, M. Tokita, J. Watanabe, Y. Liao, S. Horiuchi, *Org. Lett.* **2006**, *8*, 5453.

[5] A. D. Schlüter *J. Polym. Sci. Part A.* **2001**, *39*, 1533.

[6] Z. Bao, W. K. Chan, L. Yu, *J. Am. Chem. Soc.* **1995**, *117*, 12426.

[7] T.-A Chen, X. Wu, R. D. Rieke, *J. Am. Chem. Soc.* **1995**, *117*, 233.

[8] Y. Suzuki, K. Hashimoto, K. Tajima, *Macromolecules*, **2007**, *40*, 6521.

[9] M. Jeffries-El, G. Sauve´, R. D. McCullough, *Adv. Mater*. **2004**, *16*, 1017.

[10] a) E. E. Sheina, J. Liu, M. C. Iovu, D. W. Laird, R. D. McCullough, *Macromolecules* **2004**, *37*, 3526. b) M. C. Iovu, E. E. Sheina, R. R. Gil, R. D. McCullough, *Macromolecules* **2005**, *38*, 8649.

[11] a) R. Miyakoshi, A. Yokoyama, T. Yokozawa, *J. Am. Chem. Soc*. **2005**, *127*, 17542. b) R. Miyakoshi, K. Shimono, A. Yokoyama, T. Yokozawa, *J. Am. Chem. Soc*. **2006**, *128*, 16012. c) T. Yokozawa, H. Kohno, Y. Ohta, A. Yokoyama, *Macromolecules*, **2010**, *43*, 7095.

[12] A. Yokoyama, H. Suzuki, J. Kubota, K. Ohuchi, H. Higashimura, T. Yokozawa, *J. Am. Chem. Soc*. **2007**, *129*, 7236.

[13] S. W. Thomas, G. D. Joly, T. M. Swager, *Chem. Rev.* **2007**, *107*, 1339.

[14] A. Duarte, K.-Y. Pu, B. Liu, G. C. Bazan, *Chem. Mater.* **2011**, *23*, 501.

[15] B. S. Gaylord, A. J. Heeger, G. C. Bazan, *Proc. Natl. Acad. Sciences* **2002**, *99*, 10954.

[16] K. Doré, S. Dubus, H.-A. Ho, I. Lévesque, M. Brunette, G. Corbeil, M. Boissinot, G. Boivin, M. G. Bergeron, D. Boudreau, M. Leclerc, *J. Am. Chem. Soc.* **2004**, *126*, 4240.

[17] a) Q. Chen, Q.-Y. Cheng, Y.-C. Zhao, B.-H. Han, *Macromol. Rapid Commun.* **2009**, *30*, 1651. b) S. K. Dishari, K.-Y. Pu, B. Liu, *Macromol. Rapid Commun.* **2009**, *30*, 1645. c) B. Liu, G. C. Bazan, *J. Am. Chem. Soc.* **2006**, *128*, 1188. d) H.-A. Ho, M. Boissinot, M. G. Bergeron, G. Corbeil, K. Doré, D. Boudreau, M. Leclerc, *Angew. Chem. Int. Ed.* **2002**, *41*, 1548. e) F. Feng, F. He, L. An, S. Wang, Y. Li, D. Zhu, *Adv. Mater.* **2008**, *20*, 2959. f) H. Jiang, P. Taranekar, J. Reynolds, K. Schanze, *Angew. Chem. Int. Ed.* **2009**, *48*, 4300.

[18] C. Chi, A. Mikhailovsky, G. C. Bazan, *J. Am. Chem. Soc.* **2007**, *129*, 1134.

[19] G. Tu, H. Li, M. Forster, R. Heiderhoff, L. J. Balk, R. Siegel, U. Scherf, *Small* **2007**, *3*, 1001.

[20] U. Scherf, N. Koenen, A. Gutacker, *Acc. Chem. Res*. **2008**, *41*, 1086.

[21] a) A. Gutacker, S. Adamczyk, A. Helfer, L. E. Garner, R. C. Evans, S. M. Fonseca, M. Knaapila, G. C. Bazan, H. D. Burrows, U. Scherf, *J. Mater. Chem*. **2010**, *20*, 1423. b) A. Gutacker, N. Koenen, U. Scherf, S. Adamczyk, J. Pina, S. M. Fonseca, A. J. M. Valente, R. C. Evans, J. Seixas de Melo, H. D. Burrows, M. Knaapila, *Polymer* **2010**, *51*, 1898. c) M. Knaapila, R. C. Evans, V. M. Garamus, L. Almásy, N. K. Székely, A. Gutacker, U. Scherf, H. D. Burrows, *Langmuir* **2010**, *26*, 15634.

[22] H.-A. Ho, A. Najari, M. Leclerc, M. *Acc. Chem. Res.* **2008**, *41*, 168.

[23] L. Zhai, R. McCullough, *Adv. Mater.* **2002**, *14*, 901.

[24] A. Gutacker, N. Koenen, S. Adamczyk, U. Scherf, J. Pina, S. M. Fonseca, J. Seixas de Melo, A. J. M. Valente, H.D. Burrows, *Macromol. Rapid Commun.* **2008**, *29*, F50.

[25] G. Grynkiewicz, M. Poenie, R. Y. Tsien, *J. Biol. Chem.* **1985**, *260*, 3440.

[26] M. Knaapila, R. C. Evans, A. Gutacker, V. M. Garamus, M. Torkkeli, S. Adamczyk, M. Forster, U. Scherf, H. D. Burrows, *Langmuir* **2010**, *26*, 5056.

[27] M. Monteserín, H. D. Burrows, A. J. M. Valente, R. Mallavia, R. E. Di Paolo, A. L. Maçanita, M. J. Tapia, *J. Polym. Sci. Part B* **2009**, *113*, 1294.

[28] J. R. Lakowicz, Principles of Fluorescence Spectroscopy 3rd, *Springer*, New York **2006**, *Chapter 8*.

[29] H. D. Burrows, S. J. Formosinho, M. F. J. T. Paiva, E. J. Rasburn, *J. Chem. Soc. Faraday Trans. II* **1980**, *76*, 685.

[30] Z. Yao, Y. Li, C. Li, G. Shi, *Chem. Commun.* **2010**, *46*, 8639.

[31] C. Li, M. Numata, A. H. Bae, K. Sakurai and S. Shinkai, *J. Am. Chem. Soc*. **2005**, *127*, 4548.

[32] C. Li, M. Numata, M. Takeuchi and S. Shinkai, *Chem.–Asian J*. **2006**, *1*, 95.

[33] R. G. Pearson, *J. Am. Chem. Soc.* **1963**, *85*, 3533.

[34] C. D'Silva, X.-B. Wang and R. Pethig, *J. Phys. D: Appl. Phys.* **1989**, *22*, 1591.

[35] Z. Yao, H. Bai, C. Li, G. Shi, *Chem. Commun.* **2010**, *46*, 5094.

[36] M. L. Davies, H. D. Burrows, S. Cheng, M. C. Morán, M. d. G. Miguel, P. Douglas, *Biomacromolecules* **2009**, *10*, 2987.

Chapter 4

4. All-Conjugated, Cationic Polyfluorene-*b*-Polyfluorene "Rod-Rod" Diblock Copolymers

Abstract

All-conjugated diblock copolymers are currently of considerable interest, also for potential applications as components of biological sensors or optoelectronic devices. We report on a novel cationic diblock copolymer containing a neutral poly(alkylfluorene) block covalently bound to a ionic polyfluorene block, namely poly[9,9-bis(6-trimethylammoniumhexyl)-2,7-fluorene]-b-poly(9,9-dioctyl-2,7-fluorene) (PF6NBr-b-PFO), which was synthesized via a step-wise chain-growth Suzuki-Miyaura-type polycondensation in the first step followed by quaternization with trimethylamine as the second step. The optical properties were investigated by UV-Vis and photoluminescence spectroscopy in three different solvents: methanol, THF and THF/methanol 1:1. First indications of nanoaggregation have been obtained from imaging techniques such as confocal fluorescence microscopy in solution and atomic force microscopy (AFM) of thin films. The formation of vesicles/spherical particles was observed in THF, methanol, and in the solid state. The use of PF6NBr-b-PFO as electron injection layer of organic light-emitting diodes (OLEDs) indicated that these block copolymers can effectively reduce electron injection barriers and, therefore, serve as a promising candidate for improving charge electron injection into optoelectronic devices.

4.1. Introduction

All-conjugated block copolymers, consisting of one polyfluorene (PF) and one polythiophene (PT) block have been discussed in detail in chapter 2 and 3, especially their unique tendency to self-assemble.[1] Similar self-assembling behavior has been observed for poly(3-alkylthiophene)-*b*-poly(3-alkylthiophene) (P3AT-*b*-P3AT) diblock copolymers. An all-conjugated P3AT-*b*-P3AT diblock copolymer poly(3-hexylthiophene)-*b*-poly[3-(2-

ethylhexyl)thiophene] (P3HT-*b*-P3EHT) has been first synthesized by Zhang *et al*.[2] The P3HT-*b*-P3EHT was generated in a quasi-living chain-growth polycondensation as developed by McCullough *et al*.[3] and Yokozawa *et al*.[4] to afford well-defined diblock copolymers with narrow molecular weight distribution. This effort requires the use of catalysts that selectively transfer reactivity to the terminus of the polymer chain upon addition of each monomer unit to the chain end.[5] Subsequent reports have focused on the microphase separation in (P3HT-*b*-P3EHT)s into crystalline P3HT and amorphous P3EHT domains.[6] The observed worm-like patterns, obtained after a thermal annealing of polymer films, are also seen in conjugated poly(3-hexylthiophene)-*b*-poly(3-phenoxymethylthiophene) (P3HT-*b*-P3PT) systems (for the structures see Scheme 4.1)[7]. Recent work by Wu *et al*.[8] and Ge *et al*.[9] has yielded new types of diblock copoly(3-alkylthiophene)s like poly(3-butylthiophene)-*b*-poly(3-octylthiophene) (P3BT-*b*-P3OT) and poly(3-butylthiophene)-*b*-poly(3-hexylthiophene) (P3BT-*b*-P3HT) with high degrees of internal order within both blocks.

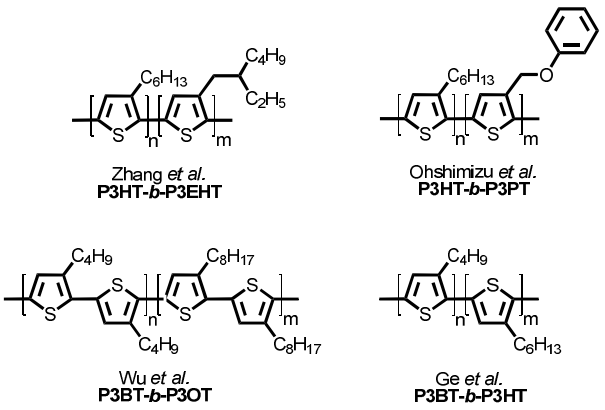

Scheme 4.1: Structures of different poly(3-alkylthiophene)-b-poly(3-alkylthiophene) diblock copolymers: P3HT-b-P3EHT after Zhang et al.[2], P3HT-b-P3PT after Ohshimizu et al.[7], P3BT-b-P3OT after Wu et al.[8], P3BT-b-P3HT after Ge et al.[9].

Motivated by these studies, we report here synthesis, optical characteristics, self assembly properties and device application of diblock copolymers that include a neutral poly(alkylfluorene) (PF) bound to a cationic poly(fluorene) block. Due to their strong blue fluorescence and their rigid, conjugated structure, PFs are very attractive as components of optoelectronic devices.[10] In particular, solid state phase formation and self-organization represent central facets in the physics of PFs.[11] Our block copolymers are macromolecular systems which have two rigid segments with identical electronic structure of the conjugated backbone and are expected to exhibit morphologies that are highly sensitive to the polarity of the surrounding medium.

Our interest in synthesis and applications of poly(fluorene)-based block copolymers prompted us to look at recent developments in the field of Suzuki-Miyaura polymerizations. Yokozawa *et al.*[12] reported the polymerization of a 7-bromo-9,9-dialkylfluorene-2-yl boronic ester using Hartwig's (*t*-Bu_3P)Pd(C_6H_5)Br[13] arylpalladium(II) catalyst. Unlike to typical Suzuki-Miyaura coupling reactions[14] using aromatic dihalides and the corresponding arylene diboronic esters, the polymeric products exhibited narrow molecular weight distributions. Under suitable reaction conditions it is possible to obtain polydispersity indexes (M_w/M_n) for the products lower as 1.3. As for polythiophenes, the reaction conditions applied by Yokozawa *et al.*[12] lead to a chain-growth mechanism of polycondensation.

4.2. Results and Discussion

4.2.1. Synthesis

Towards the poly(fluorene)-based diblock copolymers, our initial target structure were poly(fluorene)-*b*-poly(fluorene) diblock copolymers in which one of the poly(fluorene) segments contains alkylbromide substituents at the 9-position of the repeat unit. The bromoalkyl functions can subsequently be used in quaternization reactions to form charged poly(fluorene) segments. The overall synthetic strategy is illustrated in Scheme 4.2, details are outlined in the Experimental Section. In a first step, the two monomers 2-(4',4',5',5'-tetramethyl-1',3',2'-dioxaborolane-2'-yl)-7-bromo-9,9-dioctylfluorene (FO) and 2-(4',4',5',5'-tetramethyl-1',3',2'-dioxaborolane-2'-yl)-7-bromo-9,9-*bis*(6-bromohexyl)-fluorene (F6Br) were synthesized (see Figure 4.2) by mono-lithiation of the well-known dibromoderivatives under conditions that promote metal halogen exchange followed by reaction with 2-isopropoxy-4,4,5,5-tetramethyl-1,3,2-dioxaborolane.[15] The non-ionic poly[9,9-*bis*(6-bromohexyl)-2,7-fluorene]-*b*-poly(9,9-dioctyl-2,7-fluorene) (PF6Br-*b*-PFO) is subsequently generated in a step-wise chain-growth polycondensation,[12] by addition of first FO, followed by F6Br, as the two AB-type monomers. Optimization of the reaction conditions was carried out by varying reaction time (from 0.5 to 60 minutes), catalyst concentration (2.5-10 mol%), and the order of monomer addition between FO and F6Br. We found optimum conditions by firstly polymerizing FO with 10 mol% of (*t*-Bu_3P)Pd(C_6H_5)Br catalyst in a sodium carbonate solution in H_2O/THF (5:12) for 10 minutes at room

temperature. After addition of the second monomer F6Br as a solution in THF the mixture was stirred for an additional 30 minutes. The polymer solution was poured into acidified methanol and the residue was subsequently purified by Soxhlet extraction with methanol for 24 hours. The polymer PF6Br-*b*-PFO was obtained in 82% yield as a light yellow solid and is soluble in typical organic solvents, such as chloroform, tetrachloroethane, or chlorobenzene.

The resulting non-ionic PF6Br-*b*-PFO was reacted with trimethylamine in a quaternization reaction to obtain our target, an all-conjugated, cationic diblock copolymer PF6NBr-*b*-PFO (92% yield). The cationic diblock copolymer PF6NBr-*b*-PFO is soluble in polar solvents and solvent mixtures, including methanol and THF/water as well as in organic solvents such as chloroform and THF.

Standard characterization of the polymeric products was accomplished by gel permeation chromatography (GPC) analysis, nuclear magnetic resonance (NMR) spectroscopy (^{1}H and ^{13}C) and optical spectroscopy. Atomic Force Microscopy (AFM) as imaging technique (see next paragraphs) was used to characterize the self assembly properties of the block copolymers.

The results of the NMR analysis are in accordance with the proposed structure (see Experimental Section).

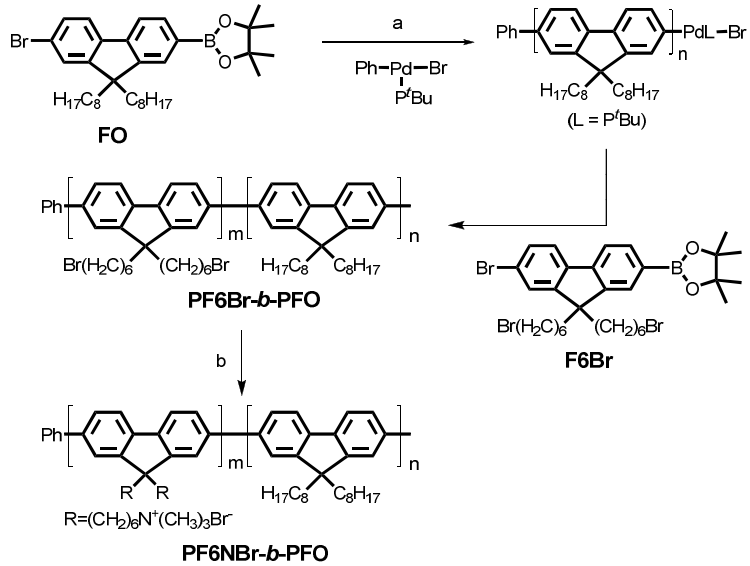

Scheme 4.2. Synthesis of the cationic diblock copolymer PF6NBr-b-PFO. a) Na_2CO_3, b) $N(CH_3)_3$.

The molecular weights afforded for the different blocks after extraction are listed in Table 4.1. PF6Br-*b*-PFO was obtained with a mean number average molecular weight (M_n) of 18,100 and a M_w/M_n of ~1.27. To calculate the mean number average molecular weights of both

blocks a GPC sample was taken before the second monomer F6Br was added to give a M_n ~ 8,100, corresponding to ca. 20 repeat units for the PFO block. The difference between the observed M_n of the PFO aliquot and the PF6Br-*b*-PFO sample reflects the M_n of the PF6Br block (M_n = 10,000, m = ~20). We could not measure the molecular weight of the cationic block copolymers by conventional GPC due to the strong interaction of the charged copolymer with the stationary phase of the GPC column (adsorption).

Table 4.1. Molecular weight data of PFO, PF6Br, and PF6Br-b-PFO.

structure	**M_n**	**M_w**	**M_n/M_w**
PFO	8,100	10,200	1.26
calculated PF6Br[a]	10,000	12,700	1.27
PF6Br-*b*-PFO	18,100	22,900	1.27

a. Calculation of M_n(PF6Br) = M_n(PF6Br-*b*-PFO) – M_n(PFO). Calculation of M_w done in an analogous way.

4.2.2. Optical Properties

Figure 4.1(a) shows the normalized absorption spectra of PF6NBr-*b*-PFO in three solvents: methanol, THF/methanol 1:1, and THF. One major absorption band is observed in THF, with an absorption maximum at about 390 nm which is typical of polyfluorene materials[10]. In methanol, one observes the emergence of a sharp, second peak of lower energy at about 430 nm in addition to the broad band previously observed in THF. The absorption in the THF/methanol (1:1) mixture is similar to that observed in methanol. The sharp peak at 430 nm has been previously assigned to the beta-phase of PFO.[11,16] Nothofer reported the formation of the PFO beta-phase when dissolving the polymer in good solvent/poor solvent mixtures of increasing "poor solvent" content. PFO shows a rich and unique packing behavior.[17] The so called β-phase is characterized by a distinct red shift of absorption and emission with remarkable well-resolved vibronic structure caused by a planar confirmation of the PFO backbone we found as the polarity of the solvent increases aggregation occurs and formation of the PFO β-phase is observed.

The photoluminescence (PL) spectra obtained by excitation at 380 nm are shown in Figure 4.1(b). The PL spectra in THF shows the characteristic polyfluorene emission bands at 414, 437 and 464 nm (414 nm: 0-0 α-phase, 437 nm: 0-0 β-phase).[18] In methanol stronger peaks at 437 and 464 nm emerge in relation to the emission band at 414 nm due to an increased β-phase content.[19] The photoluminescence of the mixture of THF/methanol (1:1) is similar to that in methanol. Protic and polar solvents favor the formation of the β-phase in our block copolymers as described for other PFO-based systems.[11]

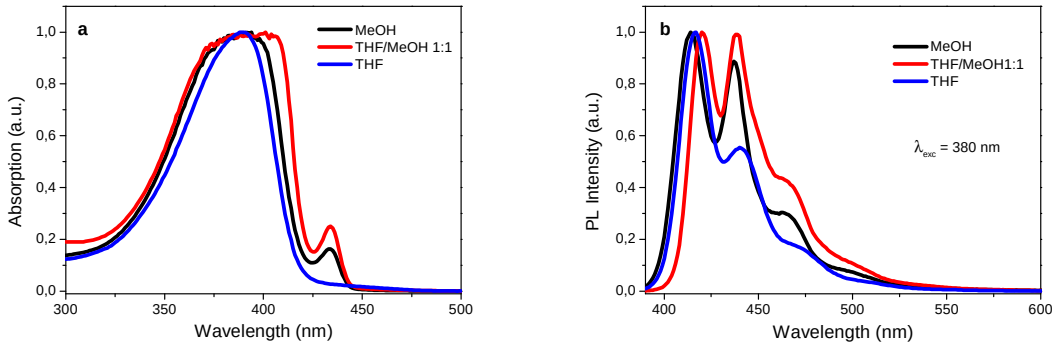

Figure 4.1. a) UV-Vis and b) photoluminescence spectra of the diblock copolymer PF6NBr-b-PFO in methanol, THF/methanol (1:1), and THF, (λ_{exc}= 380 nm).

4.2.3. Atomic Force Microscopy of Thin Films

Having first indications of aggregation from the absorption and photoluminescence spectra we also investigated the aggregation behavior of the all-conjugated, cationic diblock copolymer PF6NBr-*b*-PFO by tapping mode Atomic Force Microscopy (AFM) imaging technique. Here, the aggregation behavior in a selective solvent (methanol) for the polar block and a non-selective solvent (THF) will be discussed in detail. Figure 4.2(a+b) gives an exemplary illustration of the formation of vesicular aggregates from methanolic solution. Films spin-coated onto mica from methanolic solution (0.1% of PF6NBr-*b*-PFO) show the occurrence of clearly visible vesicular particles with a diameter of several 10 nanometers as well as larger aggregates.

Further AFM experiments have been carried out in THF for the same concentration (0.1%) of the polyelectrolyte diblock copolymer PF6NBr-*b*-PFO [Figure 4.2(c+d)]. Spin-coated a THF

(0.1%) solution (after aging for 10 days) leads to a dense coverage of the substrate most probably due to a pre-aggregation processes during aging.

The preferred formation of low curvature vesicular aggregates for rigid rod-rod-type, all-conjugated diblock copolymers was recently rationalized.[20] The self-assembly into such low curvature aggregates should be, herby, widely independent from the molecular weight of the diblock copolymers and the block length ratio.[21,22]

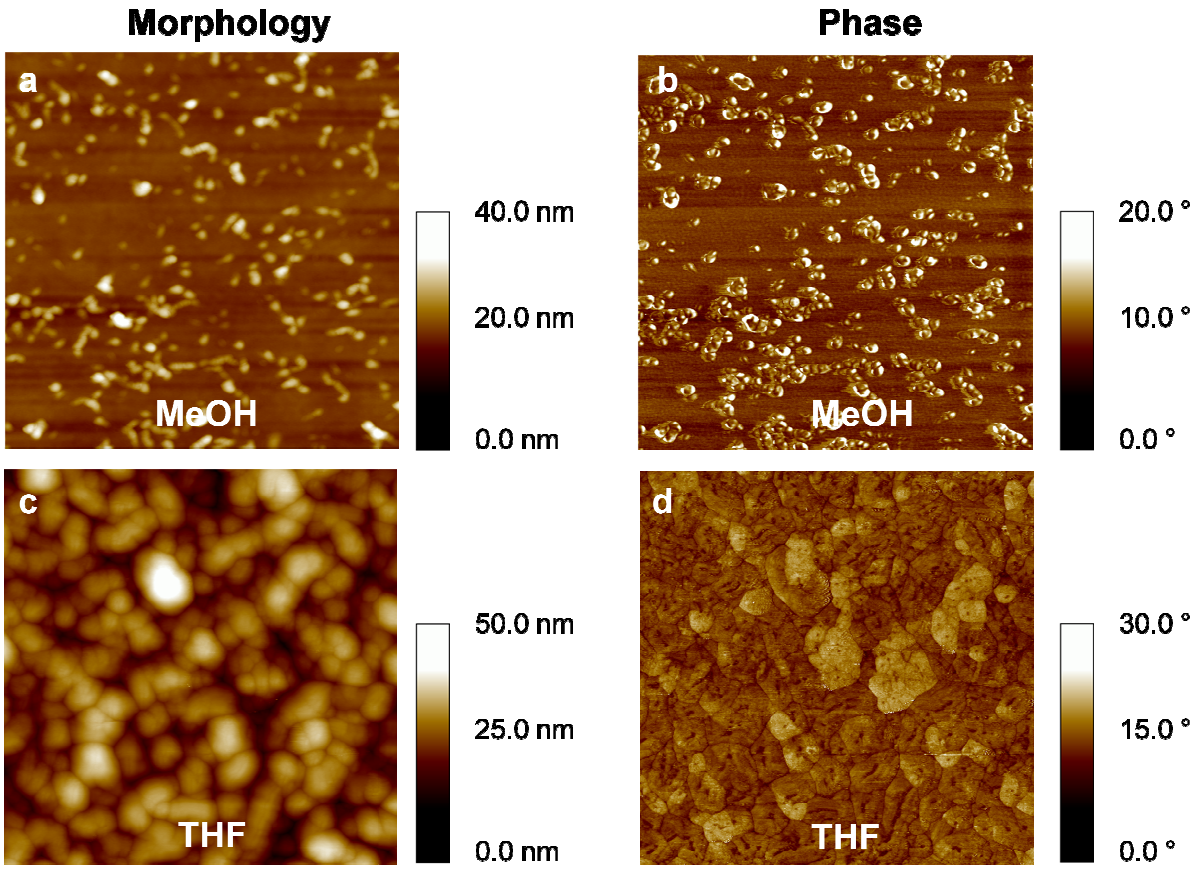

Figure 4.2. Tapping mode AFM morphology (a and c) and phase (b and d) images of PF6NBr-b-PFO, 0.1% in methanol (a and b) and 0.1% THF (c and d), spin-coated, (image size: 2.0x2.0 μm).

Furthermore, AFM also allows for differentiating between charged and neutral blocks based upon differences in the electrostatic surface potential of the blocks. Films spin-coated onto indium tin oxide (ITO) from a dilute methanolic solution (0.1% of PF6NBr-*b*-PFO by weight) show the occurrence of isolated spherical aggregates with a diameter of about 50 nanometers. The topography image of Figure 4.3(a) illustrates the formation of spherical aggregates from methanol. For comparison, AFM experiments have been carried out on films cast from THF solutions at the same concentration (0.1%) of the polyelectrolyte diblock copolymer PF6NBr-

b-PFO [Figure 4.3(c)]. In contrast to the spheres observed in films cast from methanol, films cast from THF contain cylindrical, worm-like aggregates.

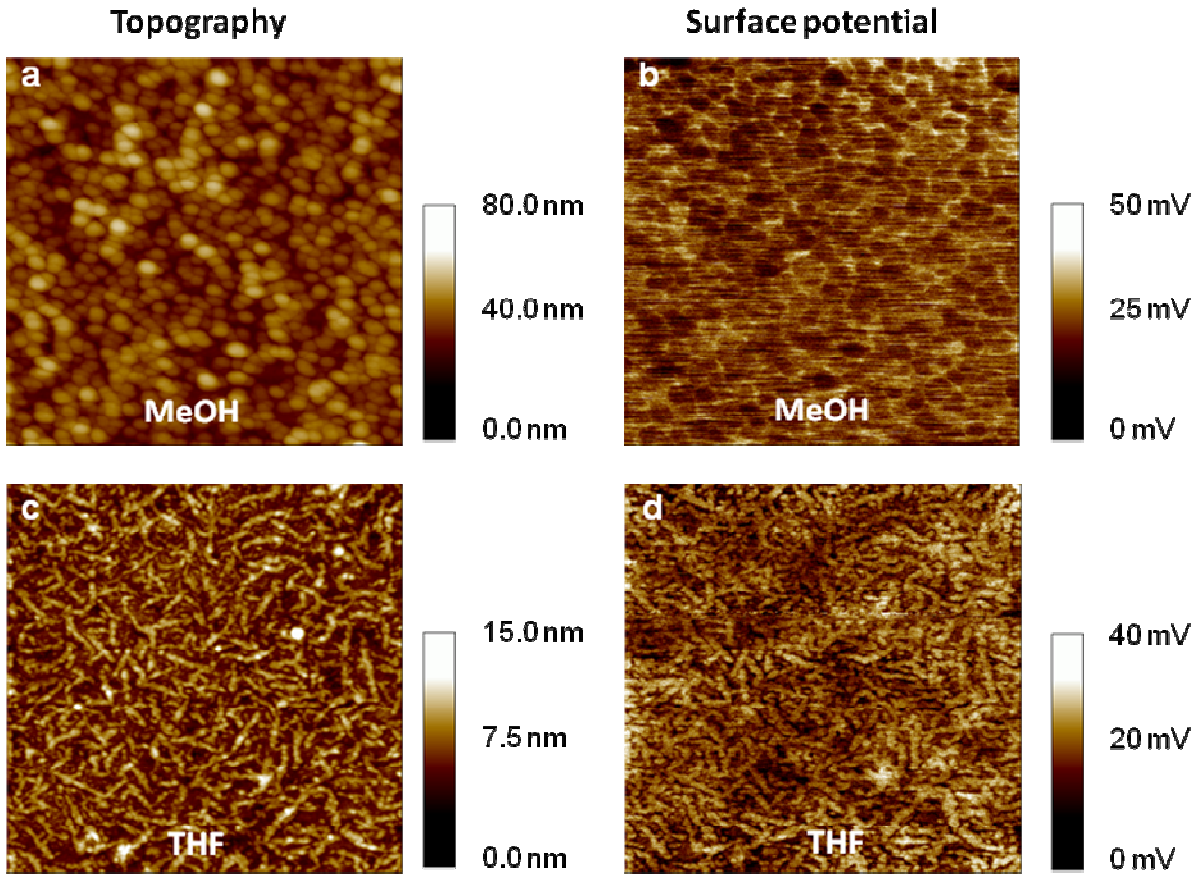

Figure 4.3.AFM topography (a and c) and surface potential (b and d) images of ITO/PF6NBr-b-PFO, 0.1% in methanol (a and b) and 0.1% THF (c and d), spin-coated, (image size: 2.0x2.0 μm).

A comparison of topography and surface potential AFM images provides information about the position of the cationic blocks [Figure 4.3(b and d)]. Since the surface potential of the aggregates from methanol is low in comparison to the high surface potential of the particles from THF we conclude that the ionic blocks are located inside (THF) or outside (MeOH) of the particles. The phenomenon of reverse block morphologies as a function of solvent polarity has been previously discussed.[23]

4.2.4. Confocal Microscopy

In addition to our AFM investigations we have studied the aggregate formation process of PF6NBr-*b*-PFO by confocal fluorescence imaging technique. PF6NBr-*b*-PFO was dissolved

in THF (1 mg/mL) and drop cast onto a glass substrate (a traditional microscope slide). The same solution was prepared in methanol in order to vary the solvent polarity, analogous to the UV-Vis analysis. The results of these experiments are shown in Figure 4.4. In THF vesicles or polymersomes (polymer liposomes) with a diameter of 12-16 μm are formed, in methanol particles with a diameter of 6-10 μm. Therefore, self-assembly of the diblock copolyelectrolyte PF6NBr-*b*-PFO is observed for both solvents. Because methanol is a good solvent for polar PF6NBr blocks it is reasonable to anticipate that the cationic blocks should be directed to the external/internal solvent phase and PFO to the interior of the polymersome walls for methanolic solutions. In contrast, because THF is a good solvent for the PFO blocks and a poor solvent for PF6NBr we expect an inversion of the block copolymer orientation within the polymersomes in THF solution as compared to the behavior in methanol.

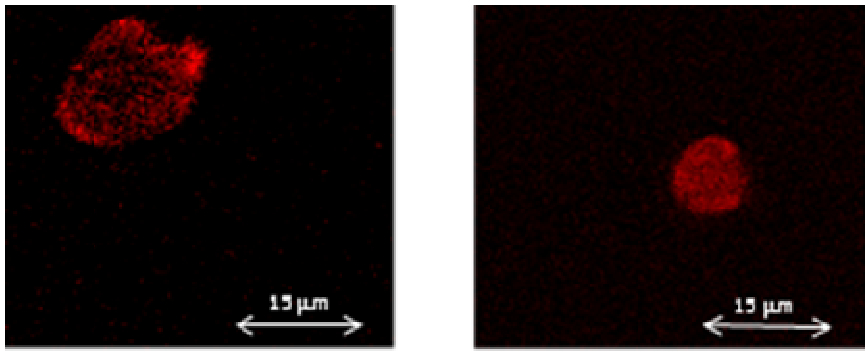

Figure 4.4. Confocal fluorescence microscopy images of two PF6NBr-b-PFO polymersomes (concentration: 1 mg/mL) on glass substrate in THF (left) and methanol (right).

By the way, the dramatically increased size of the particles (vesicles) in the confocal fluorescence microscopy images, compared to the AFM images, should result from a fusion of the primarily formed smaller vesicles.

4.2.5. Incorporation into Organic Light-Emitting Diodes (OLEDs)

One of the primary applications of conjugated polyelectrolytes was a use as charge injection layers of organic light-emitting diodes (OLEDs) leading to an improved device efficiency.[24] Here, the conjugated polyelectrolytes offer functions and device processing options not attainable by using their neutral counterparts. The conjugated polyelectrolyte (CPE) materials from layers with strong interfacial dipoles are based on their ionic functionalities. Moreover, mobile counter ions can migrate under an applied external electric field. Their solubility in

polar solvents opens the option for quenching multilayer systems in a very simple way via solution deposition.[25]

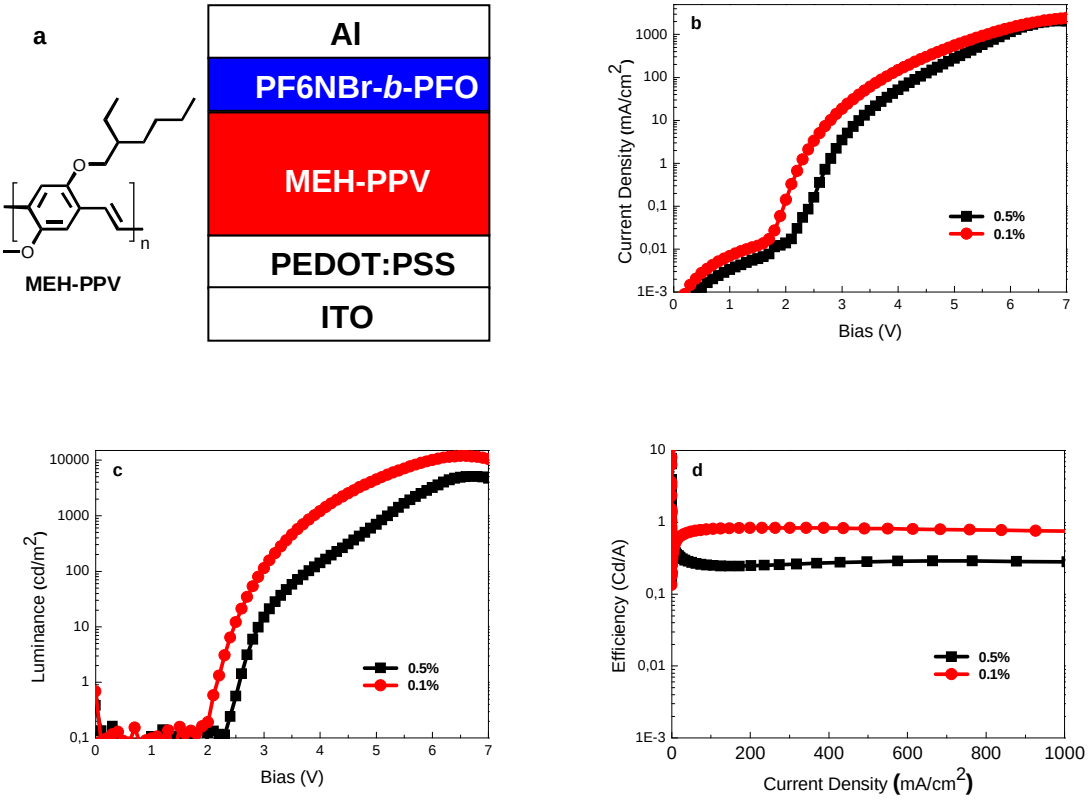

Figure 4.5. a) Chemical structures of MEH-PPV and schematic drawing of a multilayer OLED including a PF6NBr-b-PFO interfacial layer. b) Current density versus bias. c) Luminance versus bias and d) luminous efficiency versus current density characteristics of the multilayer OLEDs.

Our polyelectrolyte block copolymer was applied as an organic electron injection layer of OLEDs. We have fabricated the OLED devices with PF6NBr-*b*-PFO as the electron injection layer (EIL) via the orthogonal solvent deposition approach. Figure 4.5(a) shows the multilayer device configuration used. Poly[2-methoxy-5-(2-ethylhexyloxy)-1,4-phenylenevinylene] (MEH-PPV) is used as the emissive layer (EL) and poly(3,4-ethylenedioxythiophene):poly(styrenesulfonate) (PEDOT:PSS) as hole injection layer. The multilayer device structure can be fabricated based on the orthogonal solubility of MEH-PPV (soluble in toluene) and of PF6NBr-*b*-PFO (soluble in methanol) that allows the PF6Br-*b*-PFO layer to be cast atop the MEH-PPV layer while preventing mixing of these layers and allowing for the formation of a defined interface. The current density versus voltage (*J*-*V*), luminance intensity versus voltage (*L*-*V*), and efficiency versus current density (*E*-*J*) characteristics of devices with thin interlayers are depicted in Figure 4.5 (b-d). Herby, the

CPE interlayer is made from a solution of 0.5 or 0.1% (w/v) PF6NBr-*b*-PFO in methanol with a thickness of 40-60 nm (for 0.5% w/v) and 5-10 nm (0.1% w/v). The devices with the EIL show a low turn-on voltage (2.0-2.5 V). The results indicate that a PF6NBr-*b*-PFO interlayer can effectively reduce the electron injection barrier from the Al electrode, similar to other conjugated polyelectrolytes with only a single polyelectrolyte block. The devices with the thicker EIL show a lower maximum brightness and lower OLED efficiency as compared to the devices with a thin EIL. Based on our previous results, the difference in brightness and efficiency between devices with thick and thin EIL layers can be attributed to different primary operating mechanisms of the EIL. Thick EILs may preferably operate via ion migration whereas thin EILs preferably operate via formation of interfacial dipoles. It may be possible that the neutral PFO block of PF6NBr-*b*-PFO perturbs the ion migration for thick EIL films. These observations demonstrate that PF6NBr-*b*-PFO is a promising candidate as EIL layer for improving the electron injection from the cathode in OLED devices.

4.3. Conclusion and Outlook

In summary, we have developed a synthetic protocol towards novel, all-conjugated, cationic PF6NBr-*b*-PFO diblock copolymers. We have studied the photophysical properties and aggregation behavior of them in solution and in the solid state. We are able to tune the nanophase morphology of the all-conjugated, cationic block copolymer by using different solvents (and concentrations). The block copolymers have been used as the electron injection layer in OLEDs.

Figure 4.6 depicts our structure model for the diblock copolymer vesicles (polymersomes) that are formed by PF6NBr-*b*-PFO in methanol and in THF. In methanol the core region of the amphiphilic bilayers (vesicle walls) is generated by the aggregation of the non-ionic, hydrophobic PFO segments (in orange) while the outer shells of the vesicle walls are formed by the ionic, hydrophilic PF6NBr segments (in black). The aggregation leads to the occurrence of an interfacial dipole within the conjugated polyelectrolyte layers.[26] Aggregation in THF results in an inversion of the block orientation compared to that observed in methanol as indicated in our AFM experiments.

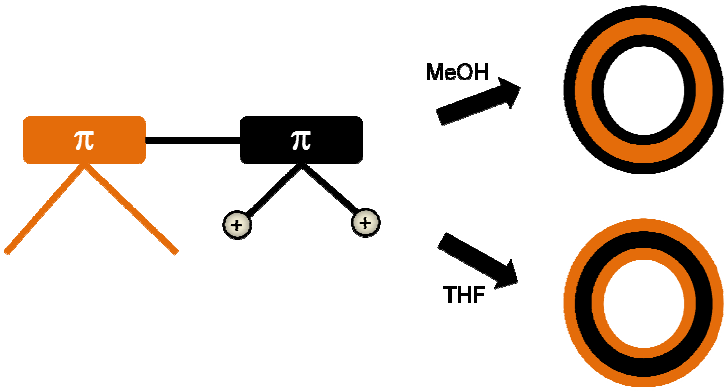

Figure 4.6. Graphical illustration of the vesicle structure formed by PF6NBr-b-PFO from methanol or THF (orange: PFO block, black: PF6NBr block).

Future work will focus on the self-assembly behavior of PF6NBr-*b*-PFO and related systems. Concerning the poly(fluorene)-*b*-poly(fluorene) diblock copolyelectrolytes, a further improvement of the electronic properties seems possible via modification of the side groups (alkyl length, polar head groups). The use of different polar side group may fine-tune the self-assembling behavior. For this, block polyelectrolytes with different quaternary ammonium groups, e.g. derived from pyridine or methylimidazole, are interesting candidates.

Additionally, the influence of different counter ions (e.g. I^-, F^-, BIm_4^-, and $BArF_4^-$, see Scheme 4.3) on the performance and device characteristics of organic light-emitting diodes should be studied.

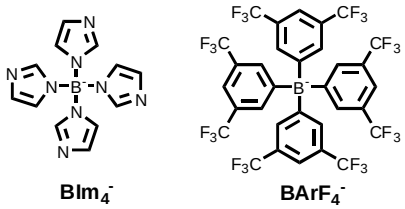

Scheme 4.3: Structures of the counter anions BIm_4^-, and $BArF_4^-$.

Several sensors based on small CPEs have already been developed for specific analytes as anions/cations, proteins, or DNA.[27,28] In this view, our block polyelectrolytes should be of considerable interest for a use in biosensors, and sensors in general.

4.4. Experimental Section

Materials

Unless otherwise indicated, all reagents were obtained from commercial suppliers and were used without further purification. All reactions were carried out using standard and Schlenk techniques under an argon atmosphere. The solvents were used as commercial p.a. quality.

General procedure for the synthesis of 2,7-dibromo-9,9-dialkylfluorene

2,7-Dibromofluorene (15.8 g, 48.8 mmol), alkylbromide (488 mmol) and tetrabutylammonium bromide (1.57 g, 4.88 mmol) were added to an aqueous potassium hydroxide solution (300 mL, 45% w/w). The mixture was stirred for 1 h at 80 °C under argon atmosphere and then diluted with water (50 mL). The aqueous solution was extracted with dichloromethane three times and the combined organic layers were washed with water, 1 M HCl, brine, and dried over magnesium sulfate. After removal of the organic solvent, the excess alkylbromide was removed under reduced pressure. The crude product, a yellow oil, was purified by silica gel column chromatography to afford 2,7-dibromo-9,9-dialkylfluorene as a colorless oil, which was recrystallized from ethanol yielding colorless crystals.

2,7-Dibromo-9,9-dioctylfluorene (BrFO)

According to the general procedure, 2,7-dibromofluorene (3.84 g, 14.76 mmol) was reacted with 1-bromooctane (28.50 g, 147.6 mmol) to yield, after purification by column chromatography (eluent: *n*-hexane), about 5.84 g (approx. 72%) of the target compound.

^{1}H-NMR 500 MHz, CD_2Cl_2). δ (ppm): 7.50 (d, *J = 8.0 Hz*, 2H, Ar-H), 7.49-7.46 (m, 4H, Ar-H), 1.95 (m, 4H, CH_2), 1.24-1.06 (m, 24H, CH_2), 0.59 (m, 6H, CH_3). ^{13}C-NMR (125 MHz, CD_2Cl_2): δ (ppm): 153.46, 139.9, 130.7, 126.9, 122.0, 121.8, 56.4, 40.7, 32.4, 30.5, 29.8, 24.3, 23.2, 22,5, 14.5. Elemental analysis: $C_{29}H_{40}Br_2$, calculated (%): C 63.51, H 9.79, measured (%): C 63.41, H 9.61. GC-MS: t_r = 8.5 min, 100% M^+: 548. Mp**:** 50 °C (± 1 °C).

2,7-Dibromo-9,9-bis(6-bromohexyl)fluorene (BrF6Br)

According to the general procedure, 2,7-dibromofluorene (15.80 g, 48.80 mmol) was reacted with 1,6-dibromohexane (117.61 g, 488 mmol) to yield, after purification by column chromatography (eluent: $CHCl_3$/hexane = 9:1), about 23.11 g (approx. 72%) of the target compound.

^{1}H-NMR 500 MHz, CD_2Cl_2). δ (ppm): 8.28 (d, *J* = 8.0 Hz, 2H, Ar-H), 8.21-8.19 (m, 4H, Ar-H), 4.03 (t, *J* = 6.8 Hz, 4H, CH_2-Br), 2.68 (quint, *J* = 4.6 and 3.7 Hz, 4H, CH_2), 2.38 (quint, *J* = 7.6 and 6.9 Hz, 4H, CH_2), 1.91 (quint, *J* = 8.5 and 6.9 Hz, 4H, CH_2), 1.81 (quint, *J* = 7.5 and 7.3 Hz, 4H, CH_2), 1.31 (m, 4H, CH_2). ^{13}C-NMR (125 MHz, CD_2Cl_2): δ (ppm): 150.9, 137.9, 129.1, 124.9, 120.3, 120.0, 54.3, 38.8, 32.6, 31.4, 27.7,26.5, 22.23. Elemental analysis: $C_{29}H_{40}Br_2$, calculated (%): C 46.19, H 4.65, measured (%): C 46.10, H 4.71. GC-MS: t_r = 7.2 min, 100% M^+: 650.

General procedure for the synthesis of 2-(4',4',5',5'-tetramethyl-1',3',2'-dioxaborolane-2'-yl)-7-bromo-9,9-dialkylfluorene

2,7-Bromo-9,9-dialkylfluorene (15.4 mmol) was dissolved in dry, degassed diethylether (300 mL) and placed in a 500 mL round bottle flask. The solution was cooled down to -78 °C and 0.98 equivalents of alkyl lithium (either *n*-butyllithium or *t*-butyllithium) was added drop-wise. The resulting solution was stirred for one hour followed by addition of 2-isopropoxy-4,4,5,5-tetramethyl-1,3,2-dioxaborolane (12.6 mL, 61.5 mmol) in one shot. The reaction mixture was stirred for one more hour at -78 °C. The mixture was then allowed to warm up to room temperature overnight followed by quenching with water (50 mL). The two-phase solution was then extracted with dichloromethane three times and the combined organic layers were washed with water and brine, and dried over magnesium sulfate. The solvent was removed under reduced pressure and the resulting yellow oil was purified by silica gel column chromatography to afford 2-(4',4',5',5'-tetramethyl-1',3',2'-dioxaborolane-2'-yl)-7-bromo-9,9-dioctylfluorene as a colorless oil.

2-(4',4',5',5'-Tetramethyl-1',3',2'-dioxaborolane-2'-yl)-7-bromo-9,9-dioctylfluorene (FO)

According to the general procedure, 2,7-bromo-9,9-dioctylfluorene (6.0 g, 10.9 mmol) was reacted 1.6 M *n*-butyllithium (6.2 mL, 10.7 mmol) to yield, after purification by column

chromatography (eluent: ethyl acetate/hexane = 95:5), about 3.20 g (approx. 49%) of the target compound.

^{1}H-NMR (500 MHz, $CDCl_3$). δ (ppm): 7.81 (d, 1H, Ar-H), 7.72 (s, 1H, Ar-H), 7.66 (d, 1H, Ar-H), 7.57 (d, 1H, Ar-H), 7.46 (s, 1H, Ar-H), 7.40 (m, 1H, Ar-H), 2.04-1.90 (m, 4H, Ar-CH_2), 1.39 (bs, 12H, $OC(CH_3)_2C(CH_3)_2O$), 1.29-1.00 (m, 20H, alkyl-H), 0.82 (t, 6H, CH_2-CH_3), 0.64-0.47 (m, 4H, alkyl-H). ^{13}C-NMR (125 MHz, $CDCl_3$): δ (ppm): 153.6, 149.5, 143.0, 140.0, 127.8, 133.9, 129.9, 128.9, 126.2, 121.4, 119.0, 83.8, 55.5, 40.1, 31.8, 29.9, 29.1, 24.9, 23.6, 22.6, 14.0. Elemental analysis: $C_{35}H_{52}BBrO_2$, calculated (%): C 70.59, H 8.80, measured (%): C 70.42, H 8.39. GC-MS: t_r = 9.8 min, 100% M^+: 596.

2-(4',4',5',5'-Tetramethyl-1',3',2'-dioxaborolane-2'-yl)-7-bromo-9,9-bis(6-bromohexyl)fluorene (F6Br)

According to the general procedure, 2,7-bromo-9,9-*bis*(6-bromohexyl)fluorene (10.0 g, 15.4 mmol) was reacted with 1.7 M *t*-butyllithium (15.1 mmol) to yield, after purification by column chromatography (eluent: ethyl acetate/hexane = 95:5), about 5.60 g (approx. 52%) of the target compound.

^{1}H-NMR (500 MHz, $CDCl_3$). δ (ppm): 7.82 (d, 1H, Ar-H), 7.72 (s, 1H, Ar-H), 7.66 (d, 1H, Ar-H), 7.77 (d, 1H, Ar-H), 7.46 (d, 2H, Ar-H), 3.30 (t, 4H, CH_2-Br), 2.00 (m, 4H, CH_2), 1.67 (quint., 4H, CH_2), 1.42 (s, 12H, $OC(CH_3)_2C(CH_3)_2O$), 1.21 (quint., 4H, CH_2), 1.09 (quint., 4H, CH_2), 0.60 (quint., 4H, CH_2). ^{13}C-NMR (125 MHz, $CDCl_3$): δ (ppm): 171.3, 153.3, 149.3, 142.9, 140.0, 134.0, 130.2, 129.0, 126.3, 121.8, 121.7, 119.2, 83.9, 60.6, 55.4, 39.9, 34.6, 32.8, 29.1, 27.9, 25.1, 23.6, 21.3, 14.5. Elemental analysis: $C_{31}H_{42}BBr_3O_2$, calculated (%): C 53.40, H 6.07, measured (%): C 53.44, H 66.08. GC-MS: t_r = 8.3 min, 100% M^+: 697.

Poly[9,9-bis(6-bromohexyl)-2,7-fluorene]-b-poly(9,9-dioctyl-2,7-fluorene) (PF6Br-b-PFO)

Aqueous 2 M sodium carbonate solution (5 mL) was added to a mixture of 2-(4',4',5',5'-tetramethyl-1',3',2'-dioxaborolane-2'-yl)-7-bromo-9,9-dioctylfluorene F8 (150 mg, 0,25 mmol) in freshly distilled THF (12 mL) in a Schlenk tube under argon. The catalyst (*t*-Bu_3P)Pd(C_6H_5)Br (9.6 mg, 0,025 mmol) in THF (4 mL) was added via a syringe and the mixture was stirred for 10 minutes at room temperature. After that 2-(4',4',5',5'-tetramethyl-1',3',2'-dioxaborolane-2'-yl)-7-bromo-9,9-*bis*(6-bromohexyl)fluorene F6Br (176 mg,

0.25 mmol) in THF (2 mL) were added via a syringe and the mixture was stirred for 30 min at room temperature. The polymer solution was then poured into acidified methanol (500 mL, containing 50 mL of 2 M HCl). The precipitate was isolated via filtration and purified by a Soxhlet extraction with methanol. The residue was re-dissolved in chloroform. The polymer was isolated by removing the chloroform via rotary evaporation. The residual solid was dried under vacuum to a constant weight to give PF6Br-*b*-PFO as a light yellow solid (178 mg, 82%).

^{1}H-NMR (500 MHz, $CDCl_3$). δ (ppm): 7.84 (m, 4H, Ar-H), 7.70 (m, 8H, Ar-H), 3.29 (m, 4H, CH_2), 2.13 (m, 8H, CH_2), 1.70 (m, 4H, CH_2), 1.22 (m, 32H, alkyl-CH_2), 0.81 (m, 6H, CH_2-CH_3). GPC Anal. (THF, 254 nm): M_n = 18 000 g/mol, M_w = 22 900 g/mol, M_w/M_n = 1.27.

Poly[9,9-bis(6-(N,N,N-trimethylammonium)hexyl)-2,7-fluorene]-b-poly(9,9-dioctyl-2,7-fluorene) (PF6NBr-b-PFO)

Condensed trimethylamine (2.5 mL) was added drop-wise to a solution of the block copolymer precursor (100 mg, M_n = 18 000 g/mol) in THF (50 mL) at -78 °C. The mixture was allowed to warm up to room temperature gradually and stired for 16 hrs. The solvent was then removed under reduced pressure. The residue was re-dissolved by addition of methanol, and a second portion of trimethylamine (2 mL) was added at -78 °C. The mixture was stirred vigorously for additional 24 h at room temperature. After removal of most of the solvent under reduced pressure the polymer solution was placed in a dialysis bag (cut-off of the dialysis membrane: 1,000 g/mol, solvent: water/methanol 1:1) for three weeks for further purification. After evaporation of the solvents the polymer was collected and dried under reduced pressure to yield about 104 mg (approx. 92%) of the target compound as a yellow solid.

^{1}H-NMR (600 MHz, MeOD). δ (ppm): 7.96-7.80 (m, 12H, Ar-H), 3.22 (m, 22H, $N^+(CH_3)_3$ and N^+-CH_2), 1.70-1.60 (m, 4H, alkyl-CH_2), 1.31-1.17 (m, 32H, alkyl-CH_2), 0.83 (m, 8H, alkyl-CH_2), 0.14 (m, 6H, CH_2-CH_3). UV-Vis (MeOH): $\lambda_{max,\ abs}$ = 390 nm. PL (MeOH, λ_{exc} = 380 nm) $\lambda_{max,\ em}$= 414, 437 nm.

Device Part

The organic thin films were prepared on indium tin oxide (ITO)-coated glass substrates (Thin Film Devices) for electrical measurements. Therefore, the ITO-coated glass substrate was first cleaned with detergent, then ultrasonicated in acetone and isopropyl alcohol, and subsequently dried in an oven overnight. The substrates were treated with UV/O_3 (UVO Cleaner 42, Jelight Co. Inc.) for an hour prior to polymer deposition.

For OLED fabrication, 0.5% w/v solutions of MEH-PPV in toluene, and 0.5% or 0.1% w/v solutions of PF6NBr-*b*-PFO in methanol, were prepared and stirred at 40 °C overnight prior to use. ITO-coated glass substrates were used as the anode onto which a PEDOT:PSS dispersion (Baytron 4083, H. C. Stark) was spin-coated at 1500 rpm for 70 s, yielding a ~60 nm thick PEDOT:PSS film. The PEDOT:PSS layer was dried at 150 °C for 1 h. The MEH-PPV solution was spin-coated at ~1000 rpm for 60 s atop the PEDOT:PSS layer to yield a ~ 80 nm thick MEH-PPV film. Subsequently, the PF6NBr-*b*-PFO interlayer was spin-coated atop the MEH-PPV layer at 3000 rpm for 60 s to yield a 5-10 nm thin interlayer by using 0.1% w/v solution of PF6NBr-*b*-PFO in methanol and a 40-60 nm thick interlayer for 0.5% w/v solution, respectively. The devices were completed by drying them under a 10^{-4} torr vacuum overnight followed by thermal evaporation of Al electrodes at a pressure of 10^{-8} torr. All fabrication, annealing and testing steps were carried out inside a nitrogen atmosphere dry glove box. The film thicknesses were determined by AFM measurements.

Instruments

NMR

The ^{1}H and ^{13}C NMR spectra were recorded on a either a Bruker Avance500 500 MHz or a Bruker Avance II 600 MHz NMR spectrometer with use of the solvent proton or carbon signals as internal standard.

GC-MS

GC-MS measurements were obtained on Shimadzu GC-17A/QP-5000 EI GCMS (column: FS-OV1-CB-0,25) under helium a gas; injection temperature: 280 °C, starting temperature: 250 °C, heating rate: 6 °C, end temperature: 280 °C, end time: 30 min.

Elemental analyses

Elemental analyses were performed on a Vario EL II (CHNS) instrument.

GPC

Gel permeation chromatography (GPC) measurements were carried out using a Waters 2695 Separation Module equipped with Column I-Series Mixed Bed High Molecular Weight Viscotek columns with separation range 1000 – 10 M (30 cm x 7.8 mm i.d.), a 2414 RI detector and a 2996 photodiode array (PDA) detector. THF was employed as the solvent and polystyrene (PSS) standards were used for calibration. The measurements were obtained at 30 °C.

UV-Vis

UV-Vis absorption spectra were recorded on a Shimadzu UV-2401 PC spectrophotometer at room temperature.

Photoluminescence spectroscopy

Fluorescence measurements were carried out on a Shimadzu UV-2401 instrument at room temperature.

Confocal flourescence microscope

Confocal fluorescence images were collected using a Leica TCS SP high resolution spectral confocal microscope equipped with a Millennia® series argon laser S-10 excitation source. The polymer samples were prepared by depositing a polymer solution onto glas slide followed by placement of a cover slip. The slide was inverted and placed onto the microscope stage (cover slip down) and the sample imaged in epi-fluorescence mode.

AFM

Atomic force microscopy measurements were recorded using a under nitrogen environment using a commercial scanning probe microscope (MultiMode and Nanoscope Controller IIIa, Veeco Inc.). Surface potential measurements were collected using a Veeco diDimension Icon atomic force microscope instrument.

4.5. References

[1] A. Gutacker, S. Adamczyk, A. Helfer, L. E. Garner, R. C. Evans, S. M. Fonseca, M. Knaapila, G. C. Bazan, H. D. Burrows, U. Scherf, *J. Mater. Chem.* **2010**, *20*, 1423.

[2] Y. Zhang, K. Tajima, K. Hirota, K. Hashimoto, *J. Am. Chem. Soc*. **2008**, *130*, 7812.

[3] R. D. McCullough, *Adv. Mater*. **1998**, *10*, 93.

[4] A. Yokoyama, R. Miyakoshi, T. Yokozawa, *Macromolecules* **2004**, *37*, 1169.

[5] A. Yokoyama, T. Yokozawa, *Macromolecules* **2007**, *40*, 4093.

[6] Y. Zhang, K. Tajima, K. Hashimoto, *Macromolecules* **2009**, *42*, 7008.

[7] K. Ohshimizu, M. Ueda, *Macromolecules* **2008**, *41*, 5289.

[8] P.-T. Wu, G. Ren, C. Li, R. Mezzenga, S. A. Jenekhe, *Macromolecules* **2009**, *42*, 2317.

[9] J. Ge, M. He, F. Qiu, Y. Yang, *Macromolecules* **2010**, *43*, 6422.

[10] a) U. Scherf, E. List, *Adv. Mater*. **2002**, *14*, 477. b) M. T. Bernius, M. Inbasekaran, J. O'Brien, W. Wu, *Adv. Mater*. **2000**, *12*, 1737.

[11] D. W. Bright, F. B. Dias, F. Galbrecht, U. Scherf, A. P. Monkman, *Adv. Funct. Mater*. **2009**, *19*, 67.

[12] A. Yokoyama, H. Suzuki, Y. Kubota, K. Ohuchi, H. Higashimura, T. Yokozawa, *J. Am. Chem. Soc.* **2007**, *129*, 7236.

[13] F. Barrios-Landeros, B. P. Carrow, J. F. Hartwig, *J. Am. Chem. Soc*. **2008**, *130*, 5842.

[14] a) N. Miyaura, A. Suzuki, Chem. Rev., 1995, 95, 2457. b) A. Suzuki, *J. Organomet. Chem*. **1999**, *576*, 147.

[15] A. J. Sandee, C. K. Williams, N. R. Evans, J. E. Davies, C. E. Boothby, A. Köhler, R. H. Friend, A. B. Holmes, *J. Am. Chem. Soc*. **2004**, *126*, 7041.

[16] G. Lakhwani, S. C. J. Meskers, *Macromolecules* **2009**, *42*, 4220.

[17] H.-G. Nothofer, *Ph.D. Thesis*, Universität Potsdam, Germany 2001; Logos Verlag, Berlin, **2001**, ISBN 3-89722-6685.

[18] a) J. Jo, C. Chi, S. Höger, G. Wegner, D. Y. Yoon, *Chem. Eur. J*. **2004**, *10*, 2681. b) S. H. Chen, A. C. Su, S. A. Chen, *J. Phys. Chem. B* **2005**, *109*, 10067. c) M. Grell, D. D. C. Bradley, G. Ungar, J. Hill, K. S. Whitehead, *Macromolecules* **1999**, *32*, 5810. d) F. B. Dias, J. Morgado, A. L. Maçanita, F. P. da Costa, H. D. Burrows, A. P. Monkman, *Macromolecules* **2006**, *39*, 5854.

[19] a) P. E. Shaw, A. Ruseckas, J. Peet, G. C. Bazan, I. D. W. Samuel, *Adv. Funct. Mater*. **2010**, *20*, 155. b) A. J. Cadby, P. A. Lane, H. Mellor, S. J. Martin, M. Grell, C. Giebeler, D. D. C. Bradley, M. Wohlgenannt, C. An, Z. V. Vardeny, *Phys. Rev. B* **2000**, *62*, 15604.

[20] a) U. Scherf, A. Gutacker, N. Koenen, *Acc. Chem. Res*. **2008**, *41*, 1086. b) U. Scherf , S. Adamczyk, A. Gutacker, N. Koenen, *Macromol. Rapid Commun.* **2009**, *30*, 1059. c) Y. Park, N. Koenen, M. Forster, R. Ponnapati, U. Scherf, R. Advincula, *Macromolecules* **2008**, *41*, 6169.

[21] T. Hayakawa, R. Goseki, M.-a. Kakimoto, M. Tokita, J. Watanabe, Y. Liao, S. Horiuchi, *Org. Lett*. **2006**, *8*, 5453.

[22] D. M. Vriezema, M. Comellas Aragonès, J. A. A. W. Elemans, J. J. L. M. Cornelissen, A. E. Rowan, R. J. M. Nolte, *Chem. Rev*. **2005**, *105*, 1445.

[23] G. Tu, H. Li, M. Forster, R. Heiderhoff, L. Balk, R. Sigel, U. Scherf, *Small* **2007**, *3*, 1001.

[24] a) J. H Seo, E. B. Namdas, A. Gutacker, A. J. Heeger, G. C. Bazan, *Applied. Phys. Lett*. **2010**, *97*, 043303. b) G. Pace, G. Tu, E. Fratini, S. Massip, W. T. S. Huck, P. Baglioni, R. H. Friend, *Adv. Mater*. **2010**, *22*, 2073. c) C. W. Tang, S. A. Vanslyke, *Appl. Phys. Lett*. **1987**, *51*, 913.

[25] C. V. Hoven, A. Garcia, G. C. Bazan, T. Q. Nguyen, *Adv. Mater*. **2008**, *20*, 3793.

[26] J. Luo, H. B. Wu, C. He, A. Y. Li, W. Yang, Y. Cao, *Appl. Phys. Lett.* **2009**, *95*, 043301. J. L. Casson, D. W. McBranch, J. M. Robinson, H.-L. Wang, J. B. Roberts, P. A. Chiarelli, M. S. Johal, *J. Phys. Chem. B* **2000**, *104*, 11996.

[27] S. W. Thomas III, G. D. Joly, T. M. Swager, *Chem. Rev*. **2007**, *107*, 1339.

[28] a) B. Liu, G. C. Bazan, *Proc. Natl. Acad. Sci*. **2005**, *102*, 589. b) K. Ding, F. E. Alemdaroglu, M. Börsch, R. Berger, A. Herrmann, *Angew. Chem. Int. Ed*. **2007**, *119*, 1191.

Chapter 5

5. Summary

Within this thesis, new all-conjugated, cationic diblock copolyelectrolytes, based on polyfluorene and polythiophene blocks, have been successfully synthesized. Their photophysical properties and aggregation behavior have been studied in solution and in the solid state. Especially PF2/6-*b*-P3MAHT shows a significant solvatochromatic effect in THF/water mixtures. Bilayer-based vesicles (polymersomes) with diameters of several microns have been observed for PF2/6-*b*-P3PyHT and PF2/6-*b*-P3TMAHT diblock copolymers. Using solvents of different polarity (THF versus methanol) leads to a tunable self-assembly for PF6NBr-*b*-PFO with a different arrangement of the components within the vesicle walls. Because of the resulting control on the formed nano-scaled arrangement CPEs are also promising materials for an incorporation into optoelectronic devices. The application of P3TMAHT and PF2/6-*b*-P3TMAHT as thin electron extraction layers of BHJ-type organic solar cells leads to an increase of the PCE from ca. 5.3 to ca. 6.5%. Further on, PF6NBr-*b*-PFO has been used as thin electron injection layer of OLEDs. Such CPEs are promising candidates for improving the electron injection into the organic layers of OLEDs.

Furthermore, ionic surfactants, organic acids or biomolecules as DNA lead to a selective quenching and/or a characteristic red shift of the polythiophene-based emission band of PF2/6-*b*-P3TMAHT in due to a conformational re-organization. In this perspective PF2/6-*b*-P3TMAHT seems to be a very attractive material for sensors/biosensor applications.

A Acknowledgement

At the end of the day, my thesis is really a product of the love and support I have received. It would not exist without it. Therefore, I would like to express my gratitude to all those who gave me the possibility to complete this thesis. They will recognize themselves even if I do not mention them.

First of all, I would like to express my sincere gratitude to my advisor, Ullrich Scherf who offered me the exciting opportunity to work in the field of polymer chemistry. His broad scientific knowledge as well as the thoughtful considerations and the great, wide scope I was given helped me along this thesis. Furthermore, I would like to thank him for making my stay at the University of California, Santa Barbara, USA possible as well as for his excellent support.

My special thanks go to Guillermo C. Bazan from the University of California, Santa Barbara (UCSB), USA for enabling me to work in his group for one year, that I was most welcome during my stay at UCSB and all the numerous constructive discussions and the friendly relationship. I would like to thank him also for co-refereeing this thesis.

I am grateful to Thuc-Quyen Nguyen and Alan J. Heeger from the University of California, Santa Barbara, USA for the discussions and helpful suggestions.

I would also like to thank Hugh D. Burrows with coworkers from the Universidade de Coimbra, Portugal, Matti Knaapila from the Institute for Energy Technology, Kjeller, Norway as well as Rachel C. Evans from the Trinity College, University of Dublin, Ireland for all the measurements and investigations. Additionally, I would like to thank Rachel C. Evans for co-refereeing this thesis.

My thanks extend also my friends and former colleagues from the Scherf, Bazan and Nguyen group for sharing all their talent, time and support.

My sincere appreciation goes to all my family and friends who accompanied me along my education in Germany and during my stay at UCSB. They helped me balancing my time with work and play.

Finally, I would like to thank my parents and my sister for their love and support in easy and hard times, as well as for their encouragement, understanding and affection.

B List of Publications

Publications concerning this thesis:

Synthesis, photophysics and solution behaviour of cationic fluorene-thiophene diblock copolymers

A. Gutacker, N. Koenen, S. Adamczyk, U. Scherf, J. Pina, S. M. Fonseca, J. Seixas de Melo, A. J. M. Valente, H. D. Burrows, *Macromol. Rapid Commun*. **2008**, *28*, F50.

All-conjugated block copolymers

U. Scherf, A. Gutacker, N. Koenen, *Acc. Chem. Res*. **2008**, *30*, 1059.

All-conjugated, rod-rod block copolymers-generation and self-assembly properties

U. Scherf, S. Adamczyk, A. Gutacker, N. Koenen, *Macromol. Rapid Commun*. **2009**, *30*, 1059.

All-conjugated polyelectrolyte block copolymers

A. Gutacker, S. Adamczyk, A. Helfer, L. E. Garner, R. C. Evans, S. M. Fonseca, M. Knaapila, G. C. Bazan, H. D. Burrows, U. Scherf, *J. Mater. Chem*. **2010**, *20*, 1423.

Solvent dependent assembly of a polyfluorene-polythiophene rod-rod block copolyelectrolyte: influence on photophysical properties

M. Knaapila, R. C. Evans, A. Gutacker, V. M. Garamus, M. Torkkeli, S. Adamczyk, M. Forster, U. Scherf, H. D. Burrows, *Langmuir* **2010**, *26*, 5056.

Cationic fluorene-thiophene diblock copolymers: aggregation behaviour in methanol/water and its relation to thin film structures

A. Gutacker, N. Koenen, U. Scherf, A. Adamczyk, J. Pina, S. M. Fonseca , A. J. M. Valente, R. C. Evans, J. S. de Melo, H. D. Burrows, M. Knaapila, *Polymer* **2010**, *51*, 1898.

Improved high efficiency organic solar cells via incorporation of a conjugated polyelectrolyte interlayer

J. H. Seo, A. Gutacker, Y. Sun, H. Wu, F. Huang, Y. Cao, U. Scherf, A. J. Heeger, G. C. Bazan, *J. Am. Chem. Soc*. **2011**, *133*, 8416.

Publications concerning different topics:

Fractal aggregates of polyfluorene-polyaniline triblock copolymer in solution state

M. Knaapila, V. M. Garamus, L. Almásy, J. S. Pang, M. Forster, A. Gutacker, U. Scherf, A. P. Monkman, *J. Phys. Chem. B* **2008**, *112*, 16415.

Improved injection in n-type organic transistors with conjugated polyelectrolytes

J. H. Seo, A. Gutacker, B. Walker, S. Cho, R. Yang, T.-Q. Nguyen, A. J. Heeger, G. C. Bazan, *J. Am. Chem. Soc.* **2009**, *131*, 18220.

Surfactochromic conjugated polyelectrolyte (CPE) - surfactant complexes of a cationic polythiophene with SDS in water

M. Knaapila, R. C. Evans, V. M. Garamus, L. Almasy, N. K. Szekely, A. Gutacker, U. Scherf, H. D. Burrows, *Langmuir* **2010**, *26*, 15634.

Conjugated polyelectrolytes for organic light emitting transistors

J. H. Seo, E. B. Namdas, A. Gutacker, A. J. Heeger, G. C. Bazan, *Appl. Phys. Lett*. **2010**, *97*, 043303.

Reconstruction of conjugated oligoelectrolyte electron injection layers

Z. Chen, X.-D. Dang, A. Gutacker, A. Garcia, H. Li, Y. Xu, L. Ying, T.-Q. Nguyen, G. C. Bazan, *J. Am. Chem. Soc*. **2010**, *132*, 12160.

C Curriculum Vitae

Andrea Gutacker was born in Wuppertal, Germany on November 8th in 1981. During receiving her diploma degree in chemistry from the University of Wuppertal, Germany, in 2007 under the supervision of Prof. Dr. Ullrich Scherf she joined the group of Prof. Dr. Hugh D. Burrows for an internship in Coimbra, Portugal. From October 2007 up to April 2011 she was a Ph.D. student under the supervision of Prof. Dr. Ullrich Scherf focussing on the synthesis of all-conjugated, cationic diblock copolymers. In 2009 she joined the group of Prof. Dr. Guillermo C. Bazan for a one year research internship at the University of California in Santa Barbara, USA. The results of her investigations are collected in this thesis. In May 2011 she started to work as a chemist at Henkel AG & Co. KGaA in Düsseldorf, Germany.